DESIGN, SYNTHESIS, AND CHARACTERIZATION OF WATERBORNE POLYURETHANE DISPERSIONS FOR SELF-HEALING, ANTI-FOULING, AND UV-CURABLE COATINGS AND FILMS

by

Ekin BERKSUN

Submitted to the Graduate School of Engineering and Natural Sciences in partial fulfillment of the requirements for the degree of Doctor of Philosophy

SABANCI UNIVERSITY

JULY 2024

ABSTRACT

DESIGN, SYNTHESIS AND CHARACTERIZATION OF WATERBORNE POLYURETHANE DISPERSIONS FOR SELF-HEALING, ANTI-FOULING AND UV-CURABLE COATINGS AND FILMS

Ekin BERKSUN

Material Science and Nano Engineering, PhD. Thesis, July 2024

Thesis Advisor: Asst. Prof. Serkan ÜNAL

Keywords: Polyurethane; waterborne polyurethane; elastomer; acetone process; self-healing polymers; antifouling polymers; UV-curable polymers

Polyurethanes are one of the most important and versatile types of polymers, appearing in different forms and applications in every aspect of our lives, from insulation to biomedical applications. Examples of these products include polyurethane foams and coatings, as well as thermoplastic polyurethanes, flexible polyurethanes, rigid polyurethanes, polyurethane ionomers, and waterborne polyurethanes. These products, which have had a significant market share in the industry since the 1940s, are produced through various methods. However, the majority of traditional methods involve chemicals that pose risks to the environment and human health, particularly volatile organic compounds (VOCs).

For this reason, the development of environmentally and human-friendly polyurethane materials has become inevitable. These new generation polyurethane structures must meet all necessary performance criteria and replace traditional products in the market. The new products to be developed should be designed with a more sustainable approach, containing lower volatile organic compounds, consuming less energy, producing less waste, and having a longer material lifespan. With this mission, unique water-based polyurethane dispersions tailored for different applications have been synthesized using the acetone method and characterized. In the studies included in this thesis, systematic syntheses aimed at self-healing, anti-fouling, and UV-curing applications were conducted on structures containing different isocyanates, polyols, ionic groups, and branching amounts, and the structure-property relationships were clarified alongside various sensitive parameters such as the effects of branching degree and curing energy in highly branched water-based polyurethanes. Solid content and particle size measurements (DLS) of the water-borne polyurethane dispersions, as well as mechanical (UTM), thermal (TGA, DSC), and surface properties (VLM, SEM) of the obtained elastomeric films, were reported

ÖZET

KENDİKENDİNİ ONARABİLEN, KİRLENMEYE DİRENÇLİ VEYA UV İLE KÜRLENEBİLEN KAPLAMA VE FİLMLER İÇİN SU BAZLI POLİÜRETAN DİSPERSİYONLARININ TASARIMI, SENTEZİ VE KARAKTERİZASYONU

Ekin BERKSUN

Malzeme Bilimi ve Nanomühendislik, Doktora Tezi, Temmuz 2024

Tez Danışmanı: Dr. Öğr. Üyesi Serkan ÜNAL

Anahtar Kelimeler: Poliüretan, Su bazlı poliüretan, Elastomer, Aseton metodu, Su bazlı boya bağlayıcısı, Kendi kendini iyileştiren polimerler, Antifuling polimerler, UV-kürlenebilir polimerler

Polimerik malzemelerin en önemli sınıflarından biri, poliüretanlardır. Poliüretan malzemeler izolasyondan biyomedikale, otomobilden tekstile, yaşamımızın her alanında, farklı formlarda karşımıza çıkar. Bu ürünlere örnek olarak poliüretan köpükler ve kaplama uygulamaları başta olmak üzere, termoplastik poliüretanlar, esnek poliüretanlar, sert poliüretanlar, poliüretan iyonomerler ve su bazlı poliüretanlar verilebilmektedir. 1940'lı yıllardan bu yana sanayiide çok önemli bir pazar hacmine sahip bu ürünler, farklı metodlar aracılığı ile üretilmektedir. Ancak, geleneksel yöntemlerin büyük bölümü, çevre ve insan sağlığına risk oluşturduğu anlaşılan kimyasallar ve özellikle, uçucu organic bileşikler (VOC) içrmektedir. Bu sebeple, çevreye ve insana duyarlı, yeni nesil poliüretan malzemelerin geliştirilmesi kaçınılmaz hale gelmiştir. Yakın gelecekte geliştirilmesi gereken çevre dostu poliüretan yapıları, gerekli tüm performans kriterlerini sağlamalı ve pazardaki geleneksel ürünlerin yerini almalıdır. Geliştirilecek bu yeni ürünler, daha sürdürülebilir bir anlayışta dizayn edilen akıllı polimerler olmalı, düşük miktarda uçucu organik bileşik içermeli, daha düşük miktar enerji tüketimi, atık üretimi ve maaliyet ile üretilebilmelive daha uzun malzeme ömrüne sahip olmalıdırlar.

Bu misyon ile, farklı uygulamalara hitap eden, özgün nitelikteki su bazlı poliüretan dispersiyonları aseton metodu ile sentezlenmiş ve karakterize edilmiştir. Tez dahilindeki çalışmalarda, poliüretanın segmentli yapısının sunduğu avatajlardan faydalanarak, sert kısım etkisi, yumuşak kısım etkisi ve iyonik grup etkileri ile birlikte, A2+B3 metodu ile sentezlenmiş yüksek dallanmış su bazlı poliüertanlarda dallanma derecesi ve kürlenme enerjisinin etkileri gibi birçok hassas parametre incelenmiştir. Farklı izosiyanatlar, polioller, iyonik gruplar ve dallanma miktarları içeren yapılarda, kendi kendini iyileştirme, antifuling ve UV-kürlenme uygulamalarına yönelik sistematik sentezler yapılmış, yapı-özellik bağlantıları açıklığa kavuşturulmuştur. Su bazlı poliüretan dispersiyonlarının katı miktarları ve parçacık boyutu ölçümleri (DLS), elde edilen elastomerik filmlerin mekanik (UTM), termal (TGA, DSC) ve yüzey özellikleri (VLM, SEM) rapor edilmiştir.

ACKNOWLEDGEMENTS

First of all, I would like to extend my deep thanks to my advisor, Dr. Serkan Ünal, for leading me through this unique adventure. PhD is one of the most notable and challenging periods of our careers. Therefore, it is extremely impactful who you go through this journey with. I feel really lucky to have Dr. Serkan Ünal with all his wisdom and decency. I am very proud to have been able to benefit from his knowledge and experiences.

I would like to express my sincere gratitude to Prof. Dr. Yusuf Z. Menceloğlu who founded such a wonderful research environment and facilities for everyone willing to make an impact. His vision, experiences and extensive knowledge inspired many researchers. It was a great honor to be his student and feel his endless support throughout my PhD journey.

I would like to thank my thesis committee, Prof. Dr. Ersin Serhatlı, Assoc. Prof. Bekir Dizman, Assoc. Prof. Nuray Kızıldağ for their interest and support.

I have to reflect my admiration for Dr. Hayriye Unal who also shaped my research with her indispensable touches, for her endless research passion and perseverance besides her kindness and supportiveness. I am also grateful to Prof. Dr. Fevzi Çakmak Cebeci for everything he taught me not only as a polymer professor, but also as a wonderful personality who lights my way. I also thank my professors, Assoc. Prof. Özge Akbulut and Assist. Prof. Nur Mustafaoğlu, for their kind collaboration and contributions.

I owe a huge thanks to Cüneyt Erdinç Taş and Buket Alkan Taş for being such a special role- model and mentor to me as a grad student, researcher and family**.**

Being a part of the Ünal research group was a privilege. The former and present members of my research group: Serkan Güçlü, Billur Seviniş Özbulut, Ayşe Durmuş Sayar, Soner Kızıl, Deniz Anıl, Murat Tansan, Necdet Ozcelik, Tuğçe Çinko, Yeşim Sepici, Serra Kori and Çiğdem Uçar, thank you for everything we shared.

I want to extend my sincere gratitude to my Mat.Grad. friends, Yeşim Menceloğlu, Deniz Köken, Tuğçe Akkaş, Omid Mohammad Moradi, Yelda Yorulmaz, Mervenaz Şahin, Cihan Arlı, Lyn Zemberekçi, Öykü Demirel, Sena Yüce, Selin Gündoğdu, Gökmen Tamer Şanlı, M.Aybike Ersin, Nilüfer Çakır and especially Sarp Kölgesiz for sharing this adventure.

I would like to thank all laboratory specialists in FENS and SU-IMC for their valuable cooperation.

Alongside all the academic support, the most crucial role in completing this journey actually belongs to my secret heroes. They have been very special people who supported me in every difficult moment and rejoiced with me in every happy moment. I want to thank Ogeday Rodop and Ayşe Ay, who literally changed my life, for all their confidence and joyful friendship. The most heartfelt thanks go to Yusuf Kumtepe, who has brightened my life since the day we met, for all his encouragement and unconditional support.

Above all, I am endlessly grateful to my parents, who provided me with all the opportunities, always stood by my side, and supported me with all their hearts.

Ekin Berksun

2024

TABLE OF CONTENTS

LIST OF TABLES

LIST OF FIGURES

LIST OF ABBREVIATIONS

AA: Adipic Acid

AEAS: 2-[(2-aminoethyl)amino]-ethane sulfonic acid monosodium salt

AFM: Atomic Force Microscope

BD:1,4- Butanediol

DBTL: Dibutyltin Dilaurate

DLS: Dynamic Light Scattering

DMA: Dynamic Mechanical Analysis

DSC: Differential Scanning Calorimeter

EDA: Ethylenediamine

EG: Ethylene Glycol

FTIR: Fourier Transform Infrared

GPC: Gel Permeation Chromatography

HD: Hexanediol

HDI: Hexamethylene-1,6-diisocyanate or 1,6-Diisocyanatohexane

IPDI: 3-Isocyanatomethyl-3,5,5-trimethylcyclohexylisocyanate or isophorone diisocyanate

MFFT: Minimum Film Formation Temperature

NP: Neopentyl Glycol

NMR: Nuclear Magnetic Resonance

OM: Optical Microscope

UTM: Universal Testing Machine

PEG: Polyethylene Glycol

PDI: Polydispersity Index

PTMO: Poly(tetramethylene oxide)

PU: Polyurethane

TGA: Thermogravimetric Analysis

TMA: Thermomechanical Analysis

WPU: Waterborne Polyurethane

LIST OF SYMBOLS

cm: Centimeter

^{o}C: Celsius Degree

rpm: Revolutions per Minute

g: Gram

h: Hour

kDa: Kilo Dalton

mL: Milliliter

Mn: Number Average Molecular Weight

Mw: Weight Average Molecular Weight

T_g: Glass Transition Temperature

T_m: Melting Temperature

Wi: Weight Initial

W_f : Weight Final

%: Percentage

E': Storage Modulus

E'': Loss Modulus

CHAPTER 1: INTRODUCTION

1.1.Dissertation Overview

Polyurethanes are unique materials that can exhibit elastomeric, thermoplastic, or thermoset properties depending on the chemical structure. In this respect, polyurethanes appear as one of the most versatile polymeric materials due to their segmental chemical structure and highly compatible nature with several materials.

The segmented structure of a polyurethane chain allows tuning the chemical, physical, and mechanical properties of the resulting structure. In this scope, modifications can be made by taking advantage of various synthesis methods, types, and ratios of isocyanates, polyols, and chain extenders. Therefore, it is possible to attain functional properties in polyurethanes with chemical approaches. Although the incorporation of organic or inorganic particles is a commonly preferred approach as an alternative, the main challenge is to design and synthesize intrinsically smart polyurethane structures due to concerns about toxicity, incompatibility with polymer matrices, and homogeneity problems of the additive particles.

Waterborne polyurethanes (WPUs) present further versatilities as environmentally friendly alternatives to traditional solvent-based systems. Due to these unique aspects, WPUs have been widely utilized in various applications pertaining to high-performance coatings, adhesives, sealants, binders, paints, and sizing agents. Their low or zero volatile organic compound (VOC) emissions make them an attractive option for applications where environmental regulations and safety concerns are paramount.

The inherent versatility of polyurethanes also extends their ability to be formulated into coatings, films, foams, and elastomers with specific properties tailored to meet the demands of diverse industries. For instance, in the automotive industry, WPUs are employed in interior coatings that require durability and a high-quality finish. In the textile industry, they are used to create breathable yet water-resistant fabrics.

Overall, the adaptability of polyurethanes, particularly waterborne polyurethanes, underscores their importance in modern material science. Their ability to be engineered for specific applications, combined with their environmental benefits, positions WPUs as a crucial component in the advancement of sustainable and high-performance materials across a broad spectrum of industries.

1.2. Objectives

This dissertation aims to design, synthesize and characterize environmentally friendly and functional WPU dispersions and their films for prospective applications. All the studies were designed concerning the impact of conventional, solvent-borne polyurethanes on global warming, environmental pollution, and public health. In this sense, smart, high performance and environmentally friendly WPUs were developed focusing on self-healing, anti-fouling, and UV-curing applications. Basically, self-healing WPU coatings were designed to significantly enable prolonging the service-life of products; inherently anti-fouling WPU coatings are capable of replacing toxic ingredients of marine coatings thus, contributing to wildlife protection, and finally WPUs for efficient UV-Curing processes provide significantly reduced manufacturing energy consumption and offer new potential applications in 3D printing.

1.3. Dissertation Structure

The main skeleton of this dissertation is based on the synthesis and characterization of smart and environmentally friendly WPU dispersions and films for a variety of industry-oriented applications.

In the first chapter, a detailed background information and literature review is presented on polyurethanes and WPUs from the discovery to process methods developed to synthesize them up to now.

In the second chapter, the synthesis and characterization of WPU dispersions for self-healing films and coatings were reported. In order to reach high self-healing efficiencies, key parameters were systematically investigated including the effect of soft segment structure, soft segment content, chain extension degree, ionic group type, ionic group content and several environmental factors as external stimuli potentially affecting the course of the healing process.

The third chapter is focused on the preparation of WPU binders for anti-fouling marine coatings. Herein, the harsh and complex environment was a challenging factor requiring a sensitive design in terms of the balance of hydrophobicity and hydrophilicity, surface properties and thermal properties. Yet, via the strategy of combining various polyols with different structures and hydrophilicity/hydrophobicity balances, drastic results were obtained from novel WPUs synthesized in this study.

The fourth chapter is studied with the aim of obtaining UV-curable WPUs with novel topologies for an efficient UV-curing process with a minimum energy, also fulfilling the consumer needs such as homogeneity, transparency and mechanical performance. For this purpose, oligomeric A_2+B_3 polymerization technique was used to obtain the main skeleton of a branched WPU with acrylate chain ends and a suitable photoinitiator was implemented to the system.

Lastly, overall conclusions were dedicated within a holistic perspective. As a future work, an ongoing study on the design of direct-ink writing (DIW) 3D printing ink was shortly presented.

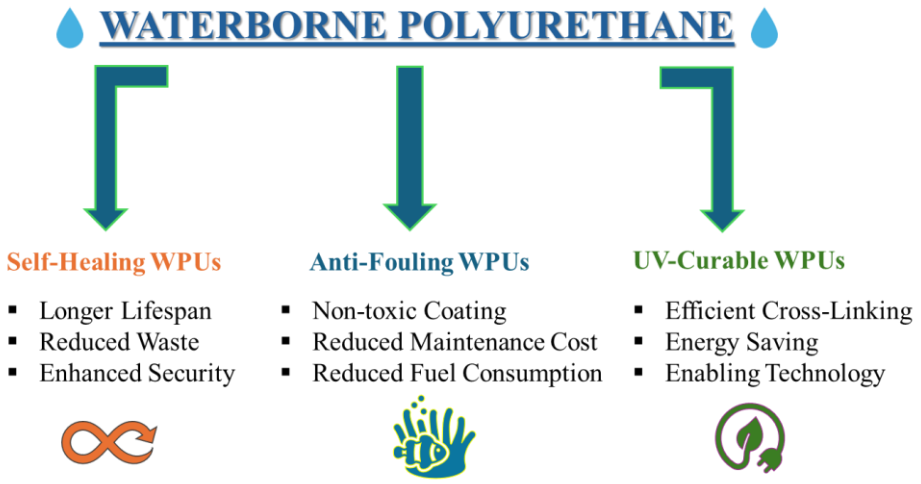

Figure 1: Dissertation structure

CHAPTER 2: LITERATURE REVIEW

2.1. History of Polyurethanes

Back in the 1930-1940s, huge competition emerged between the chemists and chemical companies which started an invention era. Polyamides (Nylon) were discovered by Carothers and patented by DuPont. Meanwhile, Otto Bayer from IG Farben in Leverkusen, Germany, was trying to produce rival synthetic polyamides. However, he used a different chemical and performed the same method with isocyanates. Thereby, he made his milestone invention in 1937 and polyurethanes appeared on the world stage[1]. The first polyurethane, Perlon U, was obtained from the reaction of 1,6-diisocyanatohexane and 1,4-butanediol[2,3]. Later on, scientist succeeded to obtain processable PU elastomers, foams, adhesives and coatings during the Worl War II. Afterward, Schlack reported the first water-based polyurethane in 1942. By the 1970's, Dietrich et al. developed segmented PU ionomers with high industrial importance. In the course of time, Du Pont's Lycra product became one of the most famous polyurethane products. Since then, as described in Figure 2, the journey of polyurethanes continues in numerous applications with an increasing global market size [3].

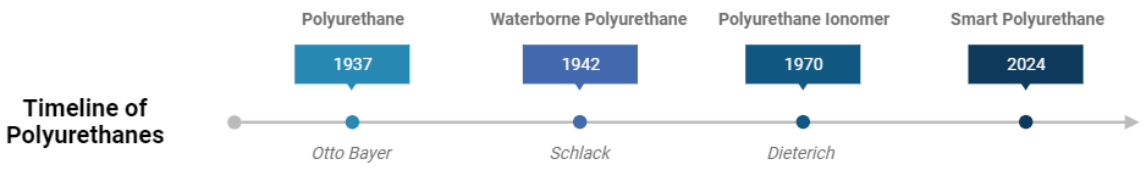

Figure 2: Evolution of Polyurethanes

The U.S. polyurethane market, measured by product size from 2020 to 2030 in USD million, has shown a steady growth trend. Starting at $12.4 million in 2020, the market experienced a slight increase to $12.7 million in 2021. From 2022 onwards, the market size continued to expand, reaching its peak in 2030. The market is segmented into various products, including rigid foam, flexible foam, coatings, elastomers, adhesives and sealants, and others. Throughout the forecast period, rigid foam and flexible foam maintained significant portions of the market share, with notable contributions from coatings, elastomers, and adhesives and sealants.

In 2022, the global polyurethane market was diversified across several end-use segments. The largest share was held by the construction sector, indicating the extensive use of polyurethane in building materials and insulation. Following construction, the furniture and interior industry constituted a significant portion of the market, driven by the demand for comfortable and durable furniture materials. The automotive industry also held a notable share, reflecting polyurethane's role in manufacturing car seats, interiors, and components. The electronics and appliances sector, packaging, footwear, and others comprised smaller but important segments, highlighting polyurethane's versatility and wide range of applications.

2.2. Polyurethane Chemistry

Polyurethane (PU) is a class of synthetic polymers bonded by carbamate (urethane) linkages. Since their discovery, polyurethanes have been serving in many forms such as foams, adhesives, sealants, and coatings. The building and construction sector (insulator and flame retarders), automotive industry, biomaterial technologies, textile and sizing industries, flooring and packaging applications essentially profit from versatility of polyurethanes[4].

A typical polyurethane, Figure 3, is obtained from the reaction of isocyanate and polyol with at least two functionalities, via step-growth (addition) polymerization. Furthermore, the molecular weight of PU structure can be increased by low molecular weight aliphatic diol/triol or diamine/triamine terminated chain extenders. Based on this diversity of raw

materials, polyurethane materials exhibit a segmental structure as block copolymers, which ensures the tunability of physico-chemical properties[5].

Hard segment is formed by the reaction of isocyanates with low molecular weight, alcohol or amine terminated chain extenders. The hard segment represents a polar segment and mainly responsible for the mechanical properties of the resulting material [6,7]. On the other hand, the soft segment is constituted by non-polar, high molecular weight polyols. Usually more than 60% (weight) of the PU chain is formed from the soft segment having control on the molecular mobility, crystallinity, solvent resistance, thermal stability, and phase separation[8].

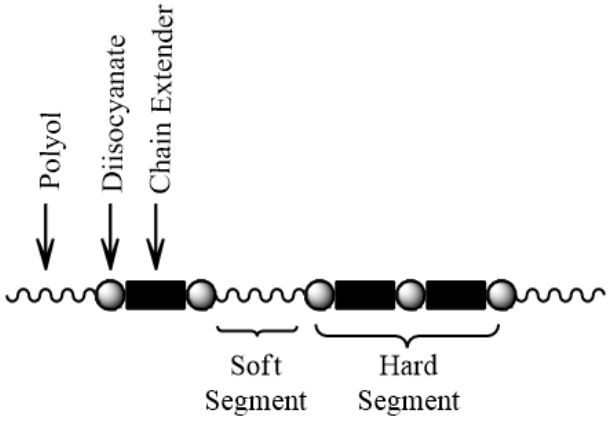

Figure 3: Polyurethane Structure

2.2.1. Diisocyanates

Diisocyanate monomers play crucial role in determining the physico-chemical properties of PUs since they are the main constituent of the hard segment. Depending on the type and structure of the diisocyanate preferred, the reaction temperature, reaction rate, catalyst need is altered together with the final mechanical properties. It has been reported that two main types of diisocyanates are being used in the PU production, i.e. aliphatic diisocyanates and aromatic diisocyanates[9].

Aliphatic diisocyanates are often used for higher thermal stability and high-performance needed applications. Aliphatic isocyanates that are attached to sp3 carbon atoms possess a prolonged lifetime and yellowing stability against UV exposure in comparison to aromatic isocyanates. The most utilized aliphatic diisocyanates are HDI, IPDI and H_{12}MDI. Aliphatic isocyanates are also compatible with additives such as pigments and stabilizers[10–12].

Aromatic diisocyanates are preferred for their lower cost, however, their higher volatility toxicity and photo-oxidative (yellowing) issues shrink their application window. Their inherent properties direct their application area toward rigid and thermoset materials. Their low stability against UV light also limits their outdoor application[13].

Activity of the isocyanate group, –N=C=O, is very high due to the presence of two cumulated double bonds.

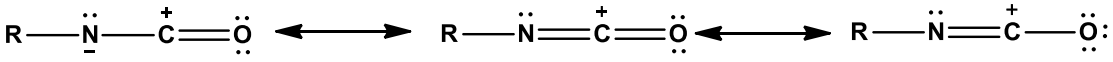

Figure 4: Resonance Structure of PU unit

The resonance structure of the isocyanate is vital for the polyurethane reaction. As seen in Figure 4, the negative partial charges are generated at either nitrogen or oxygen atom due to the electronegativity difference and it makes the positively charged carbon center susceptible to nucleophile attacks with active hydrogen (i.e., R-OH). The isocyanate reactivity can be boosted with an electron-withdrawing R group, such as an aromatic group. This is the reason why aromatic diisocyanates such as methylene diphenyl diisocyanate and TDI are used in the industry.

On the other hand, depending on the type and nature of the diisocyanate used (aromatic or aliphatic) higher reaction temperatures and/or various catalysts are needed to promote urethane formation reactions at a reasonable rate.

Another important point about the isocyanates is their biuret formation. When isocyanate and water get in touch with each other, water hydrolyzes the isocyanate group very quickly. For this reason, it is essential to store the isocyanate containers at moisture-free conditions[14].

2.2.2. Polyols

Polyols, also referred to as macrodiols, typically possess multiple hydroxyl (-OH) groups. The selection of these polyols plays a crucial role in regulating factors such as crystallinity, phase separation, and the elastomeric properties of the resulting polyurethane. On the other hand, isocyanates are introduced into synthesis by using compounds that contain hydroxyl groups due to their high reactivity, although this reaction tends to be slow at room temperature. This slow rate can be attributed to the phase incompatibility between the polar and less dense polyol phase and the relatively non-polar and denser isocyanate phase. Consequently, the incorporation of suitable surfactants and catalysts can be needed to facilitate this reaction. The most commonly employed types of polyols include polyether, polyester, and polycarbonate macrodiols (Figure 5)[15].

Polyether polyols offer flexibility, hydrolytic stability with reduced viscosity and cost. However, their contribution in oxidative stability, and mechanical strength is not significant[16]. Polyester polyols make a difference with their capability of making stronger hydrogen bonds between hard and soft segment which leads to increased intermolecular forces. Thus, enhanced intermolecular forces give rise to lower phase separation, higher thermal stability, and flame resistance together with good mechanical properties. The disadvantageous sides of polyester polyols are their higher price and high viscosity. On the other hand, the ester group make them highly sensitive to hydrolysis attack. From the thermal stability point of view, ester-based polyols are found to be more stable than ether-based ones due to the additional hydrogen bonding[17,18]. Polycarbonate polyols give rise to excellent resistance to organic solvents, high hydrolytic stability, good elastomeric properties at low temperature, and good weathering together with fungi resistance [19].

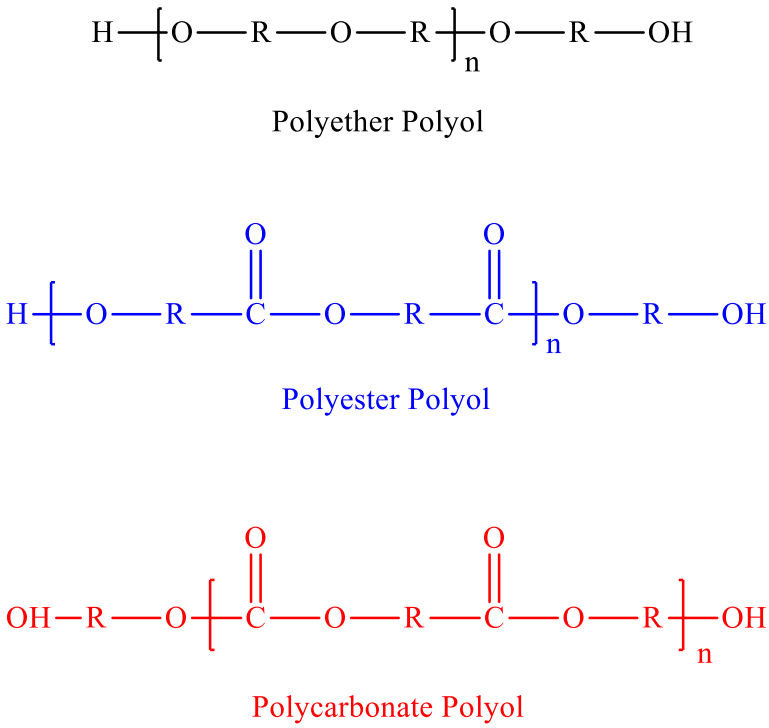

Figure 5: Polyol Structures

The fact that the reaction between a diisocyanate and a diol follows second-order kinetics is well-documented. However, as the polymerization process progresses and the concentration of urethane groups increases, there is a secondary reaction where isocyanate groups may also initiate reactions with NH groups within the polyurethane linkages. This leads to the creation of allophanate and biuret groups. Consequently, this deviation from second-order kinetics results in higher order reaction kinetics. Furthermore, additional reactions involving the NH groups found in the allophanate linkages with isocyanate functionalities eventually lead to gelation and the development of a covalently crosslinked network. It is evident that these side reactions, which lead to branching or crosslinking, have a significant impact on the structure and overall properties of the resulting polyurethanes[20].

Besides, as renewable biomass resources, vegetable oils and biodiesel-derived crude glycerol have garnered increased attention in recent years due to their low cost, potential biodegradability, and functional diversity. Vegetable oil-based polyurethane (PU) films have

demonstrated thermal and mechanical properties that are comparable or superior to those of petroleum-based polyols [21–23].

2.2.3. Chain Extenders

Polyurethanes are originally hydrophobic structures and require emulsifiers to disperse them in water. Using internal emulsifiers such as ionic groups including carboxylate, sulfonate or quaternary ammonium salt, or non-ionic groups within the polymer is more advantageous than using external emulsifiers. The incorporation of internal emulsifiers imparts waterborne polyurethanes with environmentally friendly characteristics, such as flexibility, good strength, and abrasion resistance.

Chain extenders are low molecular weight, difunctional compounds such as glycols and diamines and incorporated with the role of introducing rigid domains in the polymeric structure. They are generally used to increase the molecular weight by reaction with the terminal NCO end groups therefore, they form part of the hard segment[24,25].

The addition reactions of alcohols and amines with isocyanates lead to the formation of urethane and urea linkages respectively, as shown in Figure 6. Since amines are much more nucleophilic than the hydroxyl groups, urea formation reactions take place almost instantaneously at room temperature.

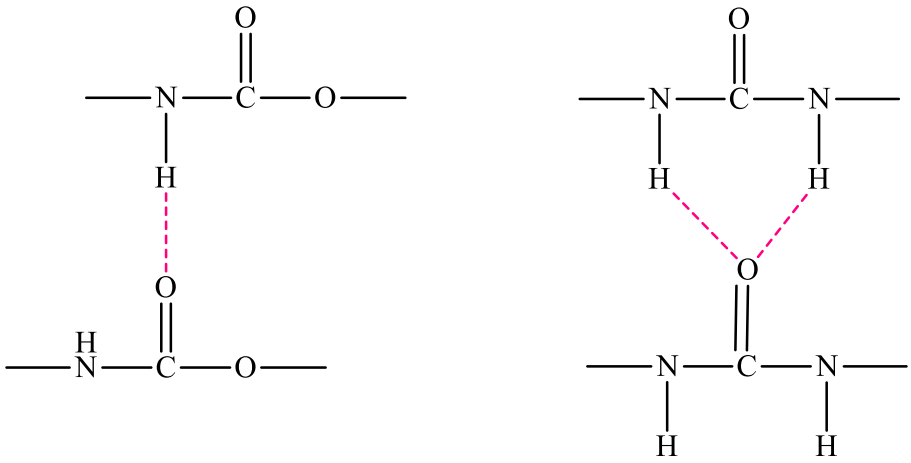

Figure 6: Hydrogen bonding in urea and urethane.

Dimethylolpropionic acid (DMPA) is an internal emulsifier commonly used as a hydrophilic chain extender in the synthesis of anionic waterborne polyurethane dispersions (WPUDs). However, DMPA has some drawbacks, such as a high melting point and low solubility, which necessitate the heavy use of solvents. Therefore, there has been significant interest in developing liquefiable emulsifiers with reactivity compatible with polyols.

It is also essential to determine the concentration of the NCO group and use the appropriate amount of chain extender to ensure an equimolar reaction between the two components. An excess of chain extenders can lead to poor chain extension efficiency and a subsequent deterioration of the mechanical properties of the polyurethane dispersion. Additionally, understanding where the chain extension reaction occurs, whether on the particle surface or inside the particle is crucial for comprehending the reaction mechanism and controlling particle morphology[26].

Grzelak et al. have detailly showed that the length of the chain extender significantly impacts formulations made with hexamethylene diisocyanate, leading to increased phase separation and haze as the chain length increases. Diethylene glycol, however, was found to enhance phase mixing in hexamethylene diisocyanate-based materials. In contrast, the influence of chain extenders on isophorone diisocyanate-based materials was found to be minimal [27].

2.2.4. Catalyst

The kinetics of step-growth polyaddition between diisocyanates and polyols is especially important for commercial production of linear polyurethanes. Catalysts enhance the reactivity between polyols and isocyanates and allow the reaction to take place at mild conditions. Basically, the catalysts act on polarization of either the isocyanate or hydroxyl compound through polar interactions. Alcohol, amine, water structures contain unstable hydrogen atoms and the catalytic activity of isocyanates with these chemicals can be catalyzed by tertiary amines or organometallic compounds. For instance, the organometallic tin catalysts mainly conduct the gelling reaction, although the amine catalysts exhibit a more varied range of blow/gel balance [28].

1,4-diazabicyclo-[2.2.2]-octane (DABCO) is the most used amine catalyst. Among the organometallic catalysts Sn, Pb and Fe containing complexes are predominant such as dibutyltindilaurate (DBTDL) and dibutyltindioctanate. Their chemical structures are shown in Figure 7. Less frequently used catalysts are the catalytic salts of Bi, Fe, Ti, Co, Cd and Zn [2].

Although the exact mechanism of the activation reaction is not fully established, Bloodworth and Davies proposed a route that is the most accepted mechanism to date. Their proposed mechanism includes the nitrogen from isocyanate coordinating with the organotin, forming the intermediate N-stannylurethane, which thenundergoes the alcoholysis. These catalysts are used in the liquid form in most cases, either in pure form or diluted solution, at ppm level [1] .

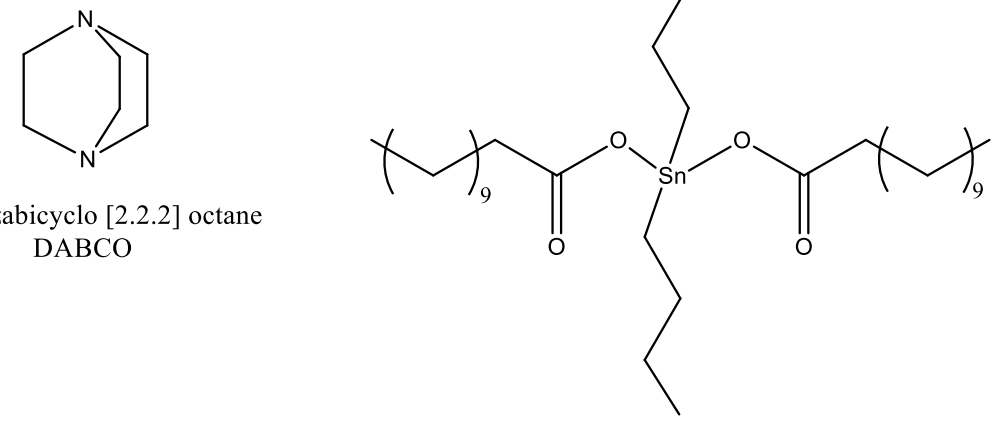

Figure 7: Catalysts used in PU reactions.

Other than the above-mentioned main components, polyurethane formulations can contain plasticizers, pigments, blowing agents, surfactants, fillers, stabilizers, anti-foaming agents and flame-retardants.

2.3. WPU Chemistry

Water-borne polyurethane (WPU) dispersion can be defined as a binary colloidal system in which PU particles are dispersed in a continuous aqueous medium where the hydrophilic-hydrophobic nature enables the formation of micelles (latex particles) resulting a milky-white appearing dispersion.

The physico-chemical properties of WPUs are mainly determined by their segmental structure and its chemistry just like solvent-borne PUs. They are essentially influenced by the size and cohesion of each segregated domain, segment length, the degree of phase separation, ionic content, hydrogen bond density and molecular weight [29].

2.3.1. WPU Ionomers

WPU polymer should contain ionic and/or nonionic hydrophilic segments in their structure to be dispersible in water. WPU ionomer is a copolymer that includes a PU backbone, with its repeat units carrying pendant acid groups that either completely or partially neutralized to create salts [30]. WPU ionomer micelles possess high surface energy, which aids in the formation of a film once the water evaporates therefore, dispersions are often kept for at least six months before being used. The longevity of these colloidal systems is impacted by their particle size distribution. A minimum level of ionic content is crucial for creating a stable polyurethane ionomer, depending on the type of ionic groups present.

The development of WPU ionomers resulted in two distinct types: anionomers, where PUs have pendant acid groups, and cationomers, where they have tertiary amine groups integrated into their backbones. Prior to dispersion, these groups are neutralized to create internal salts. Additionally, there are nonionic PUs available, which utilize nonionic stabilizing moieties. These ionic groups serve as an internal emulsifier and can take various forms, such as (i) cationic-like quaternary ammonium groups, (ii) anionic-like carboxylated or sulfonated groups, or (iii) nonionic groups, such as polyols with ethylene oxide end groups [31]. Herein, the placement of the ionic groups, the degree of ionization, the length of the spacer group between the polymer backbone and the ionic groups, and the choice of neutralizing agents are all crucial parameters on defining the properties of the ionomers.

Moreover, the method of incorporating ionic segments into the chain and the counterions kind determine PUI properties, including ability to form dispersions in polar solvents, e.g., in water or ionic conductance of formed coatings. This may be attributed to additional hydrogen bounds and electrostatic interactions offered by the ionic groups.

The other parameters such as the stoichiometry of the reaction, process conditions, process temperature and time, presence and amount of the polyaddition catalyst are responsible for the formation of biuret groups, allophanate ones, carbodiimide or azaheterocyclic isocyanurate structures, or oxazolidone ones. In anionomers, the most frequently used ionic segment is produced with DMPA, while in cationomers, MDEA is the most efficient choice [32].

2.3.1.1. Anionomers

Polyurethane anionomers can be classified as linear polyurethanes which contain a small number of acidic functional groups like COO^- or HSO_3 within their chains. Anionomers, in particular, have been extensively researched and can be easily synthesized by condensing non-ionic diisocyanates with conventional polyols and anionic chain extenders, often using DMPA [33]

DMPA is the primary choice among ionic diols due to its cost-effectiveness and excellent reactivity with various PU prepolymers that have free isocyanate groups. DMPA, being an inexpensive reagent, proves to be highly effective in solubilizing polyurethanes in polar solvents, especially water, even with just a small amount of this short anionic diol. This synthetic approach also contributes to environmental sustainability by eliminating the need for polluting solvents, resulting in more eco-friendly materials and biocompatible polyurethanes. Consequently, the resulting waterborne polyurethane (WPU) anionomers exhibit significant polarity, enhancing their solubility in water compared to insoluble non-ionic polyurethanes. They also demonstrate improved solubility in polar organic solvents such as N,N-dimethylacetamide, dimethylformamide, and acetonitrile dimethylsulfoxide. Additionally, their higher propensity to form hydrogen bonds, compared to non-ionic PUs, further contributes to their unique properties [34].

In water-based polyurethane dispersion, increased hydrophilicity typically leads to smaller particle sizes. It is reasonable to presume that anionic centers, being naturally hydrophilic, are predominantly situated on the surfaces of polyurethane particles within the continuous aqueous phase.

2.3.1.3. Zwitterionimers

Zwitterionomers are a class of polymers characterized by the presence of both positive and negative charges distributed among various atoms, resulting in an overall neutral charge for the molecule. The process for synthesizing zwitterionomers closely resembles that used for cationomers. Zwitterionomers are typically produced by quaternizing N-alkyldiols using sultones and lactones, which results in the formation of these unique polymer structures.

2.3.1.4. Cationomer

Polyurethane cationomers are primarily synthesized through the reaction of isocyanate-capped prepolymers and low-molecular-weight tertiary amines containing hydroxyl groups in their structures. The suitable ion is obtained by neutralizing the amine with acid, such as acetic acid or formic acid in most cases, or by forming an ammonium salt through reactions with substances like dimethyl sulfate, alkyl chlorides, benzyl chloride, or even other polymers containing chlorine atoms. Moreover, polyurethane cationomers can be produced through the reaction of diisocyanates with nitrogen-containing alkyl diols or sulfur-containing diols. The ionic groups are obtained through quarternization of nitrogen atoms or ternization of sulfur atoms. The typical cationomers typically contain 0.1–1.2% of NHR-3 groups. In cationomers, it is found to be MDEA is the most efficient ionic group. These cationic groups enhance the crystallizability of the samples and increase cohesion between the hard segments via Coulombic forces. As a result, polyurethane cationomers exhibit superior adhesion to polar surfaces.

Moreover, these cationomers can form stable aqueous dispersions with an acidic reaction, eliminating the need for emulsifiers. This property is one of the most important characteristics of polyurethane cationomers. Additionally, if substrates contain more than two functional groups, the option to create branched and cross-linked structures becomes available.

In summary, polyurethane cationomers offer a wide range of possibilities for modification and application due to their unique chemical properties. This versatile approach allows for

the modification of the polarity of polyurethane cationomers. Regardless, the route remains open for structural modifications, typical for polyurethanes, involving various polyols and diisocyanates.

2.4. Waterborne Polyurethane Synthesis

Polyurethane ionomers (PUIs) possess a valuable characteristic in their ability to be synthesized either in bulk or within a solvent. One significant advantage of these polymers is their remarkable solubility or dispersibility in polar solvents, particularly in water.

The most well-known processes for synthesizing waterborne polyurethane (WPU) dispersions are the prepolymer blending process and the acetone process. These methods play a pivotal role in industrial applications. Among these methods, the acetone process is widely utilized for producing a large variety of products. Following the prepolymer process for creating PU dispersions, the acetone process is the most extensively adopted method.

2.4.1. Acetone Process

The acetone process was formerly patented by Bayer and consists of a two-step procedure. It starts with the synthesis of a pre-polymer in bulk through a reaction between polyol and isocyanate. This is followed by the addition of acetone to control viscosity followed with a chain extension step in a homogeneous medium, which occurs prior to the phase inversion step. Phase inversion is initiated by the vigorous stirring and addition of water to the synthesized polymer in acetone. In the acetone process, dispersion particles are formed early in the inversion step as the addition of water causes the polyurethane polymer to phase separate from the acetone-water mixture. The final step involves the extraction of the organic solvent. This process offers precise control over molecular weight, particle size, and distribution, ensuring high reproducibility, as polymer synthesis occurs in a homogeneous

solution. Notably, the use of acetone dilution alleviates viscosity constraints and allows for its recovery for reintroduction into the system. Following the dispersion step, acetone is removed through distillation, resulting in a product with either very low volatile organic compound (VOC) content or being entirely VOC-free[35].

Herein, acetone is the preferred and commonly used solvent for this process and mainly used as a solvent during the dispersion process to control the viscosity and emulsion particle size. Importantly, the low boiling point of acetone facilitates its easy removal, resulting in a product with minimal or no VOCs. In modified processes, methyl ethyl ketone can be a suitable alternative or acetone can be replaced by a portion of the NMP (N-methyl-2-pyrrolidone) in the PU dispersion, resulting in dispersions containing very low levels of volatile organic compounds (VOCs). By carefully controlling the conditions of the acetone process, stable dispersions can be achieved through low-energy emulsification methods. However, the use of significant quantities of acetone and the need for an extra distillation step can be economically undesirable. These factors may result in reduced batch yields and higher energy consumption[36].

In the industrial context, a significant number of products are manufactured using the acetone process. Among the various methods available for preparing PU dispersions, the acetone process stands out as one of the most commonly employed. In recent times, there has been a growing interest among researchers in studying and optimizing the acetone process. Notably, while the pre-polymer mixing method finds utility in the coating industry, the acetone process is often preferred for applications in the adhesive industry.

2.4.2. Prepolymer Process

The pre-polymer mixing method involves chain extension taking place in a heterogeneous phase, where a hydrophilic isocyanate-terminated pre-polymer is dispersed in water. Pre-polymer is created by reacting the appropriate amounts of diols, including polyether or polyester, with a molar excess of di-isocyanates. Typically, pre-polymers made from cycloaliphatic di-isocyanates are used due to their low reactivity with water. Ionic centers are

introduced into the reaction mixture as an internal emulsifier. After the chain extension step, the mixture is dispersed in water. To reduce the viscosity of the mixture, typically around 10-15 wt% of the organic solvent N-methyl-2-pyrrolidone (NMP) is used. In order to successfully apply this method, the dispersion step must be completed quickly, and at a temperature below the critical point where the NCO groups begin reacting with water. It is crucial to carefully control the functionality and viscosity of the mixture during this process.

2.4.3. Hot-Melt Process

The hot-melt method offers a solvent-free approach for synthesizing waterborne polyurethanes and is utilized to produce waterborne polyurethanes with a certain degree of branching and low molecular weight products. It involves the reaction of an isocyanate-terminated pre-polymer with urea to create biuret groups. Essentially, this process caps the pre-polymer with urea to obtain biuret functionality. Subsequently, this pre-polymer is dispersed in water and reacts with formaldehyde, leading to a condensation reaction and the formation of polyurethane-urea structures. In this method, controlling the formaldehyde reaction can be challenging, and side reactions involving urethane groups in the polyurethane may also occur. They can be easily dispersed in water without the need for any organic co-solvent. Consequently, this process yields waterborne polyurethanes with different polymer properties compared to the acetone process and yet, not particularly suitable to produce surface coatings.

2.4.4. Ketamine-Ketazine Process

The ketamine-ketazine process can be considered as a variation of the pre-polymer mixing method. In this process, the pre-polymer is mixed with a blocked amine or a blocked hydrazine before it comes into contact with water. Diamines, which are masked with ketones to form ketimines, can be blended with NCO pre-polymer without undergoing a reaction. In

this step, the mixture is then combined with water to create a dispersion. Subsequently, the ketimine hydrolyzes into an amine, facilitating chain extension.

In the ketazine process, in which the NCO pre-polymer reacts with a ketazine, aldazine, or hydrazone before dispersion, goes a step further. Here, hydrazine is released upon contact with water, leading to chain extension. The hydrolysis of ketazines occurs more slowly compared to ketimines. Consequently, this process is suitable for producing NCO-terminated pre-polymers from aromatic isocyanates.

Consequently, dispersion prepared using these processes results in high-performance coatings that approach the quality of waterborne polyurethanes synthesized by the acetone process.

2.5. Review on the Waterborne Polyurethanes

Polyurethanes are widely used high-performance materials in everyday life. Conventional polyurethanes are typically produced with solvent assistance such as DMF, chloroform, THF or NMP. However, due to increasing public health concerns, global warming and environmental pollution, utilization of such harsh chemicals are being restricted. New legislations all around the world limit the volatile organic compound (VOC) levels and direct the industry toward water-based systems. Hence, the replacement of solvent based polyurethanes with their waterborne analogs is inevitable. The waterborne polyurethanes (WPUs) basically have a very low level of VOC level and exhibit an environmentally friendly character. For this reason, they have been closely investigated by both academia and industry.

Besides the non-toxicity, WPUs have many advantages over their solvent based counterparts. WPUs can reach high molecular weight at low viscosity, they exhibit high flexibility, high strength at low temperature, good adhesion and rheological characteristics in the absence of external emulsifier.

WPUs are being actively used in many applications such as finishing material in textile coating, self-healing coating, antifouling, 3D-printer inks, indoor and outdoor paints, wood

coating, anticorrosive coatings, drug release matrix, antimicrobial surface coating, phase change materials, photothermal coatings, fluorescent coatings, UV-curable, shape memory polyurethanes.

Moreover, polyurethane structure is compatible with numerous nanoparticles. Therefore, WPU-nanoparticle nanocomposite applications are widely used to boost the thermal and mechanical properties, chemical stability, biocompatibility, 3D-printabality, and antimicrobial aspects. WPU nanocomposites generally contains carbon nano-tubes, halloysite nano-tubes- graphene, TiO2, SiO2, ZnO, etc[37].

Kolgesiz et al., have focused on developing waterborne polyurethane (WPU) foams as a carrier matrix for halloysite nanotubes (HNTs) to create environmentally friendly packaging materials. The WPU, engineered with ionic and hydrophilic properties, was used to form porous scaffolds that incorporated HNTs. These WPU-HNT nanocomposite foams were designed to enhance the shelf life of fresh fruits by absorbing moisture and ethylene. The process involved mixing WPU dispersion with surfactants, foaming agents, and thickeners, followed by adding HNTs at various concentrations, as shown in Figure 8. The resulting foams were flexible, light, and effective in extending the shelf life of tomatoes and bananas. Given the non-toxic nature of HNTs and the FDA approval of PU resins for food contact, WPU-HNT foams show strong potential as safe, ripening-retarding packaging materials to reduce food loss during transportation and storage [38].

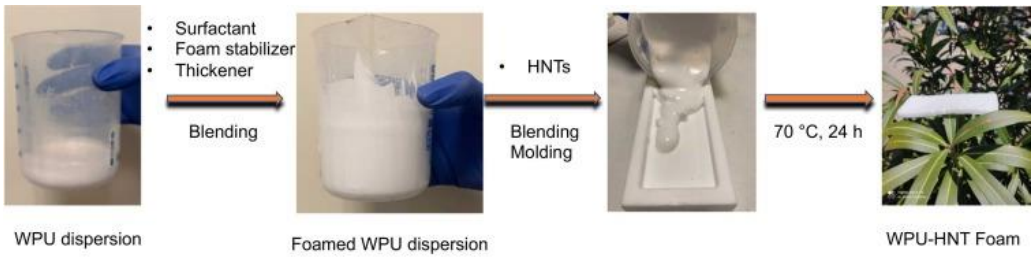

Figure 8: WPU foam preparation

Tas et al. have prepared novel polydopamine-polyurethane (PDAPU) particles by coating polydopamine (PDA) on WPU micelle surface in a dispersion state, through an effective, one-pot method. The successful coating approach was monitored by cryo-TEM and seen that the particle size increased by about 60 nm (Figure 9). The resulting PDAPU films were pointed out with the environmentally friendly nature of the WPU in addition to the highly efficient photothermal conversion upon irradiation with either solar light or NIR laser. It was seen that the PDAPU films could reach 105.8 °C when irradiated with solar light at 3 sun for 20 min and only 5 min of NIR laser light at 800 mW/cm^2 was enough to raise the local temperature from room temperature to 138.6 °C. Consequently, a remarkable potential application area such as a solar-driven water evaporation container, demonstrating a high water-evaporation capacity of the PDAPU films arising from its photothermal effect [39].

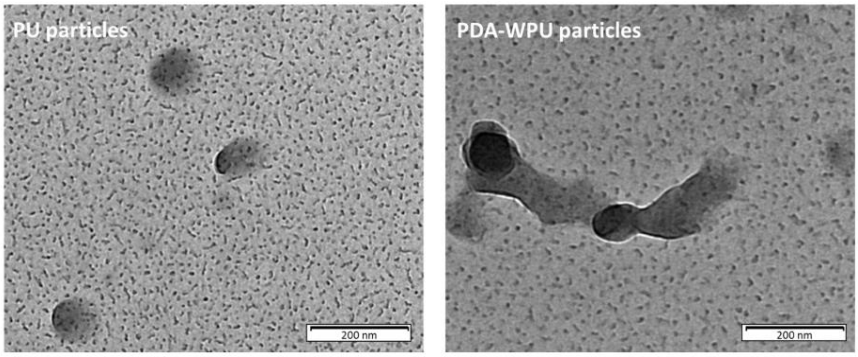

Figure 9: WPU latex structures.

Recently, Wang et al. reported an interesting study on the incorporation of boron-containing dye (BCD), a single boron containing chromophore, as chain extender to polyurethane. BCD is able to switch its emission color according to its aggregation state and it was incorporated to achieve a full-color emitting structure. The procedure is represented in Figure 10. Herein, polyurethane was chosen due to its versatile segmental structure. In this scope, PUs was synthesized from PEG soft segment (at different molecular weights), toluene diisocyanate (TDI) as hard segment, and the mixture of 1,4- butanediol and BCD as chain extender. The high amount of hydrogen bonds in the matrix, originating from the urethane linkages, was helping to the stabilization of BCD's tricoordinate state, influencing the emission color. On the other side, the phase separation between the hard and soft segment was an important

factor where the BCD moieties were separated from the PEG soft segment, thus, the interchain aggregation could be minimized. The small domain sizes provided an homogeneous distribution as well. The detailed studies also revealed that the composition and molecular weights of components were not affecting the emission color of FPU; the emission color was dictated by the density of BCD moieties in hard-segment domains and the emission color could be varied from blue to red by simply increasing the content of chromophore (under UV irradiation at 400 nm) [40].

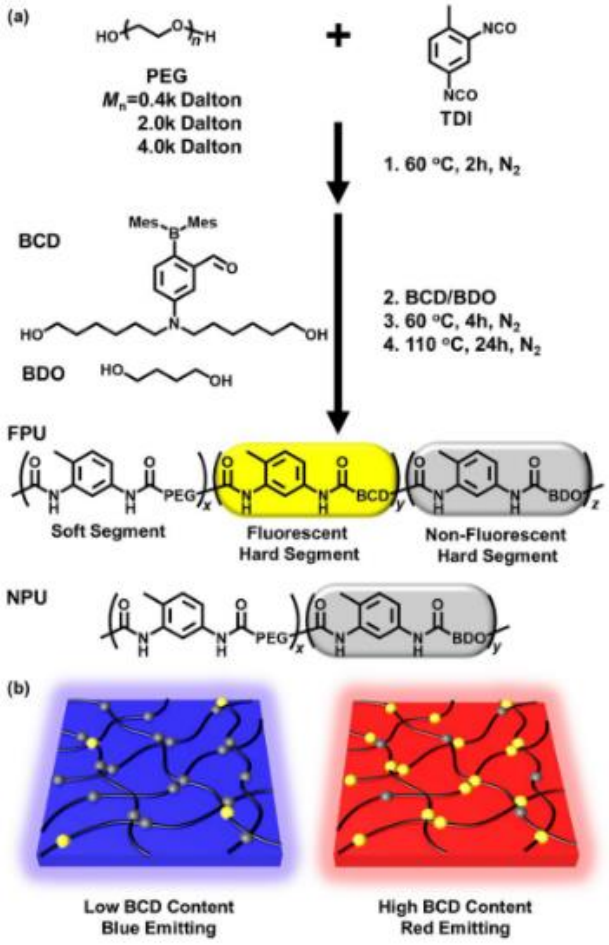

Figure 10: Fluorescent WPU structure.

Shape memory materials can “remember” their original shape and regain the initial shape from temporary shape in response to external stimulus. In shape memory polyurethanes, the key factor is found to be the thermodynamic incompatibility of hard and soft segments [41].

Recently, Yang et al. have successfully prepared biodegradable shape memory polyurethanes (SMPUs) from HDI, PCL diol and PHP chain extender, furthermore, introduced oxidized carbon black (OCB) to provide photothermal activity against NIR, as well as to reduce the transition temperature below the physiological temperature. The PHP chain extender had two chymotrypsin cleavage sites providing degradability by chymotrypsin, offering a great potential for the intestinal stand application. On the other side, carbon black particles were oxidized to enhance the dispersibility in SMPU and the introduction of OCB increased the phase separation degree besides the photothermal activity. With NIR laser exposure (808 nm, 1.2 W), the films unfold and after 20s, the initial shape was almost 100% recovered [42].

Zhang et al., prepared the first UV-Vis-NIR photochemically responsive shape-memory polymer composites that show successful biomimetic finger bendings upon light irradiation on different regions. The polyurethane matrix having originally shape-memory property was mixed with azobenzene compound 4-cyano-4′-pentyloxyazobenzene having the trans-cis photoswitching property upon UV-Vis irradiation and upconversion dopants which convert 808 nm NIR light into green fluorescence by continuous photon absorption[43]

CHAPTER 3: INTRINSICALLY SELF-HEALING WATERBORNE POLYURETHANES

3.1. Abstract

Nowadays, one of the most pressing global challenges is the excessive waste materials generated from the consumables. Self-healing materials offer a significant opportunity addressing this issue as they can enhance material durability, prolong its lifespan, and consequently reduce both costs and waste generation. Intrinsically self-healing materials, in particular, are highly demanded because they don't require additional healing agent or capsulation process. Among various types of materials, polyurethanes have emerged as a promising class due to their versatile chemistry, segmented structure, and adjustable bond composition.

Herein, our research focuses on the development of environmentally friendly waterborne polyurethane (WPU) dispersions synthesized using an acetone method from aliphatic diisocyanate and polyester polyols. The effects of the polyol type, hard segment content, chain extension, ionic group as well as ionic concentration on the synthesis, structure, and properties of the resulting self-healing waterborne polyurethane dispersions and cast films have been extensively investigated, providing promising results for the development of environmentally friendly, intrinsically self-healing coatings.

These WPU dispersions bear anionic groups on their backbone, and their intrinsic self-healing properties result from the cooperative effects of ionic interactions and H-bonding, types of non-covalent interactions, as presented in Figure 11. The WPU latexes were characterized using dynamic light scattering (DLS), and the resulting films underwent

structural, thermal, and mechanical analyses through techniques like FT-IR, TGA, DSC, and tensile tests. This study demonstrated that the resulting films exhibit exceptional self-healing capabilities at room or elevated temperatures, making them highly suitable for a wide range of applications, including next-generation smart protective coatings and adhesives.

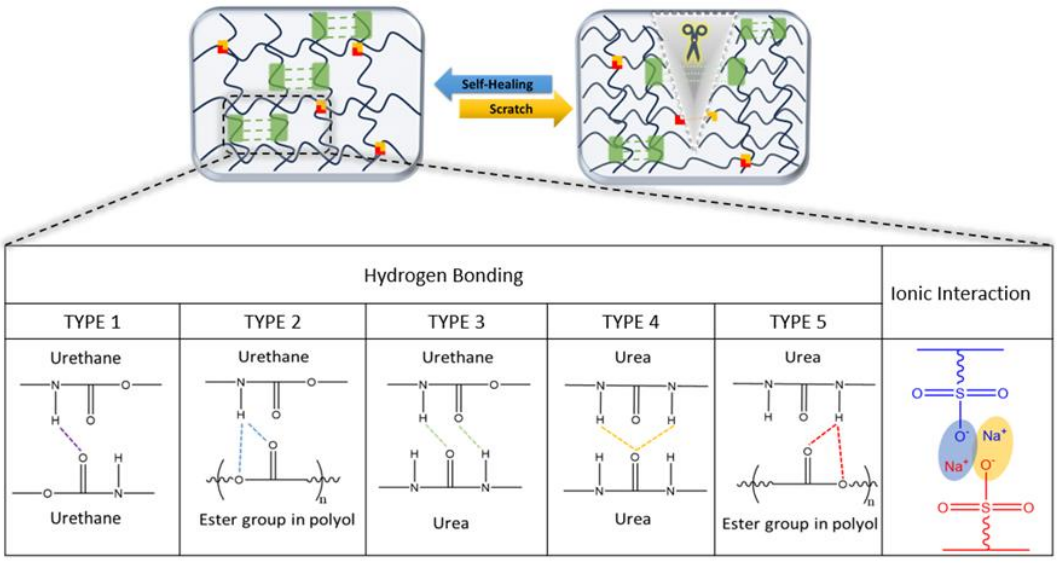

Figure 11: Self-Healing WPU Design via Non-covalent Interactions

3.2. Introduction

3.2.1. Self-Healing Materials

Natural tissues such as skin or muscles, have the fascinating ability to heal themselves spontaneously upon injuries, which plays a crucial role in the survival of the living beings[44]. Mimicking this splendid ability of living organisms to heal wounds and restore their integrity, there is a significant emphasis on the development of smart materials with self-healing capabilities in both academic research and industrial applications[45]. Basically, instead of traditional approaches to repair polymeric materials such as welding, patching, and gluing, or buying a new product, self- healing materials offer enhanced longevity, durability, and

safety[46]. Therefore, significant environmental and economic benefits can be achieved due to the enhanced durability and sustainability. Eventually, self-healing is an emerging concept in a huge scope, including construction materials, polymeric materials, hydrogels, nanocomposites and composites, on which both academia and industry has been focused[47,48]. According to the self-healing coating market report, the self-healing coatings industry is projected to experience robust growth due to the widespread adoption of self-healing coatings, with an estimated 35% increase in the period from 2021 to 2028, ultimately reaching a market value of approximately USD 45.93 million by 2028[49].

In polymeric materials, the most common type of damage is found to be mechanical damage upon scratching, cracking, puncture, delamination and so on. Aforementioned mechanical damage of polymer networks will lead to chain cleavage and/or slippage, and subsequent formation of reactive groups which may or may not proceed conformational changes in a wound area[48,49]. The reactivity of these groups determines if these entities are able to react with the surroundings to form more stable oxidative products or will autonomously reassemble to repair damaged area. Thus, the stability of reactive groups resulting from localized chain cleavage will be one of the key features for repairs. At the same time, cleaved and/or displaced macromolecular segments will experience segmental rearrangements resulting in conformational changes or diffusion leading to macroscopic network rearrangements. In particular, Wool and O'Connor discussed the self-healing mechanism and suggested a five stage-model to explain the crack healing process constituted of surface rearrangement, surface approach, wetting, diffusion and randomization[50]. Ultimately, they proposed that diffusion step plays a critical role in determining the ultimate self-healing performance. The research carried out by Wool et al. also confirmed that the phenomena of crack healing in the thermoplastics occur most effectively at or above the Tg of these materials [51].

Accordingly, since typical self-healing process involves molecular diffusion, contact with damaged surfaces, followed by the rupture and reformation of dynamic bonds or interactions, the contact of damaged surfaces appears as a crucial factor. The damage to the material often results in significant deformation or cracks within the deep part of the network, thereby hindering the effective re-establishment of dynamic connections due to the lack of proper

interface contact. Another important factor is the dimensions of the scratch, it is reported that self-healing is feasible for cracks with narrow widths (<50 μm), but not for those with larger sizes[52]. However, in real-world scenarios, the size of various damages is not controllable. Therefore, achieving the self-healing of wide scratches has also become a crucial aspect in the design and improvement of repair methods[53].

The self-healing phenomenon may occur via two fundamental strategies in polymer-based materials: i) Extrinsic Self-Healing Mechanism ii) Intrinsic Self-Healing Mechanism. Extrinsic systems benefit from physico-chemical approaches such as encapsulation of healing agents/reactive monomers and cardiovascular networks, while intrinsic systems heal the damage via dynamic covalent or non-covalent bonds. Moreover, to this classification, autonomous and non-autonomous systems are defined according to the absence or presence of an external trigger such as pH, temperature or moisture[54]. The extrinsic self-healing process incline toward commercialization, but it also faces certain limitations. Extrinsic mechanisms can cause some difficulties such as unrepeatability and improvised healing agent concentration during application. Once the capsule is cracked, healing agent is released to fill the crack by capillary force but, it is a one-time self-healing performance. On the other hand, the amount of capsule should be enough to fill the crack and they should be homogeneously distributed among the surface. Therefore, extrinsic systems don't represent the ideal self-healing mechanism in real-life applications[55,56].

In the intrinsic polymeric self-healing systems, from a chemical perspective, dynamic covalent bonds (disulfide bonds, cycloaddition reactions, Diels-Alder reactions, retro-Diels–Alder reactions, 2 + 2 cycloaddition, disulfide bond reshuffling reaction, diselenide bond reshuffling , boronic ester and non-covalent interactions (supramolecular interactions, host-guest chemistry, metal-ligand coordination, hydrogen bonds, ionic bonds and π - π stackings) are predominant[57]. Yet, due to the complex synthetic processes, toxicity of chemicals, high costs and sensitivity to external conditions of the dynamic covalent bonds, intrinsic non-covalent interactions are in demand. In this manner, recent studies endeavor to reveal the critical role of hydrogen bonds and ionic interactions for the self-healing mechanism[58].

3.2.2. Van der Waals Interactions in Self-Healing

Based on the IUPAC definition, a typical hydrogen bond can be represented as X–H and is described as an attractive interaction between a hydrogen atom from a molecule or molecular fragment X–H, where X is more electronegative than H, and an atom or group of atoms from the same or a different molecule, indicating the presence of bond formation [59]Hydrogen bonds, a kind of non-covalent interaction, have 10 times lower bonding energies than covalent bonds yet, play an important role in stabilizing the structure of polymers and conferring functionality to polymeric materials[60]. The current perspective considers hydrogen bonds as robust electrostatic interactions, with their strength approximately 40 kJ mol, according to IUPAC's definition. The nature and strength of hydrogen bond interactions depend significantly on the characteristics of the hydrogen bond donor (X) and acceptor (Y). Consequently, a diverse array of hydrogen bonds exists based on the specific atoms involved. Thanks to their relatively high strength and dynamic characteristics, including dissociation and reformation in response to external stimuli such as heat, pH, and light, hydrogen bond interactions have emerged as a critical driving force behind the self-healing properties of materials[61,62].

Even though with lower bonding energy compared to a covalent bond, the H-bond has a great influence on polymer viscoelastic properties, phase separation, and degree of crystallinity[63]. A limited number of H-bonds are not sufficient to exhibit all of the required properties such high mechanical properties. However, desired properties can be achieved by the fine-tuning degree of H-bonding interactions and rigidity in the polymer backbone. Even though hydrogen bonds lead to mechanically weak materials, the remarkable reversible nature of hydrogen bonds enhances the self-healing properties. At room temperature, multiple hydrogen bonds are saturated and directional, which gives rise to a potential crystallization and loss of self-healing efficiency[64–66]. On the other hand, ionomers step forth in recent self-healing strategies[67,68]. Polymers containing ionic groups have strong electrostatic interactions. Unlike hydrogen bonds, they are not in saturated and directional nature[69]. Generally, networks composed of supramolecular interactions take advantage of the ionic groups for self-healing behavior. Das et al. emphasized the key role of the ionic groups by

converting the commercially available rubber into highly elastic material with extraordinary self-healing properties via incorporation of reversible ionic associations[70].

3.2.3. Self-Healing Polyurethanes

Self-healing materials can be produced using several types of polymers and polymer composites[71]. Within this scope, polyurethanes stand out as particularly advantageous thanks to their segmental architecture[72]. This is because they have a soft phase that facilitates the mobility of polymer chains, which is essential for enabling the healing process. Moreover, they possess a hard phase that maintains the material's mechanical stability at the same time[73].

Waterborne polyurethanes (WPU), which are new generation environmentally friendly class of PUs, exhibit very promising self- healing behavior mainly due to their segmented structure that leads to microphase separation. A network composed of soft and hard domains distributed in the network has the capacity to reorganize itself in response to mechanical damage, enabling effective self-healing. This phenomenon is characterized by the movement of polymer chains within the material, allowing them to fill voids or occupy free volume areas. WPUs are known to be a very special class of elastomeric materials due to their environmentally friendly nature, low VOC level, versatile chemical structure with tunable hard and soft segments, and adjustable mechanical properties[37].

The polyurethane chemistry can be easily adjusted to boost the self-healing performance. While the mobility of soft segment is indispensable for a self-healing polyurethane, the hard segment and ionic group’s chemistries are also crucial. Polyurethanes can evolve into polyurethane(urea)s by the reaction of isocyanates with amines[74,75]. The incorporation of urea groups into the PU chain leads to significant improvements due to the formation of two kinds of groups in hard segments, i.e., urethane and urea, and establishment of additional hydrogen bonding. Fortunately, intermolecular hydrogen bonds can form between adjacent urethane groups, enhancing the self-healing capability of the material. While urethane groups establish singlet hydrogen bonding, bidentate linkages are formed between urea units. Moreover, the presence of hydrogen bonds between amine groups in urethane segments and

carbonyl groups further ensures efficient healing of fractures in these polyurethane materials. This additional bonding supports the self-healing process and improves the material's ability to restore its integrity after damage[76,77].

The integration of self-healing functionality with WPU presents significant advantages for restoring mechanical integrity[78]. Since the molecular structure of WPU is adaptable and customizable, the most straightforward approach is to incorporate self-healing functional groups into the main polymer chains[79]. Typically, these self-healing functional groups belong to the realm of reversible chemistry. When situated around microcracks, they have the capability to bind the crack surfaces through reversible reactions under appropriate conditions. While higher soft segment content may lead to a reduction in the density of hydrogen bonds, the interaction of sulphonate groups and the flexibility of the polymer chain are regarded as critical factors for enhancing healing efficiency[80]. Reversible hydrogen bonds offer a solid foundation for the recovery of micrometer-scale deformations, contributing to the self-healing effect. In contrast, ionic interactions are well-suited for nanoscale healing[81]. Therefore, polyurethanes are expected to exhibit superior healing performance with their combined use of both hydrogen bonds and ionic interactions.
In the WPU systems, self-healing behavior is often obtained either by nanocomposite synthesis[82–84], or dynamic covalent bonds such as disulfide or Diels-Alder[85]. Nevertheless, emerging studies incline to boost non-covalent interaction’s place in the self-healing systems due to the above explained reasons.

Recently, Rong et al. reported self-healable WPU with the synergistic reversible units of aliphatic disulfide bonds and quadruple hydrogen bonding with the help of ureidopyrimidone (UPy) functionalities[86].Peng et al. prepared a cationic WPU with tannic acid (TA) and reached successful self-healing at room temperature in one week, at 50^{o}C in 3 hours, under favour of the hydrogen bonds formed between TA and the rigid domains of WPU[66]. Xiao et al. emphasized the impact of ionic chain extender; the WPU bearing sulfonate groups had greater self-healing efficiency at 100 ^{o}C for 18 hours[81].

Although the above-mentioned strategies have unique advantages and disadvantages, the ultimate goal should be obtaining an intrinsic and autonomous self-healing system through a simple and cost-effective method at room temperature. Yet, it is still challenging to achieve

high performance WPU with remarkable self-healing efficiency at room conditions, without covalent bonds, supramolecular interactions or additional crosslinker. To the best of our knowledge, this report is a pioneer for intrinsic and autonomous self-healing of pure waterborne polyurethane chains at room temperature. To address this issue, we designed and synthesized novel, low T_g, waterborne polyurethane(urea)s (WPUU) combining the dual action of multiple H-bonds and ionic interactions for a WPU composition that originally had high mechanical properties. The self-healing property is acquired by taking advantage of the synergetic effect of H-bonds and ionic interactions through the interactions of carbonyl, urethane, urea groups and ionic sodium sulfonate groups in the presence of a low T_g polyester-based soft segment on the WPU chain backbone.

3.3. Materials and Methods

3.3.1. Chemicals

Hexamethylene diisocyanate (HDI) and DESMODUR 1652, polyol of adipic acid/diethylene glycol/butanediol/ethylene glycol (M_n=2000 g/mol) were acquired from Covestro AG. Sodium 2-[(2-aminoethyl)amino]ethanesulphonate (AEAS) was kindly donated by Evonik Industries. Ethylenediamine and acetone (99.5 %) were purchased from Sigma-Aldrich. Polyol was degassed under vacuum at 100 °C for 15 minutes before usage, other chemicals were used as received.

3.3.2. Characterization

Particle Size, Zeta Potential Analysis: Particle size (z-average diameter), size distribution (PDI) and the zeta potential of WPU latex were measured by dynamic light scatter (DLS) instrument (Zetasizer Nano - ZS, Malvern Instruments Ltd., UK) equipped with laser diffraction and polarized light detectors at three wavelengths. Dispersions were diluted with deionized water; refractive index of polyurethane is 1.50 and water is 1.30. Measurements were performed at room temperature; each measurement was made with three cycles per sample.

The surface hydrophilicity of WPUU films was analyzed by static drop shape analysis system (Kruss Drop Shape Analysis System DSA 10 Mk2) in the air, at 25 °C

A ThermoScientific Nicolet iS10 FT-IR spectroscope with an attenuated total reflection (ATR) system was used for the structural analysis of film samples, with 64 scans in the region of 4000 to 600 cm^{-1}.

Thermogravimetric analysis (TGA) of all samples was performed using a Netsch (TGA/DTA) instrument by heating film samples from room temperature up to 600 °C with a rate of 10 °C/min under N_2 atmosphere. Differential scanning calorimetry (DSC) was performed in the temperature range between -120 ºC and 150 ºC with a heating rate of 10 ºC/min by TA Instruments – MDSCQ2000. Reported T_g values were taken from the second heating cycle of the film samples.

Mechanical properties of the films were tested by a universal testing machine (UTM) Zwick Roell Z100, with a load cell of 200 N and a crosshead speed of 25 mm/min. Specimens were prepared according to ASTM D1708-10 standard. An average of at least three replicates was reported for each sample.

The self-healing process was investigated qualitatively based on the optical images taken by an upright polarizing microscope equipped with a digital camera. The field of view was 50× magnified.

The determination of molecular weight and polydispersity index of synthesized polyurethane samples was carried out by triple detection Viscotek GPCmax-VE 2001 instrument, with HPLC grade DMF containing 0.1M LiBr as the mobile phase., 0.5 ml/min flow rate at 45 ºC.

Surface morphology of the dry films were monitored by AFM at room temperature and ambient pressure, under tapping mode using Nanomagnetic Instruments device. Phase images were taken through the dried films cast on silicon wafer and captured at a magnification of 2x2 mm^2.

The thermo-mechanical analysis was performed via Mettler Toledo TMA/SDTA instrument, between 110 ºC to 200 ºC, with a heating rate of 10K/min, under N_2 atmosphere, under constant load of 0.025 N force applying. Quartz sensor was used.

The dynamic mechanical analysis were conducted with Mettler Toledo DMA instrument temperature ranging from -90 ºC to 100 ºC, The operation conditions were at a frequency of 1 Hz, 5 micrometer using titanium tension clamps.

3.3.3. Film Preparation

Films were prepared by casting the WPUU dispersions into Teflon molds. The dispersion slowly evaporated at room temperature overnight and gradually dried by heating at 70 °C for 2 h, 120 °C for 1 hour. Thereby, homogenous, bubble-free, transparent WPUU films (typical film thickness was ≈ 0.3 mm) were obtained. Consequent films were kept in desiccator to avoid moisture absorption and surface contamination.

3.3.4. Self-Healing Procedure of WPU films

For the self-healing experiments, scratches were made with a depth of ±75% of the thickness of the films using a digital blade micrometer, a standard scratch was monitored in Figure 12 by an original OM image. Scratched specimens were left to heal at room temperature (RT) and at 70 ºC for different time intervals without any external pressure. The healed samples were then immediately subjected to the tensile test using ZWICK universal testing machine, using the same test method as original samples. At least 3 specimens per combination were tested.

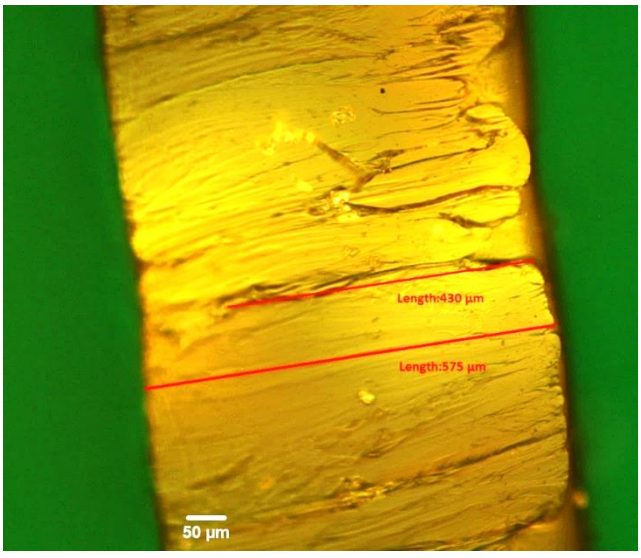

Figure 12: Cross- section of a scratched WPU film

3.4. Results and Discussion

3.4.1. Synthesis of WPU Dispersions

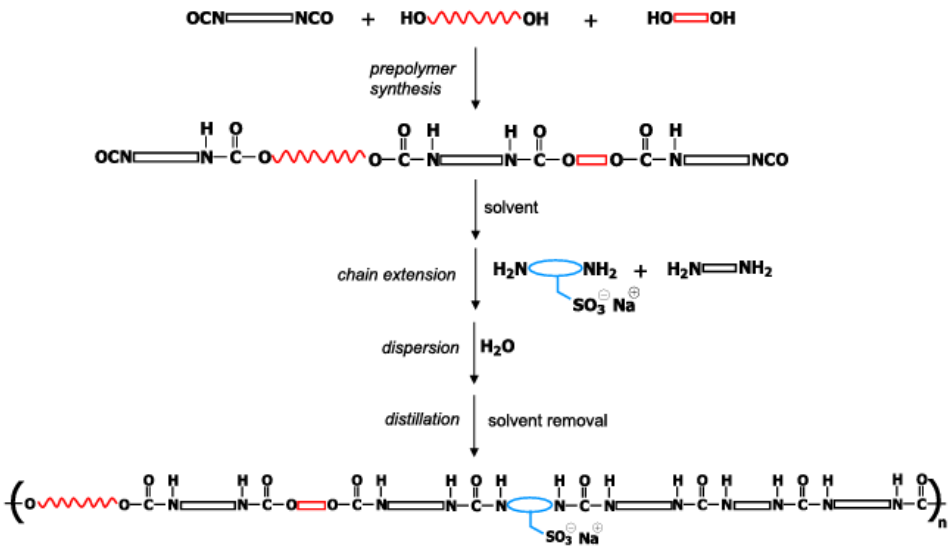

Figure 13: WPU synthesis by acetone method

Self-healing waterborne polyurethane dispersions were synthesized by acetone process, which is detailly discussed in the Introduction part. As described in Figure 13, in the first step, a four necked round-bottom flask is charged with the chosen polyol, equipped with a thermocouple, condenser, and mechanical stirrer. The polyol is degassed under high vacuum, at 100 ºC to remove the trace moisture captured. The diisocyanate is added to the polyol and reacted for the prepolymer formation at 80 ºC. The proceeding of the prepolymerization is precisely determined by the back titration method (ASTM D2572-97). Once the theoretical NCO% is reached, the isocyanate-terminated prepolymer is dissolved in acetone. For the chain extension reaction to take place, the aqueous chain extenders are slowly added into the prepolymer solution at 50 ºC. Typical diamine structures, including EDA, have limited solubilities in acetone. In addition, AEAS monomer, working as both chain extender and ionic source, is found in 50% aqueous solution form. Moreover, as a side reaction, although

they are more reactive towards hydroxyl or amino-groups, isocyanates react with water as well. Once the chain extension is performed, polyurethane chains are dispersed in distilled water under high-speed mechanical stirrring. Subsequently, the acetone removal process is realized via vacuum distillation. The WPU dispersion is vacuumed at 50 mbar, for 1 hour. Consequently, milky-white WPU dispersion is obtained, typically at a 30% solid content. In this chapter, 1,6- hexamethylene diisocyanate (HDI) was used as the single diisocyanate compound constructing the hard segment in all the following experiments.

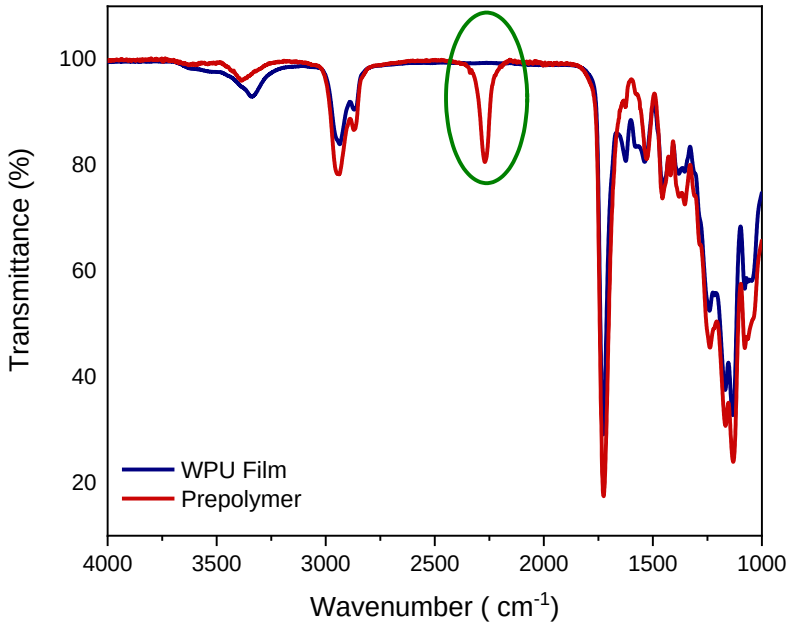

Figure 14:FTIR Spectra

During the polymerization, apart from the standard dibutyl amin back titration, the course of the reactions was also checked by FTIR spectroscopy. As is shown in Figure 14, herein, the indicator peak at 2260-2270 cm^{-1} points out the presence of N=C=O groups, arising from the isocyanate monomers. During the prepolymerization, since the reaction is not completed yet,

free isocyanate absorptions show up. However, upon the completion of the reaction and drying the WPU film, NCO peaks cannot be detected anymore.

All reactions were followed accordingly and structurally characterized usig FT-IR spectroscopy. Besides, it is possible to detect typical polyurethane structural stretching and bending peaks; N-H stretching vibrations at around 3340 cm^{-1}, $-CH_2$ stretching at 2870 cm^{-1}, C=O stretching at 1715 cm^{-1} , N-H bending at 1525 cm^{-1} , C-O-C stretching 1100 cm^{-1}[87].

3.4.2. Effect of Polyol Type

The soft segment of a polyurethane chain constitutes the majority of the structure by weight and eventually plays a critical role in achieving final properties, especially elastic properties [88]. As it is mentioned in the Introduction part, there exist several types of polyols, at different chemistries which enables the easy modification of the material with versatile structure. Likewise, prior studies mentioned the importance of polyol choice in polyurethanes leading to self-healing behavior.

The self-healing property of polyurethanes is closely related to the main chain's architecture. Soft segments of the polyurethane chains exhibit strong mobility and can easily diffuse through cracks, which is essential for effective self-healing[78] The distribution of intermolecular hydrogen bonds and the mobility of the soft segments depend on the chemical structures of both the hard and soft segments, as well as the length of the soft segments in the polyurethane chains. In other words, one must keep in mind that the primary factor in a successful self-healing process is the high mobility of the chain accompanied by the reversible interactions which enable the rearrangement and rebounding. Particularly in polyurethanes, the mobility of the chains is mainly dependent on the soft segment, thereby, the choice of the polyol is in the prior condition. Different polyol chemistries affect intermolecular interactions, hereupon the chain mobility, thermal properties, mechanical properties and self-healing behaviors are governed. Accordingly, in this chapter, the self-healing studies were conducted using the most commonly preferred polyol types in polyurethane production such as polyether and polyester polyols.

In order to conduct a systematic study over controlled chain structures, polyols at similar molecular weights (~2000 g/mol) were tentatively chosen. All synthesis parameters such as isocyanate type, hard segment content (%), ionic structure and content were kept constant, as presented in Table 1.

Table 1: Composition and properties of synthesized WPU dispersions with varying polyols

SAMPLE	Effect of Polyol Type			
	WPU-PPG	WPU-PTMO	WPU-Neopentyl Glycol/Adipic Acid/Hexanediol	WPU-Diethylene Glycol/ /AdipicAcid/ Butanediol/ Ethylene Glycol
Hard Segment (%)	17	17	17	17
NCO/OH	2	2	2	2
Chain Extension (%)	70	70	70	70
Ionic Content (%)	1.2	1.2	1.2	1.2
Particle Size (d.nm)	200	340	335	210
Mw/PDI (Da)	147.500/2.0	Not Soluble	76.200/2.1	107.600/2.2
Tg/Tm (°C)	T_g= -50	T_m= +20	T_g= -35	T_g= -43
Young's Modulus (MPa)	0.65±0.1	5.1±0.3	3.1±0.8	4.26 ±0.5
Stress at Break (MPa)	7.0±0.2	16.4±0.7	12.7±0.1	17.3±0.6
Elongation at Break (%)	1400±52	600±44	610± 33.9	1970±33

In polyether polyol-based samples, additional hydrogen bonds between the soft segments and urethane NH groups are limited. Yet, with polyester polyol based soft segments, the hydrogen bonds can also form between carbonyl groups and urethane NH groups. Therefore, the density of hydrogen bonds in the PUs containing PPG and PTMO soft segments should be lower than that in the polyester based ones. Moreover, the increase of the length of the polyether blocks would lead to the decrease in the density of the hydrogen bonds, which would weaken the ability of the self-healing. In PPG sample particularly, a methyl side-group and affect the crystallization behavior of the soft segment phase.

As it is explained in the Table 1, PPO-based WPU films gave the lowest tensile properties, mainly attributed to the fact that PPO chains are the most softest structures among all polyol types. PTMO-based WPU films showed the highest Young's modulus in original films. Yet, PTMO based WPU structures exhibit a high degree of microphase separation, which restricts the chain movement and precludes the self-healing occurrence. On the contrary, polyester based WPU films exhibit more phase-mixed microstructures due to the ester carbonyls in the polyester polyols participating in hydrogen bonding interaction with the hard segments. While this phenomenon leads to high tensile properties in polyester-based polyurethanes, it also contributes to the self-healing performance.

All samples exhibit uniform particle size distribution at a suitable diameter range of 200-350 nm, which is the typical particle size range for stable WPU micelles. Herein, the main reason of particle size variations is the different chemistries and nature of the polyol structures. Besides the functional groups, steric effects, the hydrophilicity/hydrophobicity of the polyols has a primary influence on the resulting particle size. As hydrophilicity increases, the particle size gets smaller. In general, polyester polyols exhibit more hydrophilic nature than the polyether types, therefore, poses smaller particle sizes. In the case of neopentyl glycol based polyol, the particle size is bigger than expected, which is due to the steric effect of the side methyl groups**.**

The molecular weight of the dispersions was measured using their dried films dissolved in DMF. The Mw values presented in Table 1 supports the formation of linear WPU chains at high yield where the PTMO sample couldn't be dissolved in DMF likely due to its high molecular weight.

Herein, another crucial point indicating the segmental mobility, thus the self-healing performance, is the mobility of the chains which can be monitored by DSC thermograms. The higher the melting temperature of crystalline polymers, the more restricted the chain mobility depending on the conditions of use in daily atmospheric conditions. Yet, for the amorphous polymer, the more mobile the chain, the lower the Tg value. Therefore, as discussed earlier, the lower the Tg value, the more likely the chain has the possibility of self-healing.

PTMO based WPU chains exhibit sharp melting points around 20 ºC, confirming that they are in semi-crystalline structure. Yet, polyester based WPU chains show only one glass transition temperature. Another important issue is the dedication of the microphase separation from Tg and/or Tm values of the WPUs. The fact that the polyester based WPU has one glass transition temperature at around -35 to -45 ºC means that this structure exhibits a well microphase mixed structure and its chains are highly mobile at service temperature.

As a result of these studies, mainly due to the subambient Tg values which enables the chain movement at room temperature and above, and increased number of H-bonds expected from the polyester units put forward the WPU-DEG/AA/BD/EG sample. Its self-healing potential was also visually supported by the optical images.

Two types of polyester polyols were compared. Theoretically, by only considering Tg values, we could predict that both chains would have successful self-healing performances. However, the experimental results showed that one results in higher self-healing performance which led us to dig into their chemical structures. While they both contain adipic acid and short chain diol units, the main difference in their structures appears as neopentyl glycol in one of them. It appears that those methyl groups in neopentyl glycol create a steric hindrance effect and suppress the reattachment of our non-covalent interactions during the self-healing process. On the other hand, it is also known that neopentyl glycol has a tendency to form cyclic derivatives by Thorpe-Ingold Effect, which is likely to occur. Consequently, it can be deduced that not only a low Tg is enough, but also a non-hindered chain is ineluctable for a self-healing process.

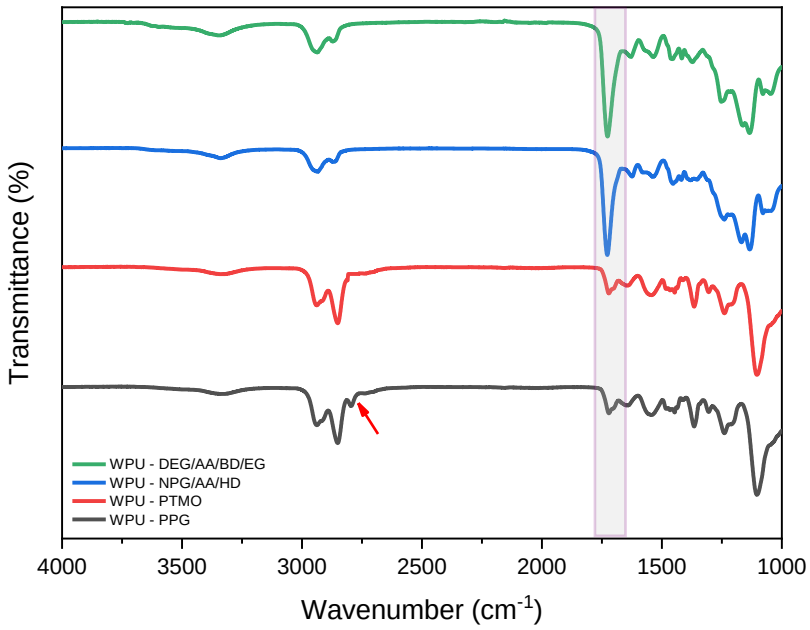

Figure 15: FTIR spectra of the WPU films with different polyols

The difference of WPU structures were also shown by FTIR spectra, in Figure 15. Spectra were recorded from the dry films of mentioned WPU dispersions. All samples showed typical -NH stretching bands at around 3350 cm^{-1}, -CH stretching at 2950-2900 cm^{-1}. Polyester based polyurethanes showed significantly intense absorption bands at 1700 cm^{-1}, due to carbonyl (C=O) groups exhibited in their soft segments, however polyether based samples showed mediocre level of carbonyl stretching bands which only comes from the urethane and urea functionalities. Moreover, PPG based WPU film showed extra -CH_2 absorption band at 2800 cm^{-1} arising from the pendant methyl group.

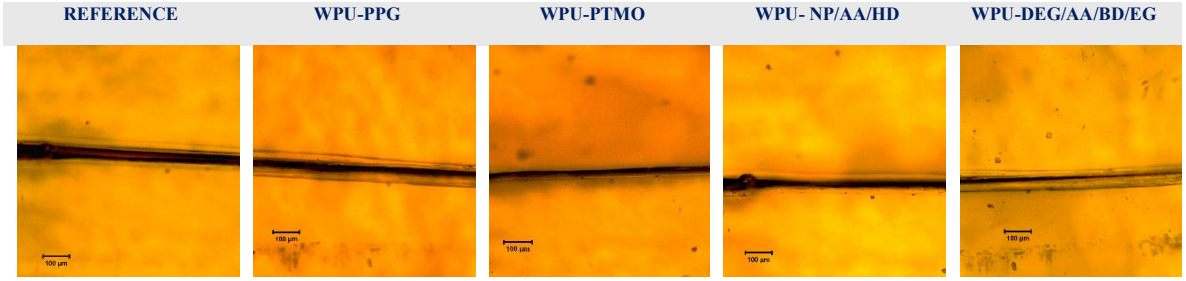

Figure 16: Optical microscope images of self-healing WPU films

Self-healing properties of the WPU films were fundamentally tested via optical microscopy, as seen in Figure 16. Dry films were scratched through a blade micrometer, equipped with digital caliper. By this means, each sample could be exactly scratched to 75% of its original thickness and left for self-healing at ambient conditions for 24 hours. Upon observations for 24 hours, it was seen that the only significant self-healing process occurred in the DEG/AA/BD/EG sample. The polyether based WPUs were almost stayed as they were freshly cut after 24 hours, arising from the lack of H-bond compared to WPU-EG/AA/BD sample and the neopentyl groups in the WPU- NP/AA/HD sample possibly lock the molecular movement and disable the self-healing. Therefore, the following experiments are focused on the DEG/AA/BD/EG sample.

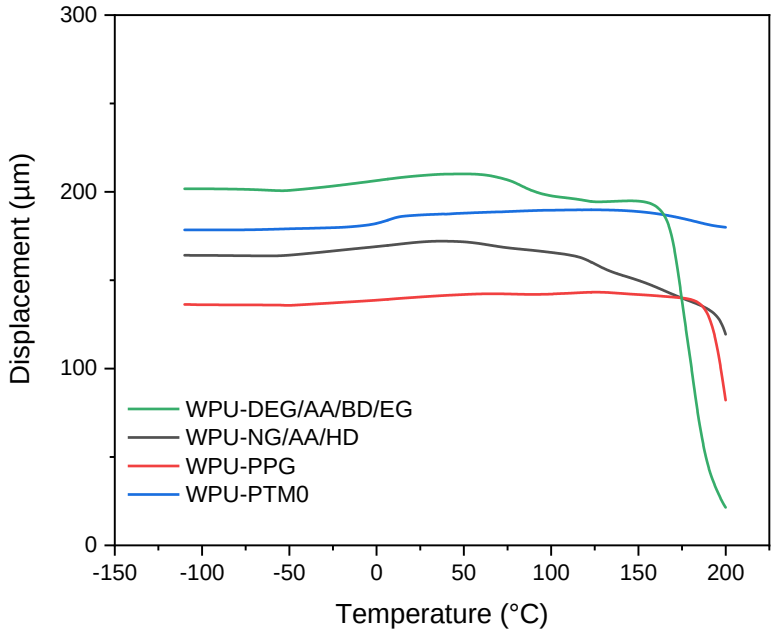

Figure 17: TMA curves of the WPU films

The TMA penetration curves are presented in Figure 17. TMA spectra offer a very clear picture about the physical cross-linking effect and relative strengths of hydrogen bonding in the hard segments of WPU films. The DEG/AA/BD/EG sample had an obvious penetration at around 70 °C besides its Tg region, which means that the deformation of the H-bonds also occurred at this temperature region. The WPU-NG/AA/HD film showed a much lower

deformation temperature than DEG/AA/BD/EG sample and got softer which is also confirmed by the UTM results. The WPU-PPG film exhibits a very long plateau region, where no significant penetration was observed except at around -50 ºC. The WPU-PTMO film showed an upward peak at around the room temperature, which is correlated with its Tm value, arising from its crystalline structure.

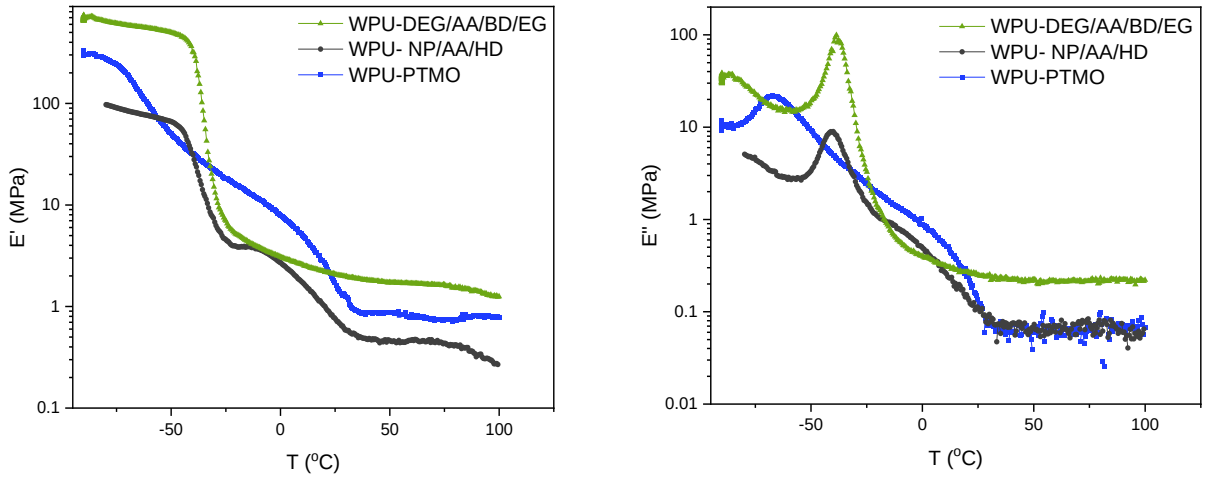

Figure 18: DMA curves of the WPU films

The storage and loss modulus profiles are presented in the Figure 18. While the E' is correlated with the mechanical properties, the E'' data gives insider information about the energy dissipation through the sample which can clarify the self-healing property.

The most obvious relaxations, located around the glass transition temperature of their composed polyols. The E′ and E'' of WPU-PPG couldn't be measured and was the lowest among the series, indicating that the nature of material was softer and difficult to resist to deformations.

The increased mechanical properties could also be verified by the increased storage modulus (E') at - 100 ºC and above 0ºC.

Herein, the most critical information can be collected via the E'' data. The loss modulus at around the Tg and room temperature clearly shows that the WPU- DEG/AA/BD/EG has the greatest ability for the relaxation and energy transfer within the material.

Therefore, the improvement in the self-healing ability of the WPU- DEG/AA/BD/EG film was confirmed to be related to the increase in the loss modulus.

3.4.3. Effect of Hard Segment

Waterborne polyurethane is a block copolymer composed of hard and soft segments that often exhibits a microphase separation structure due to the thermodynamic incompatibility between these segments. The soft segment imparts flexibility, while the hard segment provides strength, creating a special phase structure that supports the material's ability to self-heal [89] A polyurethane (PU) molecular chain typically contains polar groups such as urethane, urea, ester, and ether groups. Within the hard segment, the carbonyl group (C=O) in the urethane acts as a proton acceptor, while the –NH– group can serve as both a proton donor and acceptor. In the soft segment, the ether group (–O–) and ester group function as proton acceptors [90]

Since the soft segment is crucial for a successful self-healing process, the content (proportion) of the soft segment in the total WPU chain also plays an essential role. The suitable polyol type was identified in the previous section yet, in this section, the exact amount of soft segment is meant to be determined. In WPU chains, there exist lower and upper limits for the hard segment content to acquire adequate phase mixing and mechanical properties. In common PU formulations, the hard segment content is reported in (%) as is shown in Equation 1.

Equation 1: Hard Segment(%)= 100- Soft Segment(%)

As the length of hard segment decreased the incompatibility between the hard segment and soft segment increased. This increased incompatibility between hard and soft segments leads to a more pronounced microphase separation.

Hydrogen bonds play a direct role in mechanical properties and upon the increase in hard segment, the morphology of the backbone changes from interconnecting to isolated hard domains. Thus, three-dimensional hydrogen bonds between hard segments give strong hard domain cohesion and directly result with mechanically strong structures[91,92].

The mean particle size of WPU dispersions increased in direct relation to the hard segment content. This increase can be attributed to the expected rise in chain rigidity as the hard segment content increases. Additionally, since the ionic groups on the polymer backbone are situated on the surfaces of PU latex particles, it becomes increasingly challenging for the rigid polymer chains to reorganize these ionic centers and form spherical structures. As rigidity increases, the possibility of forming regular latex particles with the suitable hydrophobic-hydrophilic arrangement of chains decreases. Consequently, this phenomenon is believed to result in larger particle sizes during the phase inversion process as the hard segment content increases.

As the proportion of hard segments rises, there is a consistent increase in both the stress at break and Young's modulus values, as depicted in Table 2. Conversely, the elongation at break (%) shows an inverse correlation with the increasing hard segment content. This trend is explained by the stiffening effect caused by the higher concentration of urethane bonds and increased hydrogen bonding interactions within the PU backbone as hard segment content increases. Consequently, the decrease in the proportion of soft segment chains results in reduced elasticity.

A higher hard segment content in WPU film forms stronger hydrogen bonding forces within the hard domains. This intensified bonding diminishes interference with the mobility of soft segment chains, facilitating an optimal equilibrium between hard and soft segment domains. This equilibrium leads to the spontaneous formation of ordered structures within the two phases and facilitates effective phase separation.

Based on the findings presented, the extent of hydrogen bonding rises with an increase in hard segment content. This increase is linked to the increased presence of sites within both hard segment and soft segment domains, acting as hydrogen bond acceptors or donors. Consequently, these enhanced interactions lead to enhanced hydrogen bonding

Increased hard segment content acts as a physical cross-linking point, promotes hydrogen bonding, and induces microphase separation between soft and hard segments. This phenomenon directly boosts the mechanical properties of polyurethane. DLS analysis revealed that an increase in the hard segments led to an increase in particle size, ranging from 150 nm to 240 nm. Moreover, by increasing the hard segment content, the peak intensity decreased due to a reduction in the number of particles present in the dispersion.

SAMPLE	Effect of Hard Segment				
	WPU-16.5%HS	WPU-17%HS	WPU-17.5%HS	WPU-18%HS	WPU-18.5%HS
Hard Segment (%)	16.5	17	17.5	18	18.5
NCO/OH	2	2	2	2	2
Chain Extension (%)	70	70	70	70	70
Ionic Content (%)	1.2	1.2	1.2	1.2	1.2
Particle Size (d.nm)	155	170	210	240	310
Mw/PDI	107.600	117.600	133.200	138.000	131.600
Tg(°C)	-42.12	-43.47	-42.83	-42.99	-43.18
Young's Modulus (MPa)	3.49 ± 0.14	3.96 ± 0.24	4.00±0.40	5.08±0.21	5.42 ± 0.28
Stress at Break (MPa)	9.39±0.72	16.61±0.68	18.32±0.90	18.52±0.62	19.44±0.48
Elongation at Break (%)	1690±80	1980±10	1570.00±50	1480±50	1310±20

Table 2: Composition and properties of synthesized WPU dispersions with varying hard segment ratios

On the other hand, achieving a uniform dispersion with more than 18.5% hard segment couldn't be efficiently realized possibly due to the imbalanced microphase mixing effect.

The course of self-healing was constant over the increasing hard segment series. Therefore, to continue with the best performing material, the sample with the highest mechanical values was chosen for further experiments[93].

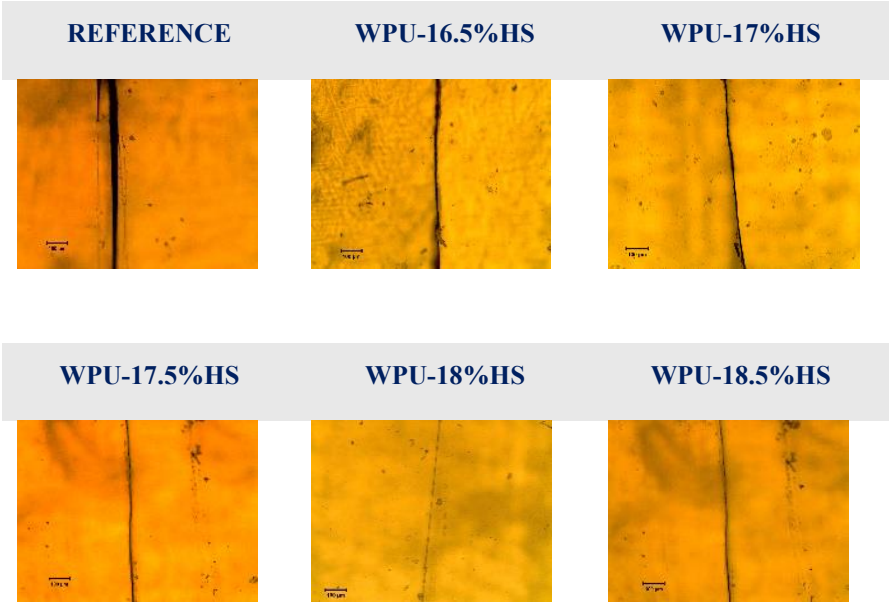

Figure 19: Optical microscope images of PU films for self-healing at different hard segment contents

As seen in Figure 19, the hard segment ratio also affects the self-healing behavior. While we see a slight self-healing for the 16-17% hard segment, the 18% hard segment is specifically more efficient. The main reason behind this scenario is the increased amount of H-bonds which offer a certain contribution to self-healing. Yet, further increment in the hard segment potentially restricts the chain movement, therefore we observe a drop on the self-healing.

3.4.4. Effect off Chain Extension Degree

The degree of the chain extension of WPU is the main factor that controls its molecular weight and chain length. Therefore, the mobility of the chain can also be affected by the bulkiness of the WPU chain. In order to achieve mechanical properties at an acceptable level, a specific molecular weight threshold must be attained[94,95].

The ionic content and the hard segment were settled to control the hydrogen bonding and ionic interactions. The degree of chain extension varied from 65 to 90 wt%, as summarized in Table 3. Herein, especially the ionic content ratio was carefully kept constant by variations with EDA content.

Table 3: Composition and properties of synthesized WPU dispersions with varying degrees of chain extension

SAMPLE	Effect of Chain Extension				
	WPU-65%ChnEx	WPU-70%ChnEx	WPU-75%ChnEx	WPU-80%ChnEx	WPU-90%ChnEx
Hard Segment (%)	18	18	18	18	18
NCO/OH	2	2	2	2	2
Chain Extension	65	70	75	80	90
Ionic Content	1.2	1.2	1.2	1.2	1.2
Particle Size	170	170	180	210	Gel Zone
Molecular Weight	60.100/2.1	121.600/1.8	133.200/2.4	138.000/2.2	Not Soluble
Tg(^{o}C)	-44.22	-43.18	-42.33	-46.5	-43.72
Young's Modulus	2.1±00.2	5.08±0.21	5.42 ± 0.28	7.7 ± 0.3	5.91±0.17
Stress at Break	3.25± 0.16	18.52±0.62	19.44±0.48	25.3 ± 1.3	5.83±0.26
Elongation at Break	1742± 80.1	1574.29±51.05	1304.96±16.37	1390 ± 25	729.42±34.03

The degree of chain extension directly affects the molecular weight which means that the length of the WPU chain grows with the chain extension step. Chain extension with short diols give rise to urethane bonds; chain extension with amine groups produces urea bonds. Therefore, additional urethane and urea bonds directly increase hydrogen bonding interactions between hard segments.

When the chain extension degree is minimal, unreacted isocyanate end groups could react with excess water in the reaction mixture, leading to the formation of excess urea groups that armake şte difficult to disperse the final polyurethane chains in water and tend to be larger in size. This may result in a particle size distribution characterized by a multi-modal particle size distribution. Conversely, when chain extension degrees are high (usually exceeding

85%), issues such as poor solubility and dispersion arise due to the exceptionally high molecular weight of polyurethane chains in the acetone process.

As the amount of chain extension went beyond 80%, tensile properties decreased. This behavior was mainly attributed to unreacted chain extender which might behave like an impurity, negatively affecting mechanical strength.

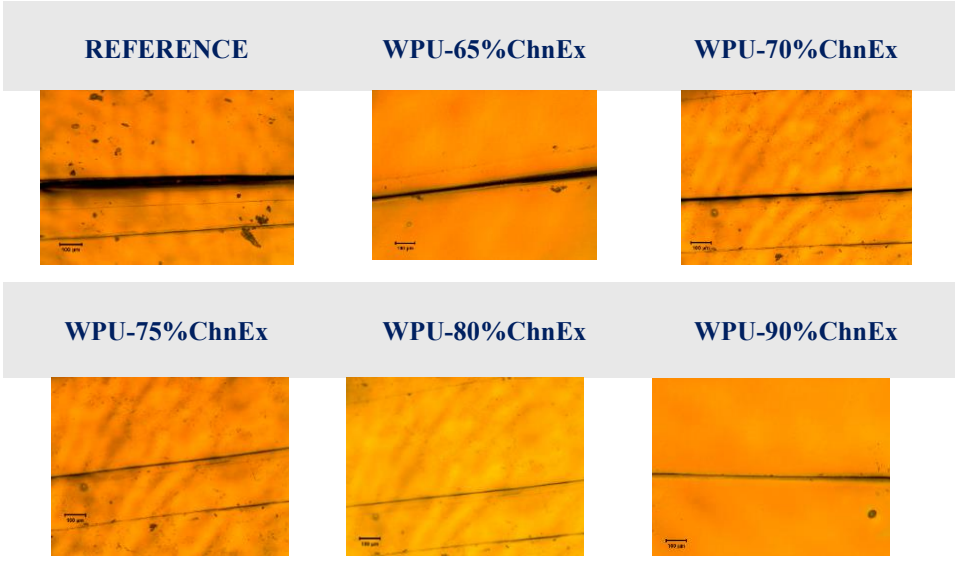

Figure 20: Optical microscope images for self-healing of different chain extension degrees

From the optical microscopy images seen in Figure 20, it is seen that the chain extension degree has a limited effect on the self-healing. Yet, the best self-healing was obtained at 80% chain extension which also showed the highest mechanical performance. Therefore, this sample is chosen as the reference for the subsequent experiments

3.4.5. Effect of ionic group type

Traditional polyurethane is either insoluble or unable to disperse in water. To make polyurethane dispersible in water, ionic or hydrophilic groups should be incorporated to the polymer chains[70,96].

As it is earlier discussed in the Introduction part, ionic groups are one of the main constituents of WPUs controlling the particle size, thermal and mechanical properties. Most typical WPUs provide the ionic group via the incorporation of DMPA thus, they bear COO^- groups[97]. Yet, it is investigated that other types of ionic groups may perform as good as their counterparts, such as SO_3^- groups. In this section, we studied the effect of ionic group type on the self-healing[98]. Basically, ionic groups interact with each other via electrostatic interactions, a class of Van der Waals forces. Therefore, they have different interaction energies which might also affect the self-healing performance of the polymer matrix they are part of.

Table 4: Composition and properties of synthesized WPU dispersions with different types of ionic groups

SAMPLE	Effect of Ionic Type	
	WPU- COO-Na+	WPU-SO_3Na+
Hard Segment (%)	18	18
NCO/(OH+NH)	1.12	1.12
Chain Extension (%)	80	80
Ionic Content (%)	1.2	1.2
Particle Size (d.nm)	560	210
Mw (Da)	139.700 / 2.8	133.500/2.1
Tg(°C)	-43.71	-46.5
Young's Modulus (MPa)	6.9 ± 0.4	7.7 ± 0.3
Stress at Break (MPa)	20.4 ± 1.5	25.3 ± 1.3
Elongation at Break (%)	1000± 110	1390 ± 30

As it is listed in Table 4, the average particle size of WPU-SO_3Na^+ is significantly smaller than WPU- COO^-Na^+. The presence of sulfonate groups, which exhibit stronger dipole-dipole interactions compared to carboxylate groups, leads to the formation of smaller ionic clusters within the polymer structure. This enhanced dipole interaction, coupled with the hydrophilic nature of sulfonate groups, reduces friction between molecular chains. Consequently, the polymer can more readily disperse in water, resulting in smaller particle sizes.

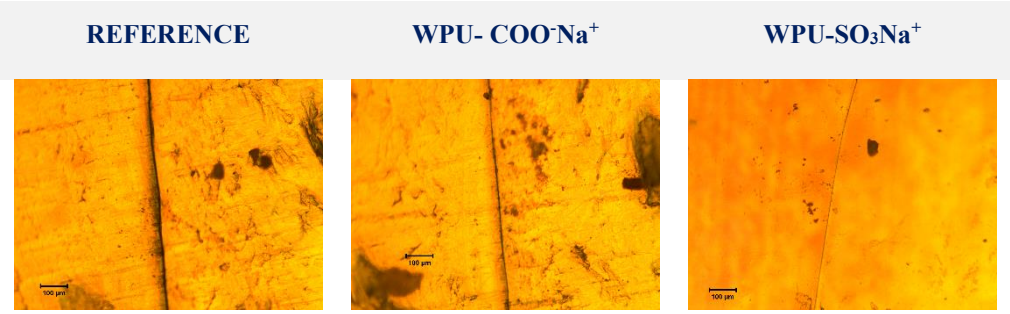

Figure 21: Optical microscope images for self-healing for different ionic groups

As it is clearly seen in Figure 21, upon switching the ionic group to COO^-Na^+, the self-healing behavior is significantly worsened. This experiment revealed the key role of the ionic group's chemistry in the rebounding process of the materials. In other words, SO_3Na^+ groups had a pronounced effect in the self-healing of PU films when compared to COO^-Na^+ groups with the same molar content. This evident difference underlines the leading role of the ionic interactions for the self-healing. Relatively weaker ionic interactions in the case of COO^-Na^+ groups couldn't be as effective which means that besides H-bonding, strong ionic interactions are indispensable for a self-healing process[99,100].

3.4.6. Effect of Ionic Content

A series of linear, anionic waterborne poly(urea)urethane dispersions were prepared via acetone method using the feed compositions given in Table 5. The NCO terminated prepolymer was obtained from HDI and polyester polyol with a low Tg; chain extension was realized using EDA and $SO3^{-}Na^{+}$ groups were integrated through AEAS molecule during the chain extension step.

Table 5: Composition and characterization of synthesized WPU dispersions with different ionic contents

SAMPLE	Effect of Ionic Content		
	WPU-0.8	WPU-1.2	WPU-1.6
Hard Segment (%)	18	18	18
NCO/OH	1.96	1.96	1.96
Chain Extension (%)	80	80	80
Ionic Content (%)	0.8	1.2	1.6
Particle Size (d.nm)	320	210	100
Molecular Weight /PDI	140.600/2.3	133.500/2.1	126.100/2.1
Tg(°C)	-48	-46.5	-45
Young's Modulus (MPa)	5.8 ± 0.2	7.7 ± 0.3	5.9 ± 0.1
Stress at Break (MPa)	16.1 ± 0.2	25.3 ± 1.3	15.4 ± 0.4
Elongation at Break (%)	1610 ± 50	1390 ± 30	1250 ± 50

GPC measurements reveal that WPUU samples show close molecular weights with slight increase possible due to increasing ionic concentrations due to the additional mass of sodium sulfonate groups. Yet, further increment of ionic content lowered the molecular weight which could also be due changing conformations of PU chains in the GPC solvent as the ionic content increases.

It is evident that the particle size distributions are uniform across all three dispersions, and as the ionic content increases from 0.8% to 1.6%, the particle size decreases from 320 nm to 110 nm. This systematic reduction in particle size indicates that both the average particle size and the width of the particle size distribution decrease as the ionic content increases.

WPU films exhibit only glass transition (T_g) temperature due to their amorphous structure, which is located at -48 to -45 ^oC range. T_g of films is directly related to the mobility and flexibility of the chains which is the key parameter of the self-healing process. The T_g value of the films slightly increased by increasing ionic content indicating the coulombic crosslinking formed between ionic centers and restricted the chain movement. Herein, the subambient T_g values ensure sufficient molecular interdiffusion for rearrangement on the cracked surface at room temperature and above.

The resulting WPU films exhibit relatively high tensile properties among their class of waterborne polyurethane films due to the enhanced H-bonding via urea groups and ionic interactions of $SO_3^-Na^+$ groups. While all the WPU films show high mechanical performance with a minimum 15MPa of stress at break and 1200% elongation, WPU-1.2 is specifically attractive with 25MPa stress at break and 1400% elongation at break.

The augmentation in the tensile strength from WPU-0.8 to WPU-1.2 is attributed to the enhanced coulombic forces and physical crosslinking between the ionic centers. The addition of 0.4% of sodium sulfonate groups increased the stress at break from 15 MPa to 25 MPa (70% enhancement) and Young's Modulus from 5.8 to 7.7 MPa. The WPU-1.2 sample exhibits the highest tensile properties with 25 MPa stress at break and 1400 % elongation at break, which can be attributed to the favorable microphase mixed structure. However, further

introduction of 0.4% ionic content in WPU-1.6 resulted with relatively weak stress at break and elongation at break presumably due to an heterogenous microphase separation.

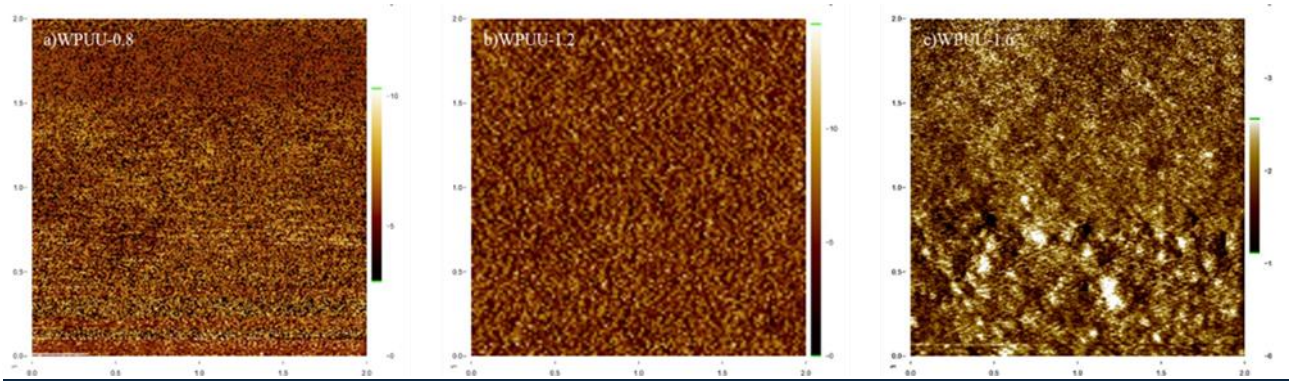

Figure 22: AFM profiles of WPU films at different ionic concentrations

Figure 22 reveals the microphase morphologies of the dry WPU films which were investigated with AFM, the phase images at room temperature were obtained at tapping mode. The dark and the light regions correspond to soft and hard domains, and the hard domains in these samples appear to be spherical shape[101,102].

As shown in Figure 22, the surface morphology of samples significantly changed with increasing ionic content. Since the hard segment ratio and H-bond density was constant among the samples, the main reason of phase separation was the increasing number of ionic interactions. In fact, in WPU-0.8 film, the formation of hard and soft segments was evident, however, due to the low ionic concentration, the phase mixing was not sufficient. Furthermore, the highest microphase mixing was achieved in WPU-1.2 sample by means of optimum ionic interaction level. On the contrary, as the concentration of ionic interaction got higher, microphase separation was more pronounced. In WPU-1.6, it is clearly seen that agglomerated structures were formed with high microphase separation due to the over ionic interaction amount.

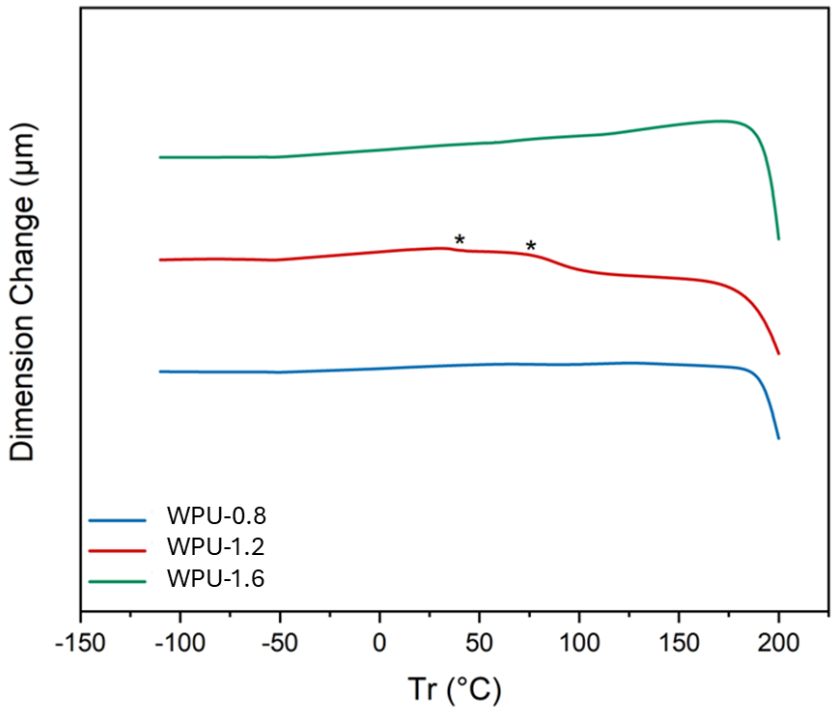

Figure 23: TMA curves of WPU films

Self-healing of a material is mainly dependent on the mobility of the chains which is controlled by the intermolecular forces. Therefore, in order to designate the self-healing conditions such as the temperature, TMA data was used to monitor the relative strength of the interactions (physical crosslinks). By using the deformation temperatures in the flow regions, it was possible to foresee suitable temperatures for an efficient self-healing, where the chains were mobile.

As presented in figure 23, TMA scans of WPU-0.8 and WPU-1.6 are stable and do not show significant deformation until 180 ºC, complete penetration of the probe takes place above 180 ºC for all samples. On the other hand, WPUU-1.2 showed earlier deformation stages around room temperature and 70 ºC. Therefore, subsequent self-healing studies were realized at room temperature and 70 ºC.

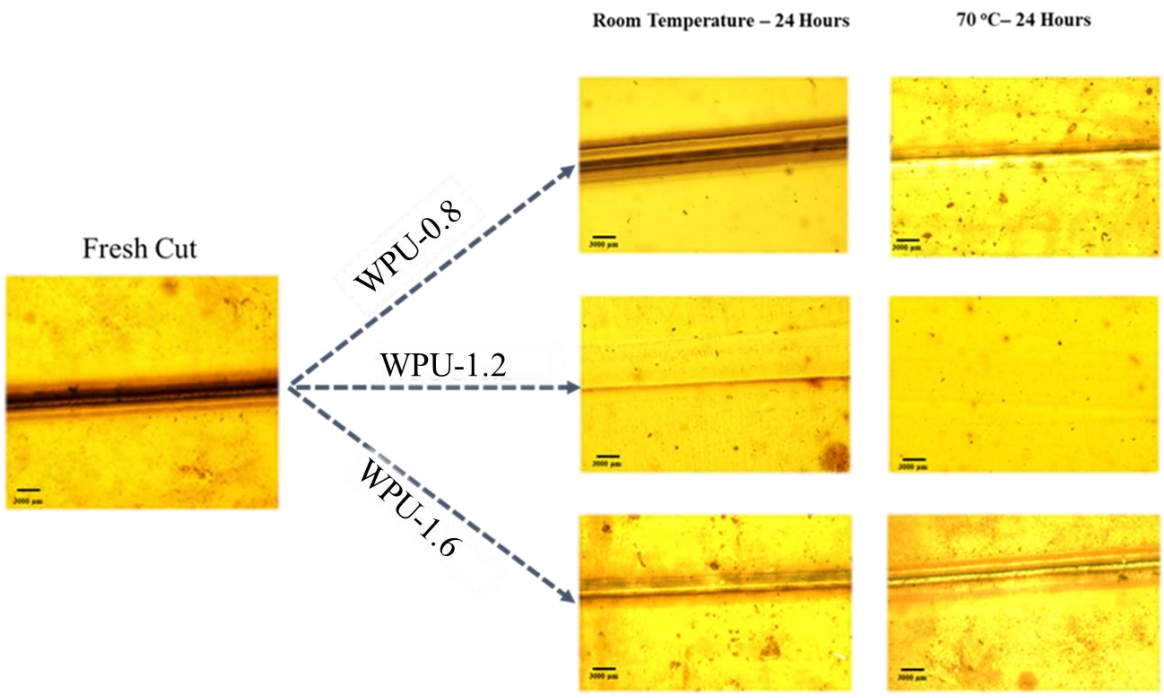

Figure 24: Optical images of self-healing for different ionic groups

The self-healing process of the WPU film samples was also observed by optical microscopy, scratches on surfaces before and after being healed at room temperature and at 70 °C (50×) were presented.

Figure 24 shows the crack closures occurred at different yields after 24 hours, it was obvious that the WPU-1.2 sample exhibited the best performance at both room temperature and 70°C, mainly due to its superior microphase mixing compared to the other samples. At room temperature, the WPU-0.8 sample displayed low self-healing performance, likely because of its lowest ionic interaction concentration which was insufficient for phase mixing. On the other hand, WPU-1.6 also underperformed due to the high microphase separation and formation of ionic aggregates.

Upon restoration at 70°C, all samples exhibited superior self-healing performance than room temperature, with cracks becoming shallower and narrower. However, the cracks in the WPU-0.8 and WPU-1.6 samples did not effectively recover and remained visible even after the 24-hour period at 70°C. In contrast, the cracks in the WPU-1.2 sample became

almost invisible under optical microscopy after 24 hours at 70°C. These results visually revealed the critical role of ionic interactions and microphase mixing in the self-healing process. No further improvement was observed after 24 hours, the self-healing process was accomplished at this period of time.

Based on the findings of this optical study, further mechanical self-healing experiments focused on the WPU-1.2 sample.

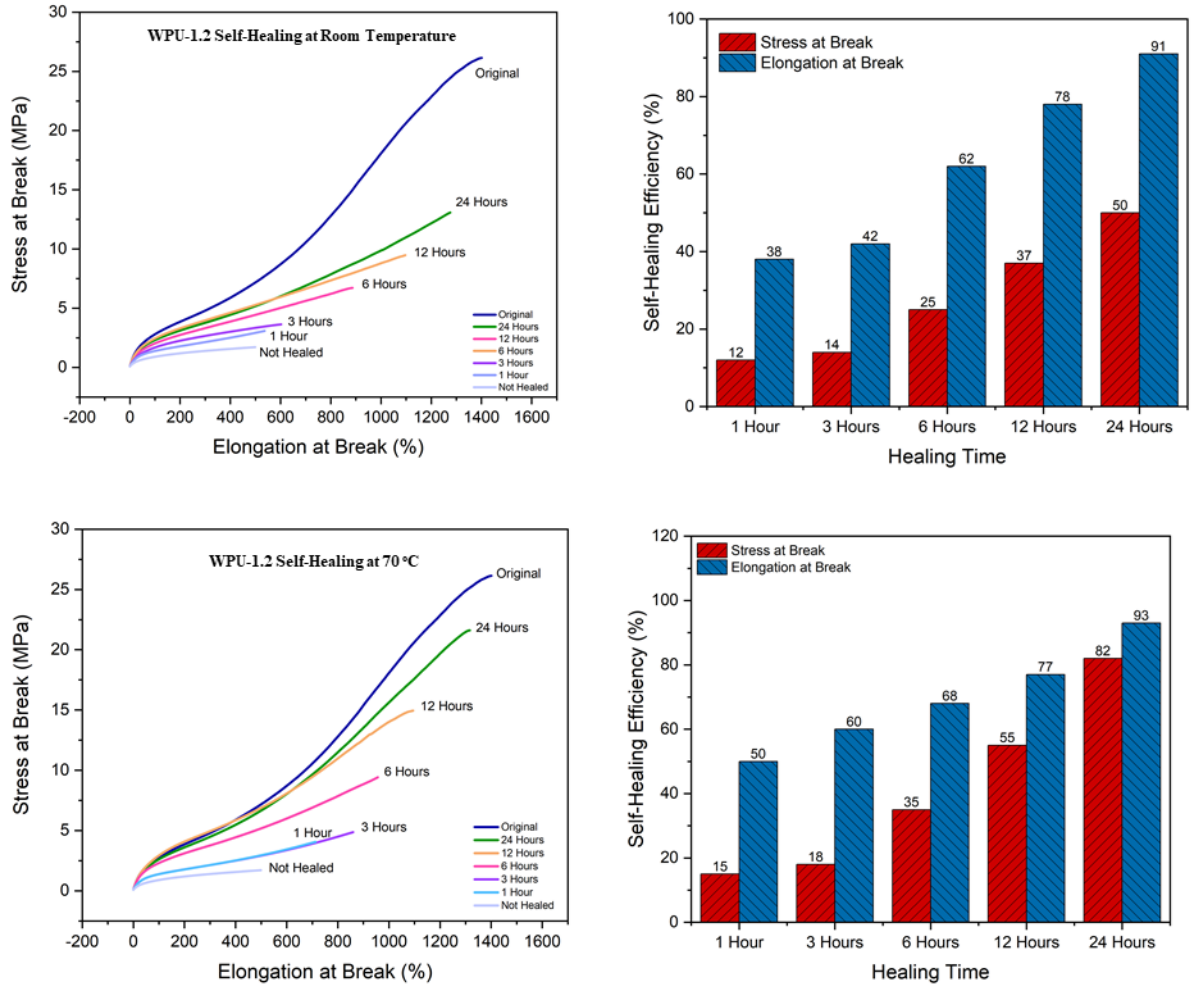

Figure 25: Self-healing efficiencies of WPU-2

WPU-1.2 sample provided efficient self-healing performance while the other two samples couldn't show remarkable self-healing performance. In our case, it is obvious that the 1.2%

of ionic content allows the necessary chain flexibility for the rearrangement of the chains in accordance with highest mechanical performance over the WPU series. As seen in Figure 25, the stress at break and elongation at break of WPU-1.2 gradually recovered over the healing period. The healing time had constructive effect on the self-healing capacity up to 1 day. After a period of 24 hours, films healed at room temperature could extend to about 1200% before failure and at 70°C, films regained their elongation about 1300% with an ideal elastomeric film profile. Hence, the WPU-1.2 is able to intrinsically recover the scratches with such a high yield in just 24 hours thanks to the synergetic effect of H- bonds and ionic interactions.

2.4.7. Self-Healing WPU- Paint Production and Application

Paint and paint chemistry play a pivotal role in the industry, serving as essential components for enhancing aesthetics, protecting surfaces, and ensuring durability in a wide range of applications across sectors such as construction, automotive, aerospace, and consumer goods[103]. They are essentially composed of binders, fillers, and pigments and mainly serve for either aesthetic or protective purposes on a variety of substrates. For instance, one of the main usages is the protection of metal surfaces from corrosion, especially in outdoor conditions. When the top paint layer is used for protection in corrosive environments, the coating's surface can be disturbed over time, resulting in the development of microcracks. These cracks can expand and expose the substrate to moisture and oxygen from the atmosphere, potentially leading to corrosion[104].

To this end, corrosion inhibitors containing chromate derivatives have been used in the industry for active protection by enhancing the resistance of metals to corrosion through the blocking of active sites where corrosion occurs. These inhibitors either form a passive film on the metal surface or chemically absorb it. However, due to health and environmental concerns related to chromate conversion coating (CCC), the industry won’t be able to use them[105] Instead, combining organic and inorganic phases in materials is thought to be advantageous where the organic phase should provide flexibility and the necessary mechanical properties. The WPU dispersions are suitable resin materials for water-based paint formulations which has been already used in the construction and automotive paint

industry, along with the protective coatings such as anti-corrosive applications. A prominent improvement had been achieved by Nissan Motor Co. that unveiled self-repairing polymer materials, including hydrophobic paints capable of self-healing, for commercial availability[106,107]

In our study, the waterborne polyurethanes act as the binder resin of the paint formulation where the ultimate goal is to obtain a self-healing, environmentally friendly paint for anti-corrosion application. To that end, the WPU dispersions synthesized in the previous chapters were supplied to the company and they were transformed into real, complete paint form. Further paint coating tests were conducted in terms of adhesion, hardness, gloss, and ageing. Therefore, in this project, it is aimed to develop products that will grow rapidly in the market in terms of both enhanced self-healing and low VOC content[78].

Upon preliminary studies realized with our WPU dispersions and paint samples produced from them, the WPU-1.2 sample showed the highest compatibility with other paint additives in addition to self-healing performance.

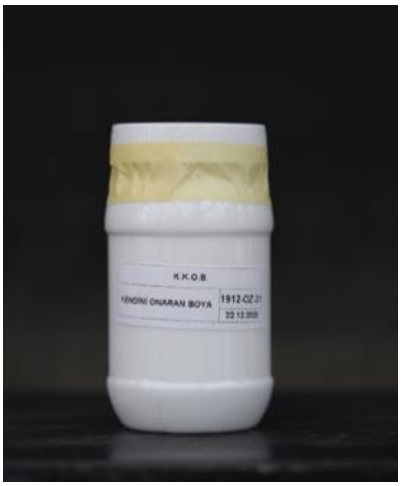

Figure 26: Product of Self-Healing WPU Paint

Therefore, it was chosen as the candidate for the scale-up production, and it is synthesized in the pilot production, as a batch of 25kg. The company successfully produced our self-healing WPU resin-based paint which is shown in Figure 26. The transformation of WPU resin to paint form was applied with such an optimized procedure, the additives with exact proportions are listed in Table 6.

Table 6: WPU-based paint composition

PAINT FORMULATION INGREDIENTS
1. Resin: (50-65%)
2. Deionized Water (5-7%)
3. Anti-Foaming Agent (0.2-0.4%)
4. TiO_2 (15-20%)
5. $CaCo_3$ (2-10%)
6. Talc (5-15%)
7. Anti-Freezer (1-3%)
8. Anti Flash (0.3-0.6%)
9. Stabilizer (0.1-0.4%)

The aforementioned produced paint was investigated in terms of surface roughness, homogeneity, stability, phase separation and dyeing. Consequently, it was approved to be applied. The fabricated paint is coated on Teflon surface and heavily scratched with razor blade and left for self-healing under the standard room temperature condition, seen in Figure 27. s. Visual observations showed that the scratch had disappeared in just three hours. This preliminary experiment enlightened us about the success of ingredients and formulation preferences.

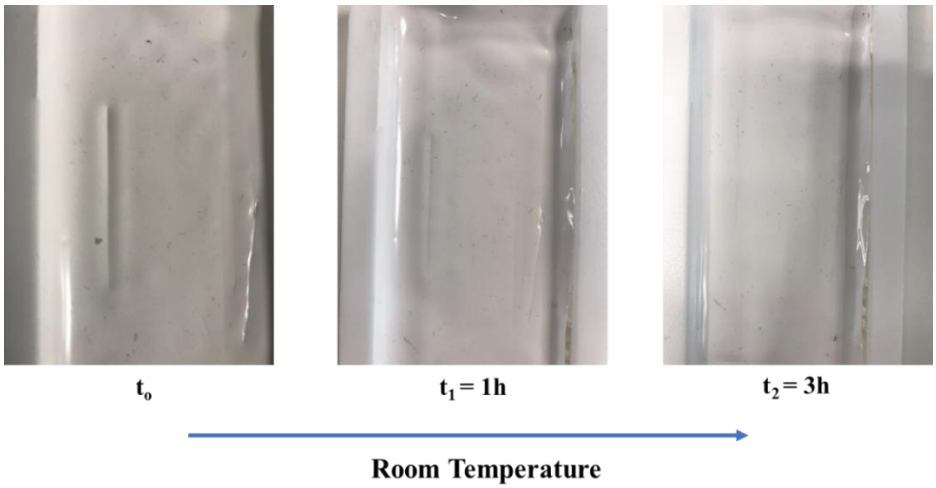

Figure 27: Self-Healing on the paint surface

Subsequently, the paints were applied on metal plates with the aim of observing their self-healing progression and anti-corrosion performance. The opaque white paint was applied using a conventional spray gun on steel strips with the dimension of 150 mm × 100 mm × 1 mm h as seen in the Figure 28.

Figure 28: Coated metal plates with WPU-based paint

Painted steel plates were tested according to universal test methods to evaluate their real-life applicability and self-healing performance as an end product as presented in the Table 7.

Our reported values indicate that our WPU-based paint has an adhesion on the surface at a maximum level (GTO) and is resistant to high impacts. Moreover, in terms of color and concealing effect, it provides a glossy white surface resistant to yellowing and ageing, in accordance with consumer desires. Consequently, the results showed that our product could successfully satisfy the industrial requirements and standards.

Table 7: Properties of the WPU-based paint

	Paint Performance	**Standard**
Solid Content	42.5%	ISO 5534
pH	9.25	ASTM E70
Density	1.19	ASTM D 2354
Viscosity (ICI)	2.37	ASTM D 526 ve ASTM D 2196
MFFT	5 ºC	ASTM D 2354
Yielding	Good	TS 4328
Spreading	Good	TS 4328
Yellow Index	91.09	ASTM E 313
White Index	0.88	ASTM E 313
Delta E - Ageing	0.8	ASTM G 154
Gloss (85 ºC)	92	ISO 2813, TS EN ISO 2813
Adhesion (Metal, Primer)	GT1-GTO	TS 4320 EN ISO 1514, TS 4317
Impact Test	80 - Very Good	ASTM D 4366
Salt Spray (1 Month)	Suitable	ASTM B 117

When protective paints are applied in environments prone to corrosion, the surface of the coating undergoes alterations in its appearance, resulting in the development of microcracks. These cracks then spread over time, allowing atmospheric moisture and oxygen to reach the underlying substrate.

A series of studies were conducted in a laboratory environment to analyze and report the self-healing behavior of WPU paint-coated plates provided by Polisan to evaluate the paint protection performance.

In the course of these studies, identical cuts were made on painted plates, and their self-healing behaviors were visually and optically examined under different cut degrees (soft and hard cuts) and different environmental conditions (room conditions and sunlight). All optical microscope images were taken in reflection mode at a 5X magnification ratio from the metal surface. The painted plates applied to the metal surface by Polisan were placed in a 5% NaCl solution in accordance with ASTM B117-11 conditions [108,109]. Two plates were subjected to the corrosion test for the paint sample. One of these plates was cut at room temperature and immediately immersed in the NaCl solution, while the second one, after being cut, was exposed to a one-hour period under a solar simulator-Sun (100 mW/cm2) and then placed in the salty water solution.

Neat surfaces were scratched by blade, the plate exposed to sunlight demonstrates higher self-healing efficiency. When comparing the two plates, the self-healing in the plate exposed to sunlight is clearly noticeable. This behavior is supported by optical microscope images, as seen in Figure 30. The reduced light reflection in the cut lines in the images of the plate exposed to sunlight indicates that the cuts on the metal plate self-heal through the self-healing polyurethane formulations

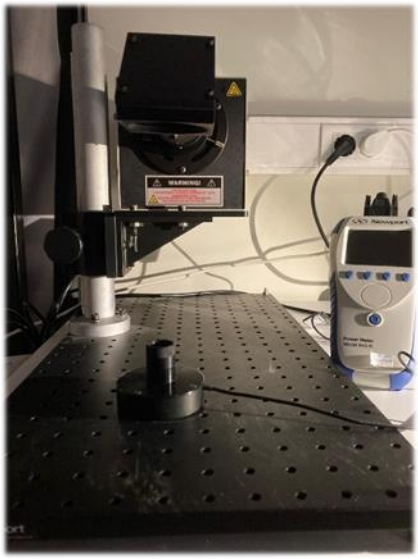

1 Sun =100 mW/cm2

2 Sun =200 mW/cm2

3 Sun =300 mW/cm2

Laser = 808 nm

Figure 29: a) Laser, b) Sun simulator, c) Corresponding energy values

When the most common external effects of surface coatings and paints are investigated, it is seen that sunlight is at the forefront[110,111]. Especially in outdoor applications, sunlight, which surfaces are exposed to for a long time, has a great effect on the surfaces. For this reason, experiments were carried out with the help of a sunlight simulator (Figure 29) in order to observe the sun rays that the obtained films can be exposed to at various power and time intervals and their possible results.

When the composition of the rays coming from the Sun to our Earth is examined, it is seen that they consist of photons in the ultraviolet light range (UV-A, UV-B, UV-C), visible (Vis.) and infrared (IR) wavelengths. In this respect, it is critical to investigate the effects of rays of various wavelengths and energies on the material and its self-repair mechanism. The power amounts of the rays falling on the material in the experiments performed with the sun simulator are given in Figure 30.

Scratched films were exposed to Sunlight simulator for different time intervals such as 1 hour and 4 hours. It should be noted that after 4 hours, the results were observed to be constant until 10 hours. Up to 10 hours, the coating started to lose its integrity, partial melting occurred. It is offered in the Figure 30 that upon sunlight a quick and efficient self-healing occurred. Especially, the initial elongation values were recovered.

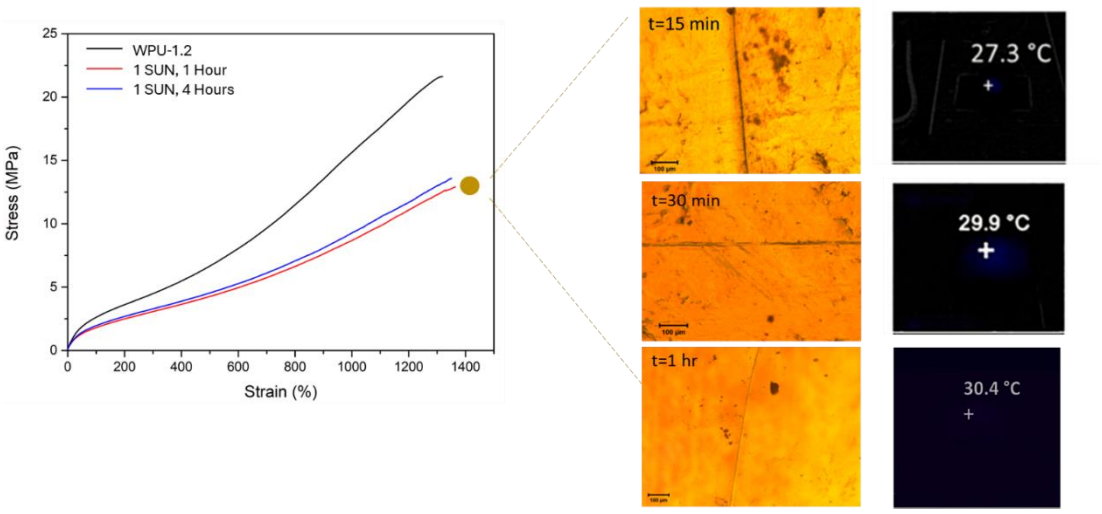

Figure 30: Sunlight exposed self-healing films

The laser with a wavelength of 808 nm is characterized by its coherence, unidirectional beam, and monochromatic light.[112] The scratched film was exposed to 808nm laser light for 1 hour. At the end of 1 hour, the local temperature was measured as 38.6 ºC which is a realistic temperature that the coating can be found on the earth, during its lifespan. As tensile properties, it was found that significant improvement was achieved in terms of Young's modulus and Stress at Break upon laser exposition compared to the not healed rival. Optical image also shows that only a slight scratch is visible after 1 hour, which is shown in Figure 31.

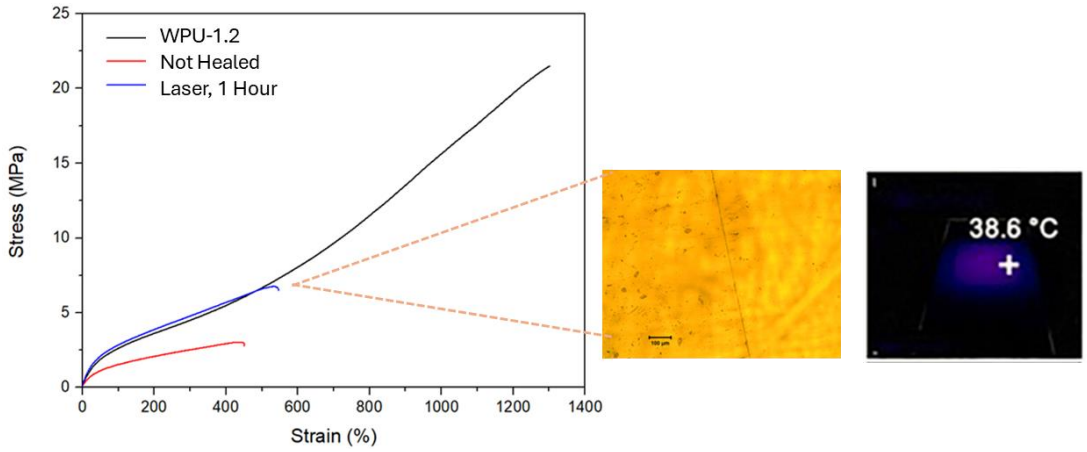

Figure 31: Laser exposed self-healing films

The painted panels applied to the metal surface were placed in a 5% NaCl solution in accordance with ASTM B117-11 conditions. Two panels from each paint sample were subjected to a corrosion test. One of these panels was cut under room conditions and immediately immersed in the NaCl solution; the other was cut and then exposed to 1 hour of urea with 1 Sun (100 mW/cm²) and subsequently placed in the saltwater solution.

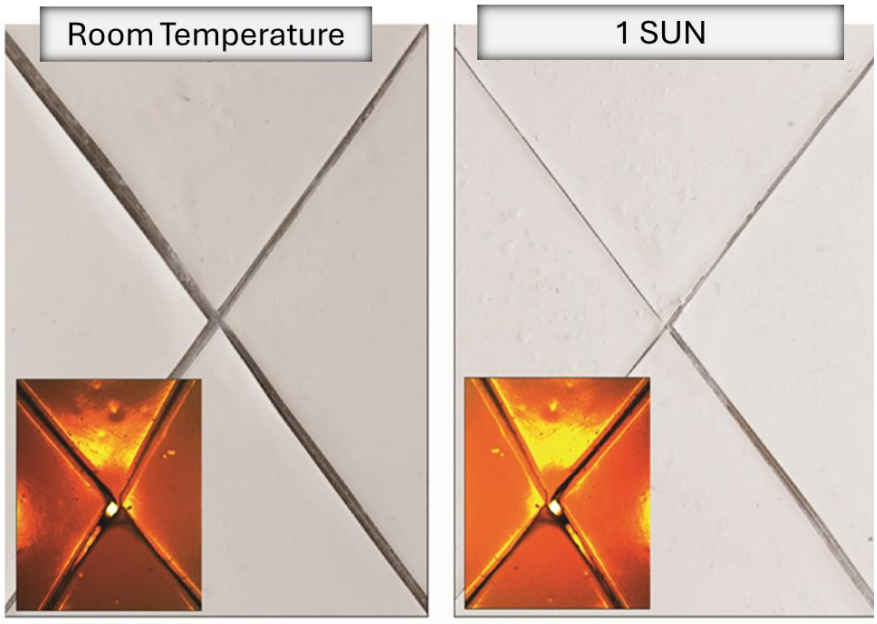

Figure 32: Corrosion plates

After immersion in NaCl solution, WPU paint-coated plates showed outstanding anti-corrosive performance. As seen in Figure 32, no rust or blister formation was observed on the plates. In fact, due to overexposure to salty water and drying, scribes paint pieces shrink at a certain level yet, beneath the coating any trace of corrosion could be observed. Furthermore, the plate exposed to Sun had obviously self-healing performance, especially on the top of the plate. This behavior support our previous results dictating that self-healing is even more pronounced with the help of outdoor conditions as well. This phenomenon proves that our WPU paint-coating could successfully protect the steel surface

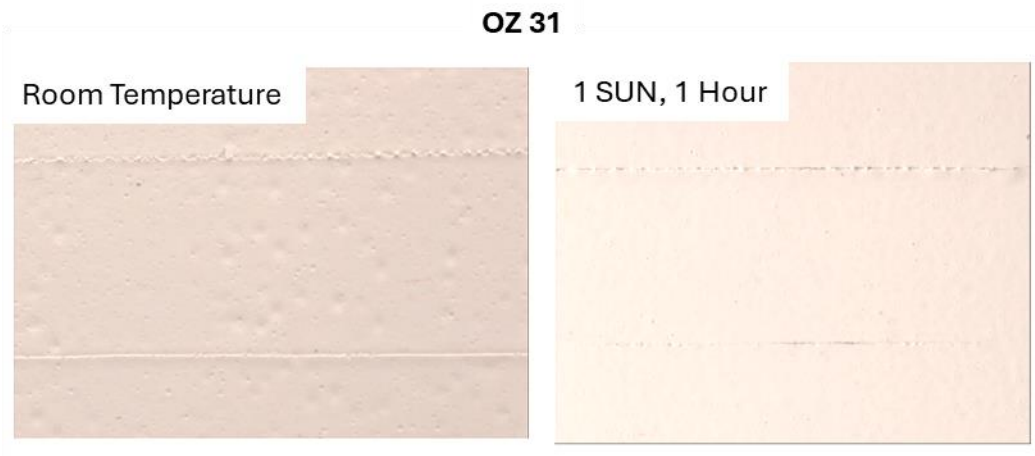

Figure 33: Self-healing on the painted plates

In the images of the plates painted with OZ 31, it is evident that there are partial closures in the scratches. Particularly, it can be observed that the strongly induced damaged line on the plate left under 1 Sun for 1 hour has successfully self-repaired. As seen in Figure 33, closure of scratches has occurred under different conditions. Consequently, our product can provide a new self- healing protection coating for industrial paint applications.

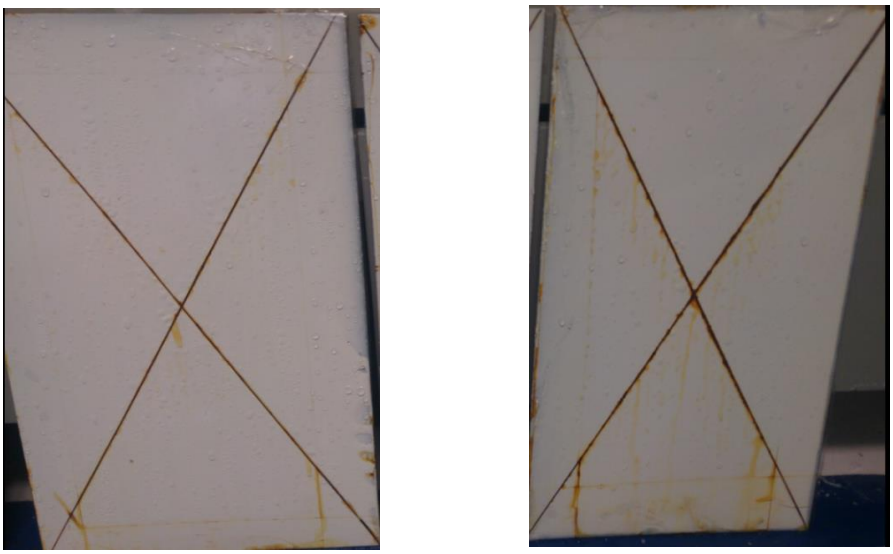

Figure 34: Blister formation on the cross -cut plates after 6 months a) reference b)WPU

Same panels were prepared for the immersion and corrosion test, with a commercial reference and our WPU formulated paint, Figure 34. After the immersion test, two panels showed almost the same level of rust formation and blisters through the crossed substrate surface[113,114]. The corrosion formation was at a competing level with the commercial competitor.

The impact test is a crucial tool in paint chemistry for assessing the performance and durability of coatings when subjected to mechanical stress. It ensures that paints meet industry standards, enhancing the overall quality and reliability of coated products. By simulating real-world conditions where coatings might experience sudden impacts or stresses, the test provides valuable insights into their performance and longevity. Its primary objective is to evaluate the paint's ability to resist deformation and potential damage from impacts, examining adhesion, flexibility, and overall integrity. The test procedure involves dropping a weight, typically a steel ball, from a specified height onto the painted surface and varying the impact force by adjusting the drop height. After the impact, the surface is inspected for any signs of cracking, chipping, or detachment from the substrate. The result often reflects the height from which a weight was dropped to cause failure in the coating.

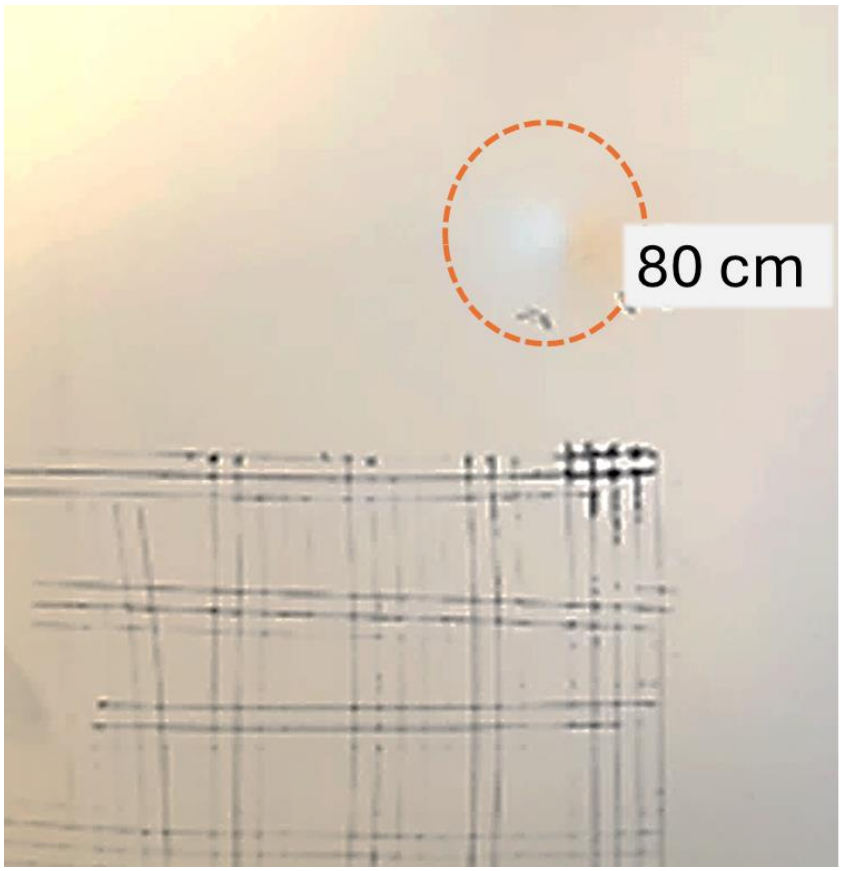

Figure 35: Impact test of WPU-based paint panel

The crosscut test is a widely used method to evaluate the adhesion of a coating to its substrate. This test is crucial in determining how well a paint or coating adheres to the material it is applied to, ensuring its durability and performance in various applications. The primary aim of the crosscut test is to assess the adhesion strength of a coating. Good adhesion is essential for the longevity and effectiveness of the coating, preventing issues like peeling, flaking, or delamination.

As a consequence of the impact test, our plate resisted the impact of 80 cm and the cross-cut test showed that the paint was strongly adhered on the plate shown in Figure 35.

3.5. Other Applications

Through the experiences gained during this project, it has been realized that the formulation and its derivatives can be easily adjusted to various different applications. Our work, which is very promising in terms of both synthesis method and chemical composition, has been redesigned for photothermal materials, energy storage and conversion, and 3D printing, which have gained critical importance in recent years.

3.5.1. Direct-Ink Writing of Waterborne Polyurethanes

Due to the new legislation and restrictions on the usage of solvent-based systems in the field of scaffold and tissue engineering, the replacement of toxic polymeric systems with their non-toxic alternatives is inevitable. Direct Ink Writing (DIW), also known as robocasting, is a type of extrusion-based additive manufacturing technology that offers high-resolution and controllable fabrication of complex structures with minimal material waste where the targeted 3D shapes can be deposited through a nozzle on a digitally controlled movable platform. Unlike conventional molding techniques offering fixed designs, DIW enables greater adaptability in fabricating structures tailored to specific material designs. Although DIW offers numerous advantages, some challenges remain such as preparing environmentally friendly, non-toxic, biocompatible inks at suitable rheological properties having necessary mechanical strengths at the same time. In this sense, waterborne polyurethanes (WPU) are prominent candidates due to their easily tunable chemical and physical properties arising from their segmental structure. While solvent-based PU inks are widely investigated in the literature, there are only a few reports on WPU-based direct writing inks[115–117]. The ability to tailor WPU formulations to mimic native tissue properties while supporting cellular functionality makes it a promising candidate for creating biomimetic constructs in cellular applications. Despite the multitude of advantages offered by WPU bioinks compared to existing polymeric scaffolds, the selection of WPU formulations and

comprehensive rheological analysis remains imperative for distinct applications. In each application scenario, the specific properties of the WPU formulation—such as stiffness, elasticity, degradation behavior, or controlled release capability—play a pivotal role. Conducting thorough rheological analyses aids in selecting the most suitable WPU formulation tailored to the specific requirements of the intended application in tissue engineering or regenerative medicine.

Figure 36: DIW printed WPU meshes

Herein, it was synthesized HDI- polyester polyol-based WPU emulsions via acetone method with high final solid content (45%). Concerning the biocompatibility character of the meshes, the usage of catalysts in the system such as DBTL is also inhibited. We systematically changed the hard segment ratio of WPU dispersions to increase H-bonding concentrations to achieve the required viscosity for ink formulation in direct ink writing (DIW) without external additives. The mechanical properties were investigated by systematic alteration of hard segment ratios (16%-18%-20% respectively) in the WPU main chain, the results are presented in Table 8. We investigated the rheological behavior and shape fidelity of inks under the influence of hard segment ratio in the WPU main chain. Further tests were conducted to determine the impact of the hard segment ratio of the inks on the mechanical properties of the WPU 3D-printed scaffolds.

Table 8: Mechanical Properties of printed WPU meshes

Sample	Mechanical Properties			
	Elastic Modulus (kPa)	Ultimate Tensile Strength (kPa)	Flexural Modulus (kPa)	Ultimate Flexural Strength (KPa)
WPU1	5.8 ± 1%	30 – 35	21.3 ± 1%	435 – 450
WPU2	19.7 ± 2%	830 – 860	56 ± 4%	910 – 940
WPU3	26 ± 2%	1220 – 1290	104 ± 4%	1650 – 1705

Considering the influence of infill patterns on the distribution and transmission of applied loads within printed structures a range of geometrical models were fabricated to demonstrate the effects of infill densities and patterns on the mechanical properties of the WPU scaffolds. Afterward, our non-additive WPU meshes were exposed to biological coating with their DIW versions. The coating of hydrophilic and biologically degradable WPU surfaces with different segmentation ratios was tested in the continuous cell culture. The study demonstrated that coated non-additive WPU formulations have enhanced cellular attachment in continuous culture than non-coated meshes. On the other hand, the least hard segmented, non-additive WPUs had more capability in continuous cell culture which migration of the cell population through mesh pores was observed.

In this sense, as seen in Figure 36, the present WPU inks provide transparent environmentally friendly, cost-effective, ready-to-use, and biocompatible products for tissue engineering applications.

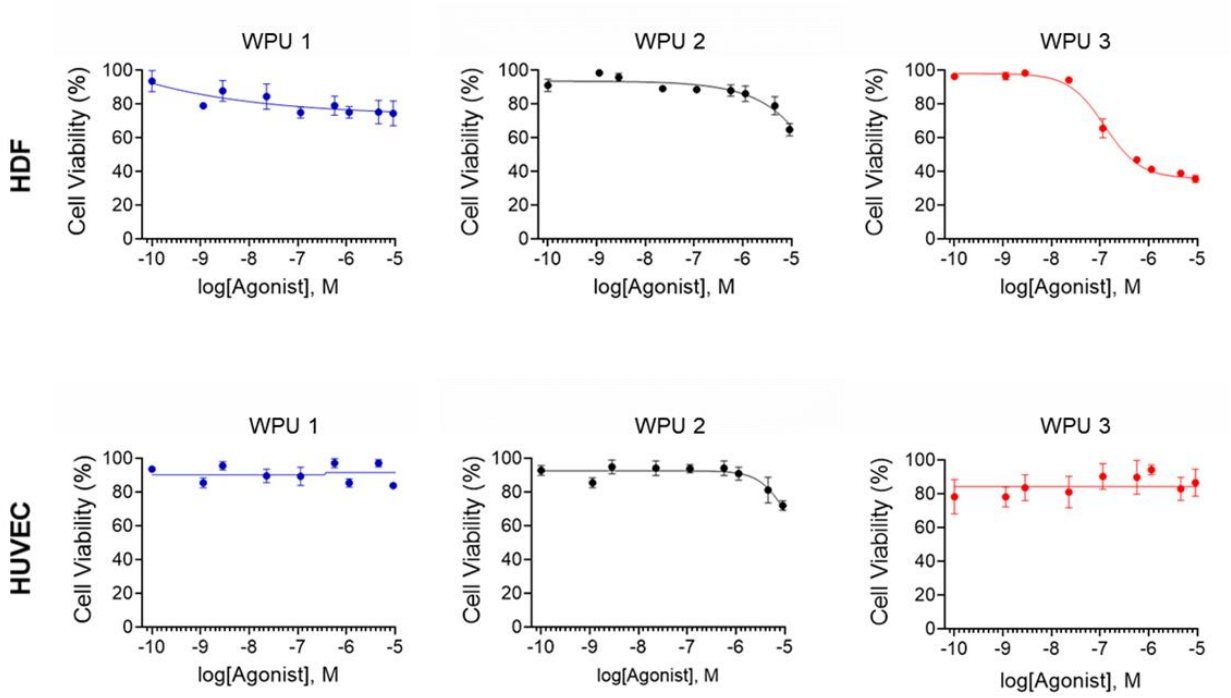

Figure 37: 2D cellular viability results of dissolved meshes. 2D MTT cellular toxicity assay results obtained from human-derived fibroblasts (HDFs) and human vein endothelial cells (HUVECs) determined by dissolved polyurethane mesh formulations. 9 serial dilutions seeded with 7,5 x 105 cells/mL, tested for 72-hour

As seen in Figure 37, 72-hour dissolved WPU meshes cellular toxicity profiles obtained by MTT assay. The results proposed that WPU1 and WPU2 indicate no toxicity even in the highest concentration for both cell lines. On the other hand, WPU3 demonstrated slight toxicity after 50 µg/mL in HDF cell line while no toxicity observed in HUVECs. Therefore, it can be concluded that the increased hard segment ratio causes a potential toxicity in the scaffold. Yet overall, considering the printed mesh concentration, all WPU formulations demonstrated safe cellular viability ranges[118].

On this opportunity, we have already demonstrated the non-toxicity of our WPU films and took advantage of their tunable characteristics to adjust the viscosity, elasticity and rheological properties for 3D direct ink-writing applications.

3.5.2. Fabrication and Testing of Multifunctional, Articulated, Magnetic Fiber Robots in Core-Shell Structure

Robotics and materials science are fields that have developed rapidly in recent years and are tightly integrated. In these fields, magnetic soft materials and robots derived from them have recently come to the forefront. Magnetic soft materials are defined as materials that can change shape or move under a magnetic field. These properties may offer great potential in various industrial and medical application areas. For instance, products made using these materials, such as magnetic grippers, surgical instruments and biomedical devices, are becoming more precise and effective. However, robots derived from magnetic soft materials are also attracting attention. These robots offer potential as devices that can easily enter complex and confined spaces, perform precise movements and even be used in biomedical applications.

The coaxial printing technique is a manufacturing method used in various industries and has gained popularity in recent years, especially in the fields of materials science and robotics. The core-shell structure is obtained by extruding materials through nested nozzles. The inner core material is pressed through a nozzle, while the outer shell material extrudes the inner core. One of the advantages of coaxial printing is that the core and shell materials can be controlled separately, which allows the properties of the core-shell structures to be fine-tuned. Furthermore, it is possible to create complex structures by combining various materials in this way. Coaxial printing can be used in many application areas, such as magnetic soft robots, offering an effective way to increase the flexibility, durability and functionality of structures.

Material selection for magnetic soft robots and similar applications has a significant impact on the performance, durability and functionality of the system. In this context, combining NdFeB magnetic particles and TPU elastomeric polymer can offer several advantages. NdFeB is a strong magnetic material and is known for its high magnetic performance. This material enables magnets to produce a strong and consistent magnetic field, which enables them to be used stably and effectively in magnetic robotic systems . The high magnetic

performance of NdFeB can be used as a powerful driving force for motion and manipulation in robotic systems.

Fiber robots with at least 65% (by weight) magnetic material content were produced in core-shell structure.During core-shell printing, a magnetic field is applied to the nozzle of the printer and magnetic alignment of the particles is ensured. Along a single fiber, different segments are aligned magnetism, that is, an anisotropic and controllable magnetism has been created.

Considering that different pressures are required for filling and printing WPU and NdFeB inks into syringes, the print size and pressure parameters were optimized. Since the obtained fiber robot still retained its transparency after WPU printing, it was observed that the core and shell structure was successfully formed in the Figure 38.

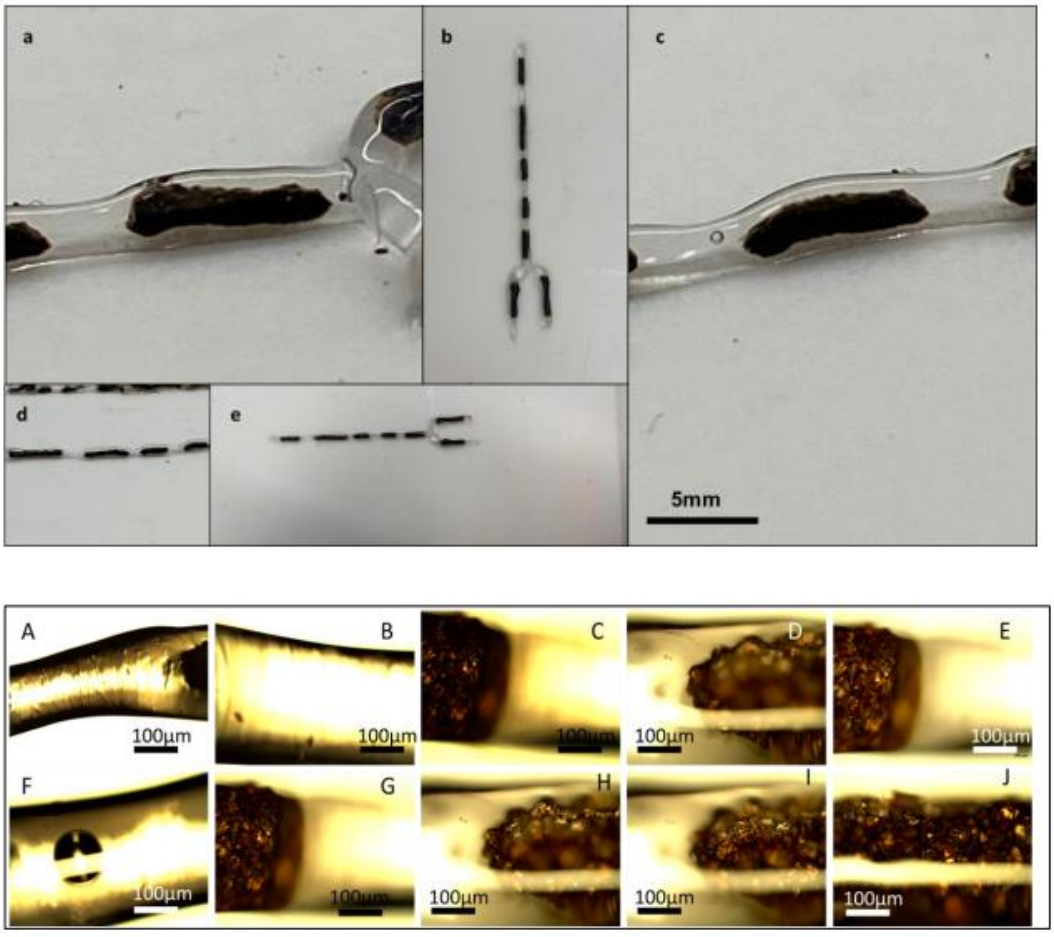

Figure 38: Core-shell structures of printed meshes

3.5.3. Photothermal Waterborne Polydopamine/Polyurethanes with Light- to-Heat Conversion Properties

The hybrid PDA-WPU polymer matrix, created through a simple post-synthesis modification of WPU dispersions with polydopamine, combines the benefits of both components, showing strong photothermal activity along with its easy-to-apply, nanoparticle-free, and eco-friendly nature. The PDA-WPU hybrid polymer matrix effectively combines the features of both WPUs and PDA, yielding photothermal materials that can be easily used as single-component films or coatings for various applications. Therefore, this matrix is a promising candidate for various photo-driven applications.

This study introduces a polydopamine-polyurethane (PDA-WPU) polymer matrix with efficient light-to-heat conversion properties capable of initiating temperature increases when exposed to light. The WPU dispersions are created from WPU solid particles that are synthesized and dispersed in a continuous aqueous phase, resulting in a safe, eco-friendly system free of volatile organic compounds. The formation of PDA-PU particles are shown in Figure 39. The waterborne polydopamine-polyurethane (PDA-WPU) polymer matrix, which has light-to-heat conversion properties, was produced by coating WPU solid particles with PDA in an aqueous dispersion. The polymerization of dopamine monomer in a pre-synthesized aqueous polyurethane dispersion resulted in hybrid particles by coating discrete waterborne polyurethane particles with photothermal polydopamine. The PDA-WPU dispersions exhibited a unimodal particle-size distribution, with particle sizes increasing based on the initial dopamine concentration and polymerization time. Films cast from these dispersions were black-colored, displayed a homogeneous morphology, and had decreasing contact angles with higher PDA content. Compared to neat WPU films, hybrid PDA-WPU films showed improved thermal decomposition behavior and thermal conductivity, while the glass transition temperatures remained unchanged, and mechanical properties were acceptable. Films with the highest polydopamine content reached 105.8 °C after 20 minutes of solar light irradiation at 3 sun and 138.6 °C after 5 minutes of NIR laser irradiation at 800

mW/cm². Additionally, PDA-WPU dispersions were molded into containers to explore their potential in solar-driven water evaporation applications.

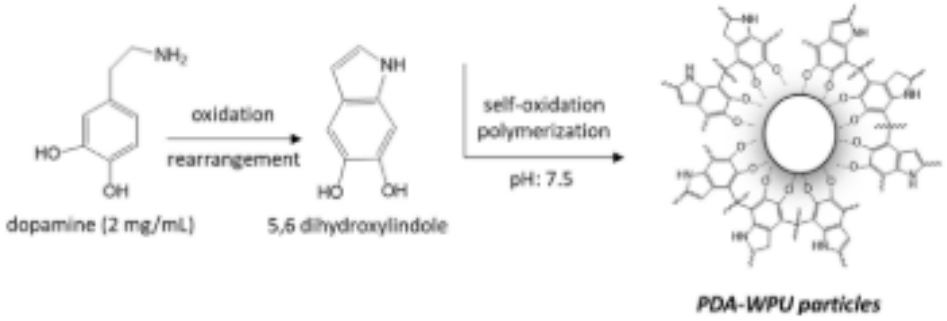

Figure 39: PDA-WPU particles

On the other hand, photothermal effect is a well-known method for the surface disinfection which can physically destroy bacteria. The fact that photothermal disinfection of surfaces provides heat- based killing that can inactivate other pathogens such as viruses as well makes this method a promising tool for a broad range of antimicrobial applications including the development of reusable personal protective equipment. The NIR-induced temperature increases in the waterborne polyurethane/polydopamine matrix enable significant antibacterial activity, leading to efficient light-activated disinfection. This design approach integrates the benefits of WPU and polydopamine into a single polymer matrix, resulting in biocompatible, non-toxic, and environmentally friendly antibacterial coatings. These coatings can be effectively disinfected using NIR light and can be easily applied on a large scale. The WPU-PDA hybrid coatings showed effective photothermal activity, reaching 155°C in just 4 minutes of NIR-laser irradiation and maintaining stability over multiple irradiation cycles. These coatings induced hyperthermia on *S. aureus*, leading to a 3.5 log reduction in viable cells, with their killing activity remaining effective for at least 20 contamination/disinfection cycles. Additionally, the coatings exhibited antibiofilm[119]properties, achieving a 3.9 log reduction in biofilm bacteria viability within 3 minutes of NIR-light exposure through physical disruption. The light-activated antibacterial

and antibiofilm coatings demonstrated here offer significant potential for NIR-light activated surface disinfection (119).

In a similar study, the polyurethane/polydopamine (WPU/PDA) matrix, which showcases the full adhesive properties of PDA, was used to immobilize lysostaphin (Lys), a key anti-staphylococcal agent, creating highly effective antibacterial and antibiofilm surface coatings. The WPU/PDA matrix was prepared by encapsulating WPU particles with PDA in an aqueous dispersion and then applied as coatings on various substrates. Simple incubation of these WPU/PDA-coated surfaces with Lys in an aqueous solution resulted in WPU/PDA/Lys coatings with Lys effectively immobilized on the surface. Non-leaching antibacterial Lys coatings exhibited a potent antibacterial effect on *S. aureus*, achieving a 4 log reduction in viable bacterial counts. Moreover, the WPU-PDA/Lys coatings demonstrated durable enzymatic activity, providing excellent storage and operational stability. Biofilm formation was significantly suppressed, with a 3.5 log reduction in surface-attached bacteria, and the bacteria adhered to the WPU/PDA/Lys coatings were effectively killed by the Lys present on the surface[120].

3.6. Conclusions

This work reports the successful synthesis of self-healing WPU anionomers exhibiting low Tg and high mechanical properties and reveals the crucial role of ionic content on the self-healing performance**.** Although a minimum ionic content (0.8%) is necessary for the preparation of a stable waterborne polyurethane ionomer, 1.6% of ionic content leads to extreme microphase separation sacrificing the mechanical properties. The intrinsic self-healing performance was achieved under favor of the optimized ionic interaction density owing to physical crosslinks in just 24 hours. This optimal ratio of $SO3^{-}Na^{+}$ groups was found as 1.2% for this formulation where the chains were mobile yielding a remarkable self-healing performance. Overall, this environmentally friendly and intrinsically self-healing WPU-1.2 sample potentially possesses a great application window in functional coatings.

CHAPTER 4: ANTI-FOULING MARINE WPU BINDERS

4.1. Abstract

This study offers a unique method for marine coating binder synthesis and design of antifouling paint that use for these issues and aims to reduce the fouling issue without using dangerous biocidal chemicals [121]. Considering these key aspects, waterborne polyurethane (WPU) based resins were designed and synthesized. The low volatile organic compound (VOC) amount, environmentally friendly character and high adhesion capability put forward the anti-fouling WPUs[122]. A series of waterborne polyurethanes with soft segment contents of 85% by weight were synthesized using acetone method using combinations of four (PTMO-PPG-PEG-PDMS) polyols and HDI. The amphiphilic property was tailored by hydrophobic-hydrophilic segments in the WPU main chain. The role of each polyol was investigated via particle size, thermal, mechanical, and surface properties. The optimum amount of hydrophilic PEG1000 polyol was found to be as 6wt% for the preparation of the anti-fouling marine coating at its highest performance.

4.2. Introduction

The term “anti-fouling” refers to all systems designed to prevent organisms from attaching to a surface. Historically, antifouling was associated solely with biocidal compounds[123]. Nowadays, the scope of antifouling strategies has extended and now it also emphasizes green, non-toxic technologies[124]. Fouling-release, on the other hand, pertains to the force needed to detach an organism that has already adhered to a surface.

Marine biofouling includes the growth of organisms like barnacles, algae, and mussels on submerged surfaces, therefore it causes serious environmental and economic problems[124]. They raise the fuel consumption along with the maintenance costs due to regularly recurring applications[125]. Due to the colonization of micro- and macro-organisms on ships or other engineered surfaces, significant impacts occur, including accelerated corrosion, clogging of water pipes, increased fuel consumption, and reduced buoyancy of maritime structures such as ships, nets/meshes, and platforms. Additionally, fouling observed on their surfaces adversely affects shipping speed. Importantly, a bacterial biofilm forms just before the accumulation of macro-organisms like mussels, algae, etc., leading to increased corrosion and the cost of ship maintenance. When antifouling paints are applied to vessels and underwater surfaces, they inhibit the growth and development of microorganisms. The enhanced smoothness resulting from the surface-coating process leads to a notable improvement in water flow overfishing vessels or yachts[126].

Biocides such as tributyltin (TBT) were developed in the mid-20th century and served as the active ingredients in antifouling paints until recently. TBT-based biocidal paints were highly effective in reducing biofouling. However, the use of TBT-based paints has been banned due to their harmful effects on non-target organisms and the environment. In response to this ban, copper, zinc, and various organic compounds have been adopted as the active antifouling components[127].

Traditional marine coating and hull paints contain biocides and toxic chemicals such as harsh solvents, Cu, Ag, Au nanoparticles[126,128]. Yet, new regulations limit the usage of such environmentally polluting materials. Therefore, development of new generation, environmentally friendly paint and coatings is inevitable for the marine coating industry.

However, sea water is a multi-component environment with a complex eco-system. A successful marine coating should be able to withstand several uncontrollable parameters such as: temperature, pH, salinity, oxygen amount and water flow. On the other hand, its formulation should also fulfill the requirements of non-toxicity and high adhesion, durability, and applicability [129,130]. In this manner, waterborne polyurethanes are promising binders enabling the necessary properties as described in Figure 40.

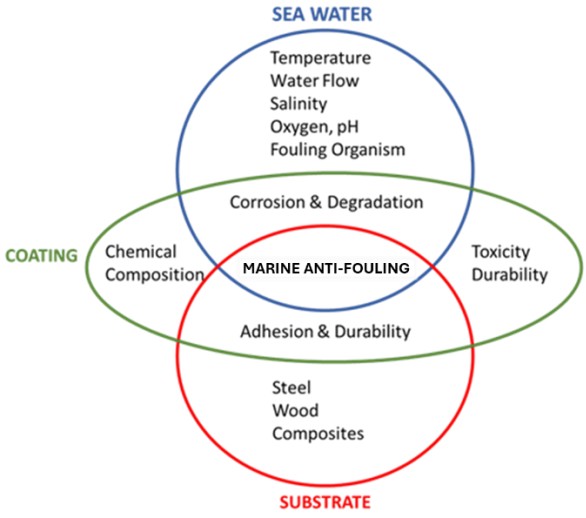

Figure 40: Marine anti-fouling systems

Waterborne polyurethanes (WPUs) are highly versatile materials used in several applications mainly in the paint, coating, adhesive, textile, and biomaterial industries. Due to environmental and public health concerns, new legislation encourages the replacement of conventional solvent-based polyurethanes with WPUs since they exhibit an environmentally friendly character with low VOC level. The key aspect behind their remarkable functionality is the segmental structure, which enables numerous chemical modifications. Hence, their final properties are dictated by the chemistry of the hard and soft segments. While the hard segment is essentially responsible for the mechanical properties, the soft segment is known for controlling thermal stability, crystallinity, molecular mobility, and solvent resistance. Macrodiols i.e.polyols, which constitutes the soft segment, can be chosen depending on the final application requirements. However, utilization of a single polyol system is not always

enough to adjust properties and to overcome the shortcomings of WPUs such as hydrolytic stability, fouling issues, or applicability. Herein, blended polyol composition of soft segment through different polyol combinations having different chemical structure, molecular weight, and physicochemical properties appear as an effective strategy to tine the physico-chemical properties and acquire the desired properties[131]. The complementary roles of varying polyols provide an extended and customized application area.

Amphiphilic polymers possess both hydrophilic and hydrophobic units in their structure and hereby, they play a crucial role in various fields such as surface modification, drug delivery, emulsifiers, environment responsive and biocompatible materials [132]Polyether polyols are one of the most preferred polyol types due to their low cost, remarkable resistance to light and ageing, and stability against hydrolysis. Furthermore, their low viscosity, low cost and hydrophobic properties makes them one of the most preferred polyol types.

Poly(tetramethylene ether) glycol, is especially preferred in high-performance coating, wetting, and elastomer applications[133]. PDMS polyols exhibits super hydrophobic properties thanks to their low surface energy and non-polar structure. On the other hand, they are known for their non-toxic (biocompatible), and inert structure alongside several favorable properties such as; heat stability, oxidation resistance, molecular flexibility, impact resistance and resilience[134]. Poly(oxypropylene) polyols (PPG's) are usually low-viscosity amorphous liquids and are available in a wide variety of molecular weights[135,136]. On the other hand, PEG is a hydrophilic, biocompatible, polymer with very low toxicity and known for its high resistance to protein adsorption and cell adhesion. It is widely used in biomaterials and antifouling applications. PEGylation involves attaching polyethylene glycol (PEG) to a surface. The recent advancement of 'PEGylation' utilizing mussel adhesive proteins suggests that they could be employed to attain high densities of protein-resistant polymers on surfaces[137].

Although the surface energies of poly(ethylene glycol) (PEG) and its oligomers generally exceed the low cell adhesion range defined by Baier, these materials are well known for their resistance to protein adsorption and biofouling. The protein resistance mechanism in high molecular weight PEG is well explained by steric repulsion. Andrade and de Gennes suggested that protein adsorption involves the removal of water from the PEG structure, a

process that is thermodynamically unfavorable due to the confinement of polymer chains, which previously had high conformational entropy[127]

From a broader perspective, researchers focusing on the strong interactions between water molecules and polymers have provided further evidence of the correlation between strong polymer hydration and resistance to protein adsorption. When hydrophilic polymers come into contact with bulk water, water molecules penetrate the polymer film, forming a hydrogen-bond network within the polymers. These highly hydrated polymer films exhibit nonfouling properties; therefore, any reduction in surface hydration may decrease their resistance to nonspecific protein adsorption [138]

Unfortunately, studies are mostly focused on single or double polyol-based polyurethanes. Recently, Meng et coworkers have prepared waterborne polyurethane starting from PTMG and PPG based amphiphilic diol mixture to obtain breathable waterproof textile coatings[139]. Ultimately, Yang et al. have prepared PEG-PPG-PTMG polyol-based binary and ternary waterborne polyurethanes by a modified acetone process[135]. Hence, there is a lack in multicomponent polyol based waterborne polyurethane design and synthesis strategies. To the best of our knowledge, there doesn't exist a systematic study on mixed polyol WPUs with more than three components. In this study, the structure-property relationship of four-blocked polyol WPUs with amphiphilic properties was explored. The amphiphilic behavior was provided by the PTMO-PPG-PDMS-PEG polyol mixture where the hydrophobic segment was balanced with hydrophilic PEG content.

4.3. Materials:

4.3.1. Chemicals:

Hexamethylene diisocyanate (HDI) and PPG polyol (Mn=2000 g/mol) were provided by Covestro. PTMO 2000, Dibutyltin dilaurate (DBTL), ethylenediamine and acetone (99.5 %) were purchased from Sigma-Aldrich. PDMS polyol and AEAS were supplied by Evonik Industry. PVP 10.000 and PEG 1000 was provided by Merck. All polyol ingredients were vacuumed to remove trapped moisture before use, other chemicals were used as received.

Ultrapure Tris base (Tris (hydroxymethyl) aminomethane) was purchased from MP Biomedicals,LLC. Tryptic soy broth (TSB) and agar powder were procured from Medimark (Italy). Staphylococcus aureus (*S. aureus*) (ATCC29213) bacteria were used for the antibacterial activity tests.

4.3.2. Characterization:

Particle size (z-average diameter), size distribution (PDI) WPU micelles were measured by dynamic light scatter (DLS) instrument (Zetasizer Nano - ZS, Malvern Instruments Ltd., UK) equipped with laser diffraction and polarized light detectors at three wavelengths. Dispersions were diluted with deionized water; refractive index of polyurethane is 1.50 and for water index is 1.30. Measurements were performed at room temperature; each measurement was made with three cycles per sample.

The surface hydrophilicity of WPUU films was analyzed by static drop shape analysis system (Kruss Drop Shape Analysis System DSA 10 Mk2) in the air, at 25 ºC.

A ThermoScientific Nicolet iS10 FT-IR spectroscope with an attenuated total reflection (ATR) system was used for the film samples, with 64 scans in the region of 4000 to 600 cm^{-1}.

Thermogravimetric analysis (TGA) of all samples was performed using a Netsch (TGA/DTA) instrument by heating film samples from room temperature up to 600 °C with a rate of 10 °C/min under N_2 atmosphere. Differential scanning calorimetry (DSC) was performed in the temperature range between -100 ºC and 150 ºC with a heating rate of 5 ºC/min by TA Instruments – MDSCQ2000. Reported values were taken from the second heating

Mechanical properties of the films were tested by a universal testing machine (UTM) Zwick Roell Z100, with a load cell of 200 N and a crosshead speed of 25 mm/min. Specimens were prepared according to ASTM D1708-10 standard. An average of at least three replicates was reported for each sample.

The surface morphology of the cast WPU films were monitored using a Zeiss LEO Supra 35VP scanning electron microscope (SEM) by employing a secondary electron detector at ambient temperature, in a vacuum, and at a 5 kV accelerating voltage 5, by coating with Au−Pd.

To analyze the antibacterial properties on the prepared samples, biofilm was formed on polymer films using the static biofilm method. The procedure was completed as follows. S. aureus cells (ATCC 29213) were grown for 24 hours in 3 mL of TSB growth medium at 37 °C and 200 rpm in a shaker incubator. Cells were centrifuged, washed twice with sterile Tris buffer (pH 7.5), and suspended in Tris buffer at a concentration of 10 8 CFU/mL to obtain bacteria solution. Followed, the samples were cut into 1 cm × 1 cm squares. Prepared samples which are 10% PVP, 1-11 +PVP + 3% PEG and PNV-PU and the pure bacterial solution were placed in a 12-well plate. 1.5mL of bacteria solution dropped on the polymer films surfaces to completely cover it. The completed assembly was incubated at 37 °C for 24 hours. To refresh the bacteria solution onto the samples, 0.5 mL of a bacteria solution containing 10 8 CFU/mL was added to the samples on the second day and placed in the incubator overnight. On the third day, the samples were dried in the incubator. The samples were taken out and washed right after incubation in 5 mL of Tris solution. Bacterial suspensions were serially diluted and then plated on TSB agar plates after 2 minutes of vortexing. For 24 hours, plates were incubated at 37 °C. The viability was measured by colony counting and expressed as log 10 CFU/mL.

4.3.3. Synthesis of Waterborne Polyurethanes:

WPU dispersions were synthetized by acetone process and a scheme of the synthesis is represented in Figure 41. The calculated amount of polyol mixture (PTMO, PPG, PDMS and PEG) was poured in a four necked round bottom flask equipped with a thermocouple, mechanical stirrer and condenser. The polyol mixture was degassed under high vacuum to remove all trace moisture in polyols. The isocyanate (HDI) and 0.5 ppm DBTL catalyst were added and the prepolymerization reaction was realized at 80ºC. The NCO was checked with standard di-butyl amine back titration according to ASTM D2572-97. Upon reaching the

theoretical value, chain extension was performed with EDA and AEAS at 50 ºC. Finally, distilled water was added, and phase inversion was established. The acetone was completely removed from the system with vacuum distillation and dispersion with 30% solid content were obtained.

4.3.4. Film Formation:

WPU films were prepared by casting the dispersions into Teflon molds. The dispersion slowly evaporated at room temperature overnight and gradually dried by heating at 70 °C for 2 hours, 120°C for 1 hour. Thereby, homogenous, bubble-free, transparent WPU films (typical film thickness was ≈ 0.2 mm) were obtained. Consequent films were kept in desiccator to avoid moisture absorption and surface contamination.

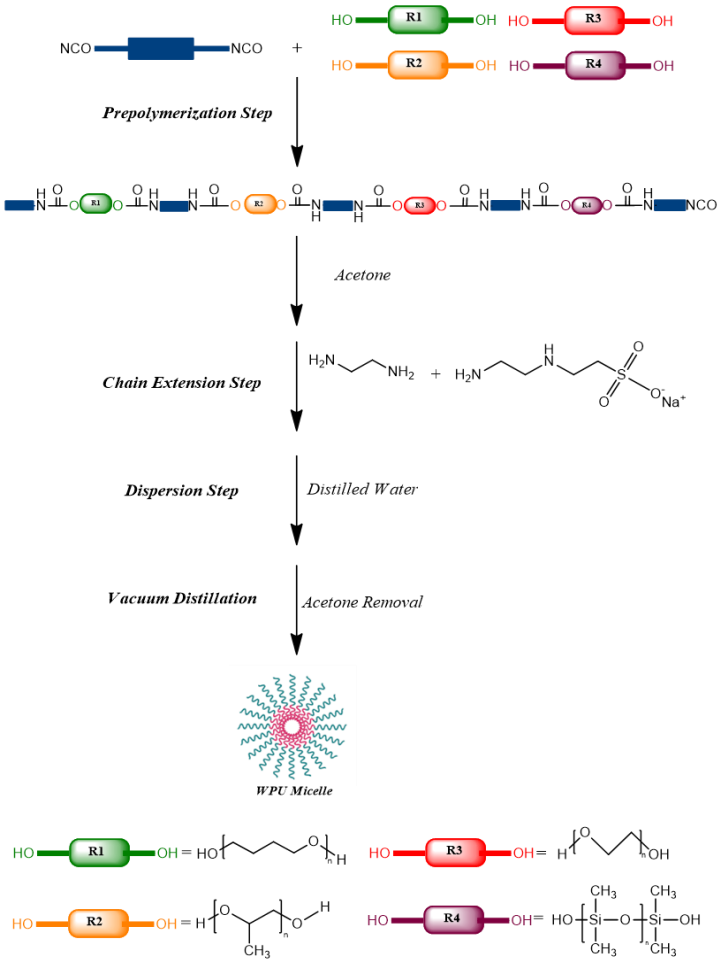

Figure 41:Synthesis Scheme of WPU Dispersions

4.4. Results and Discussion:

The waterborne polyurethane anionomers are stabilized in water by their hydrophilic segments. Herein, AEAS structure with sodium sulphonate groups ($SO3^-Na^+$) were used as ionic chain extender at 1.2 wt%. Yet, amphiphilic characteristics were enhanced by incorporating hydrophilic PEG unit in the soft segment. The hydrophilic content of a WPU anionomer and the balance of hydrophobic-hydrophilic segments is crucial having a great impact on their particle size, surface properties and mechanical properties. Although our preliminary examinations showed that PEG polyol having Mn<1000 g/mol couldn't be sufficient to prepare stable WPU dispersions due to dominance of hydrophobic parts in the chain; using PEG polyol having Mn>1000 g/mol caused a tremendous increment in the viscosity due to augmented molecular weight which devastate the applicability. Hence, in order to investigate the role of each macrodiol in the polyol composition, a series of WPU dispersions have been successfully synthesized and characterized.

Throughout the study, the same experimental procedure was used for all WPU synthesis, except the PTMO-PEG-PDMS-PPG weight ratios in the soft segment. As it is explained in Table 9, a decreasing trend in the PPG content was tuned with varying PTMO, PDMS and PEG 1000 ratios where the hard segment content, chain extension and ionic content parameters were kept constant. Herein, the soft segment constitutes 85%wt of total resin solid and the hard segment forms 15 %wt. It should be noted that PEG diol chains with lower molecular weights were also synthesized but, their resulting films didn't show any anti-fouling performance possibly due to the insufficient PEG content. Similarly, higher molecular weighted PEG diols were also examined yet, due to imbalanced hydrophilicity and the strong tendency of gelation, their resulting dispersions were not successful.

Table 9 :Nomenclature and Formulations of Anti-fouling WPU dispersions

SAMPLE	SOFT SEGMENT				HARD SEGMENT
	PTMO (wt%)	PEG 1000 (wt%)	PDMS (wt%)	PPG (wt%)	HDI (wt%)
WPU-1	30	3	3	49	15
WPU-2	30	6	3	46	15
WPU-3	30	9	3	43	15
WPU-4	35	6	3	41	15
WPU-5	35	6	5	39	15

The effect of PEG content in the composition was studied with an increasing ratio from 3% to 9% wt. It was seen that formulations having more than 9%wt PEG 1000 couldn't be effectively distributed in water and agglomerations were observed due to imbalanced hydrophilicity. In terms of particle size, distribution and mechanical properties, the best dispersion and film were obtained at 6%wt PEG 1000 content. Thereby, to reveal the effect of PTMO and PDMS components, two alterations were made as well, by tuning their proportion in the polyol mixture in samples WPU-4 and WPU-5, respectively. Always keeping PEG 1000 content at 6%wt; PTMO content was increased to 35%wt from 30% and, PDMS ratio was raised from 3% to 5%wt.

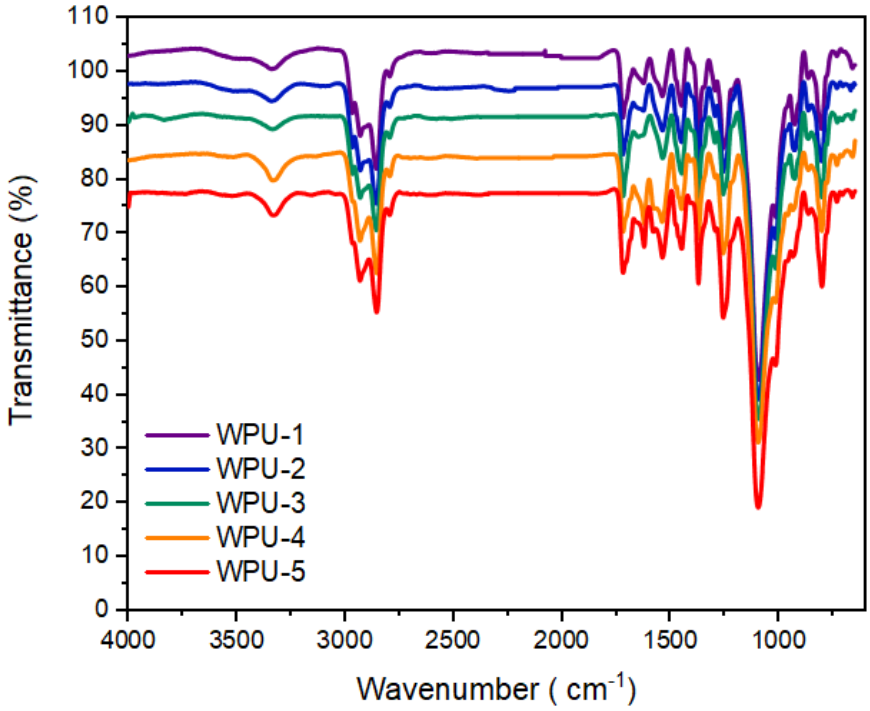

Figure 42: ATR-FTIR Spectra of WPU Films

ATR-FTIR spectra of WPU films were recorded to examine the chemical structure of WPU chains and it is presented in Figure 42. The stretching bands appear at around 3300 cm^{-1}, indicating the presence of NH groups in the WPU structure. Other significant peaks were observed at 1725 cm-1 (C=O groups of urethane), 1640 cm-1 (C=O groups of urea), 1535 cm-1 (C=O-NH groups), 2780-2900 cm^{-1} (–CH_2 stretching), and 1095 cm-1 (ether groups of soft segments), all of which confirmed the formation of WPU products. The successful integration of PDMS unit was also distinguished by peaks at 1090 cm^{-1} (Si-O-Si stretching) and 1260 cm-1 (CH_3 in $SiOCH_3$ symmetry bending).

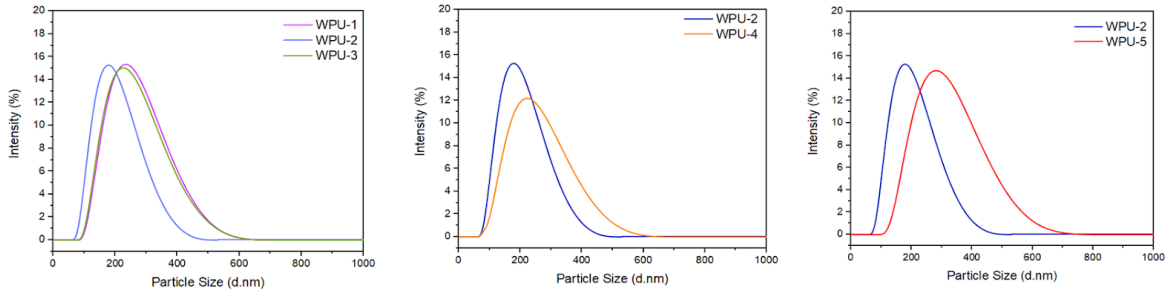

Figure 43: Particle Size Distribution of WPU Dispersion: a) Effect of PEG content b) Effect of PTMO content c) Effect of PDMS content

The particle sizes and distribution profiles of WPU dispersions were presented in Figure 43. It is clearly seen that, all over the dispersions, particle sizes exhibit unimodal distribution. In Figure 43a, the effect of PEG 1000 content was analyzed, and it is seen that the smallest particles (d. nm= 180 nm) were obtained at 6%wt. With increasing PTMO content, the particle size also increased to 210 nm (Figure 43b) and similarly, increasing PDMS ratio resulted in bigger particle size with 230 nm (Figure 43c). The bigger particle size profile observed with enhanced PTMO and PDMS content can be attributed to not only their hydrophobic character but also their pendant methyl groups in the main chain.

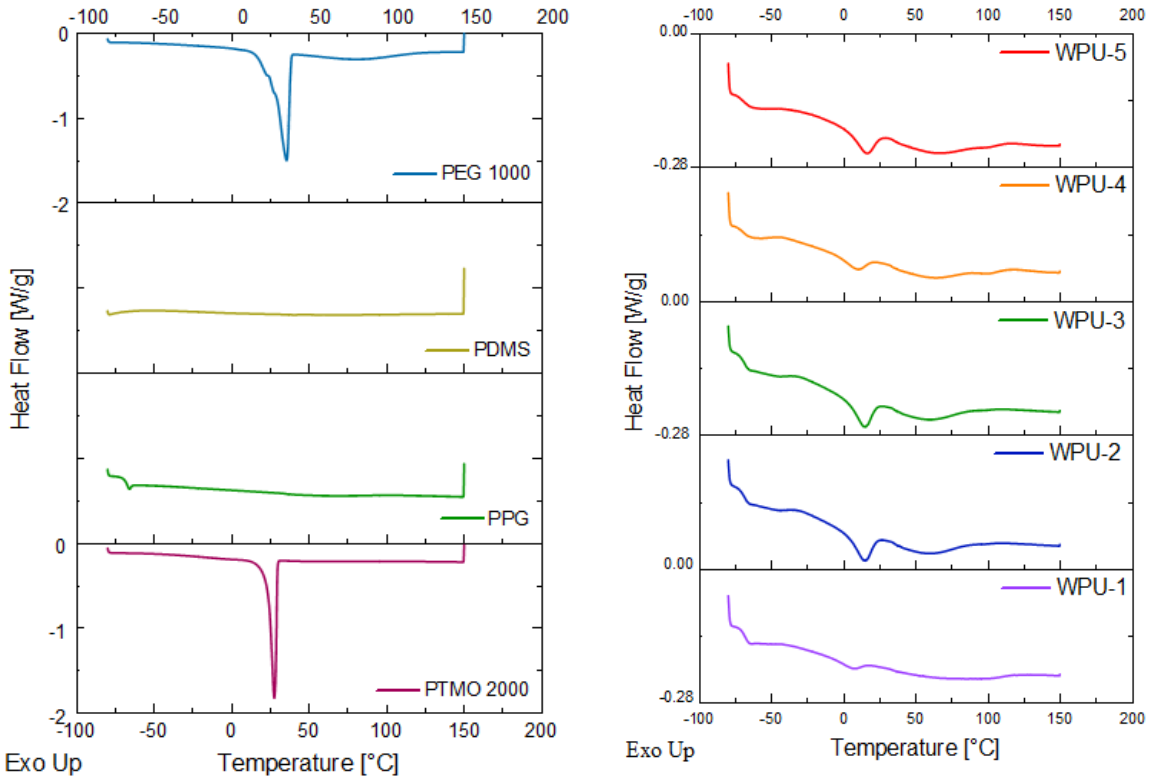

Figure 44: DSC curves a) Polyols b) WPU Films

Table 10: Thermal Properties of WPU Films

Sample	T_{g1}	T_{g2}	T_m
WPU-1	-68.2	8.1	40
WPU-2	-68.5	13.5	42
WPU-3	-67.8	16.5	44
WPU-4	-68.7	13	42
WPU-5	-68.8	20.4	41

It is well known that the soft segment affects the thermal behavior of WPUs therefore, the role of polyols may be identified through their DSC thermograms. Figure 44a represents the DSC studies revealing the glass transition and melt behavior of polyols i,e, PEG, PDMS, PPG and PTMO, respectively, in a broad range between -80 and + 150 C and Figure 38b shows the DSC profiles of all WPU films at different co-soft segment compositions. Glass transition temperatures T_g, melting temperatures T_m. were reported in Table 10.

PTMO 2000 exhibits a sharp melting point at 25 °C , PPG has Tg at -68°C, PDMS shows a slight Tg at –125 ºC and PEG 1000 has a remarkable melting point at 30ºC. All samples show characteristic Tg at around – 68°C coming from PPG Tg values. As PEG content increases, Tm point value increase. (WPU-1 vs WPU-2 vs WPU-3)Increased PTMO content didn't had an significant effect on the Tm and Tg points. Yet, increased PDMS content significantly increases Tm point. (WPU-2 vs WPU-5)

Herein, one of the crucial points is that the WPU films poses two Tg points, which enhances the easy-clean and anti-fouling properties by giving them a soft and slippery surface.

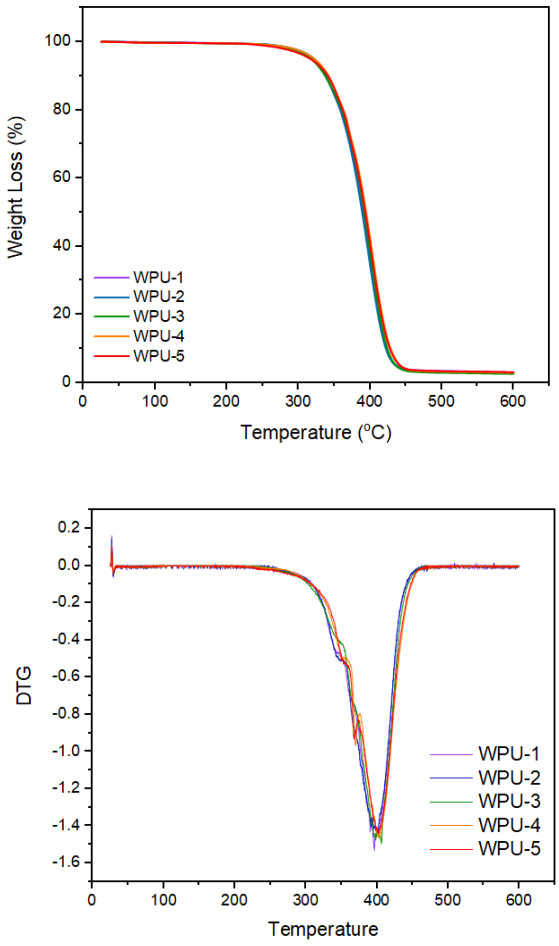

Figure 45: TGA curves of WPU Films

As shown in Figure 45, thermal degradation curves display a slower initial and then a more rapid degradation process, suggesting a two-step mechanism for the degradation. All WPU films showed high thermal stability independent from their polyol composition. The first-weight loss stage, in the temperature range of 300–350 °C, was indicating the decomposition of urethane and urea bonds to form isocyanates, alcohols, primary and secondary amines and olefins and loss of carbon dioxide from the urethane bond. The second degradation stage around 400 °C was attributed to the decomposition of polyether soft segment.

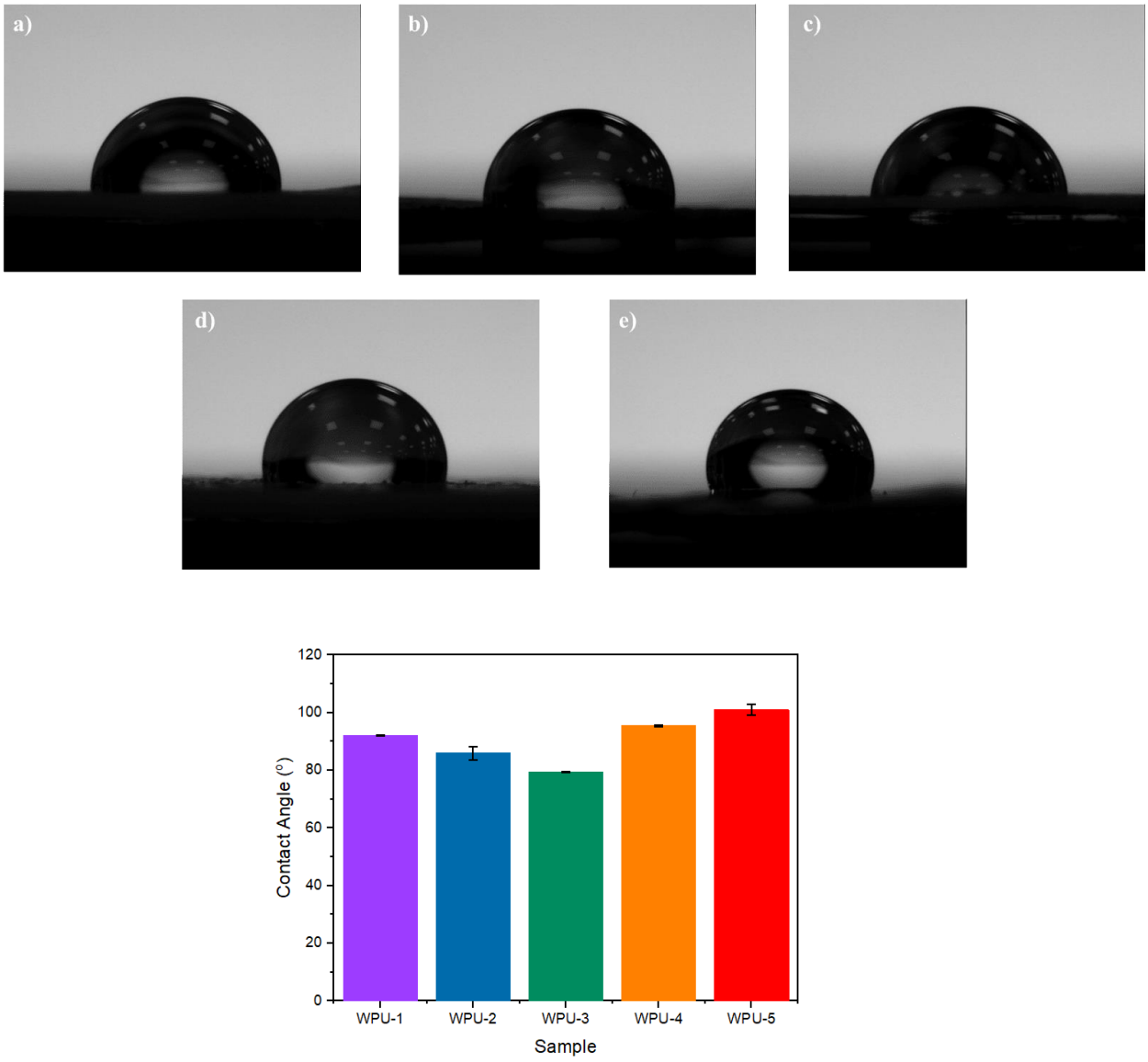

Figure 46: Contact Angle of WPU Films

The surface hydrophilicity plays a key role for WPU applications such as paints and coatings and the water contact angle measurement are a very effective technique in predicting the relative hydrophobicity or hydrophilicity of polymer surfaces. It is known that a water contact angle above 90° indicate a hydrophobic surface whereas a surface is accepted as hydrophilic if the contact angle value is less than 90◦.

The water contact angles, and the data obtained of the WPU films with polyol contents are presented in Figure 46. While the WPU-1, WPU-4 and WPU-5 samples show hydrophobic

surface property, WPU-2 and WPU-3 present hydrophilic surfaces. The contact angles of the samples decreased with an increase in the PEG1000 content in the soft segment, reducing the θ value from 91 º to 80 º indicate more hydrophilic surface. The contact angle for WPU-2 is about 85°**,** whereas it increases to the value of 95° for the WPU-4 sample depending on the increased PTMO content.

Eventually, due to its low surface energy, WPU based on predominantly PDMS soft segments display the highest water contact angles around 101º affirming the formation of extremely hydrophobic surface. Overall, at constant PEG content, comparing WPU-2, WPU-4 and WPU-5 contact angle values are ordered as follows: PDMS>PTMO> PEG polyol.

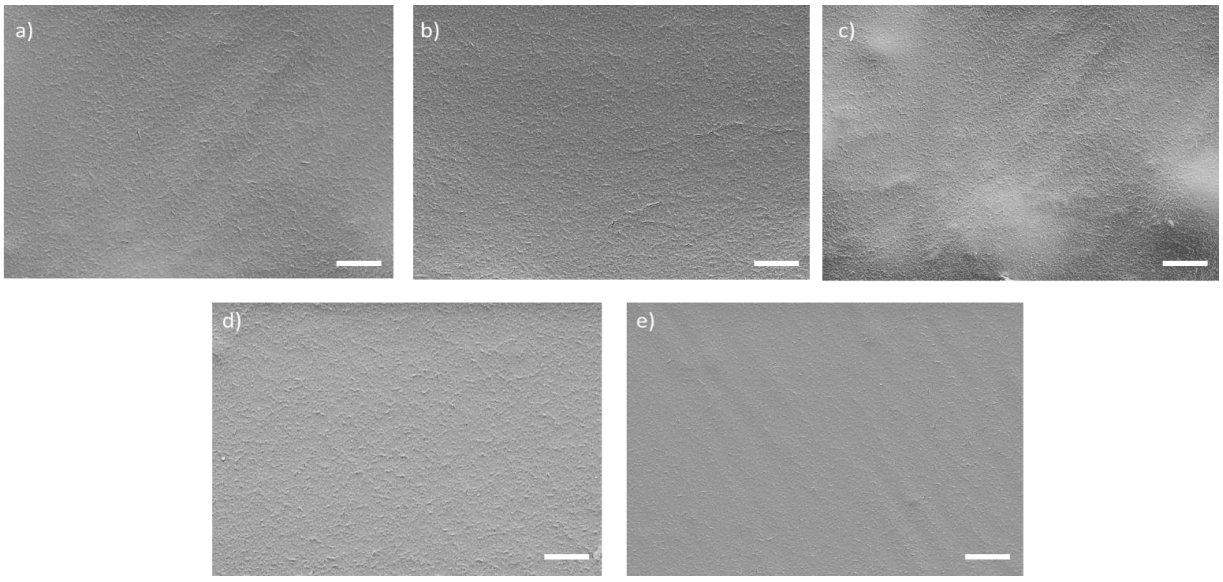

Figure 47: SEM images of WPU Film Surfaces

Surface chemistry plays a crucial role in the formation, stability, and release of fouling organisms adhering to surfaces. The surface of WPU films composed of varied polyols was investigated using SEM to evaluate their surface morphologies. Except Figure 47c, all surfaces present fairly smooth and uniform surfaces which confirms the successful film formation and drying process. However, in Figure 47 a,b,d,e, a rough surface appearance is attractive. Because of increased amount of PEG (9wt%), agglomerated structures have been formed which may be attributed to the formation of excess amount of intermolecular H-bonding and improper amphiphilic balance.

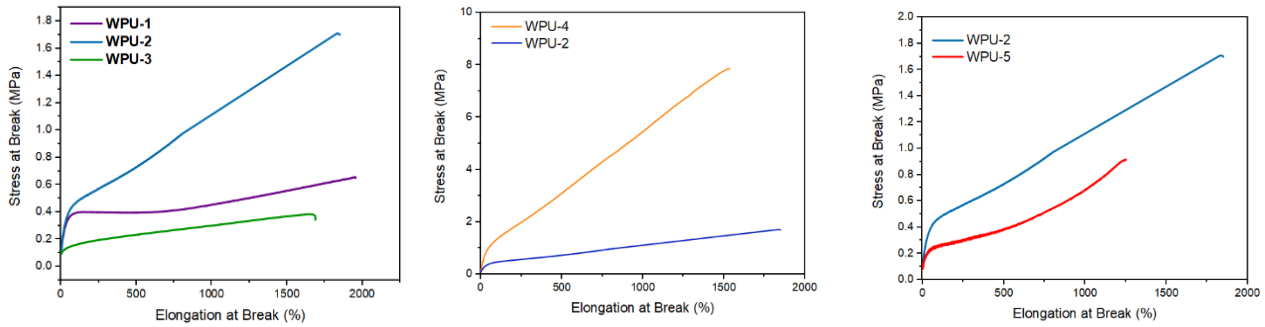

Figure 48:Tensile Properties of WPU Films

Figure 48 shows the stress–strain curves of WPU films. As mentioned before, the incorporation of PEG units requires a sensitive balance. In this manner, it is clearly seen that WPU-2 sample exhibits the highest tensile properties among the PEG variation study due to its optimal amount of PEG 1000 content (6wt%).

Table 11: Mechanical properties of WPU films

	E_t (MPa)	σ_b (MPa)	ε_b (%)
WPU-1	1.28 ± 0.20	0.67 ± 0.10	1938.50 ± 14.40
WPU-2	1.38 ± 0.08	1.75 ± 0.06	1832.00 ± 8.70
WPU-3	0.25 ± 0.02	0.41 ± 0.04	1538.84 ± 161.60
WPU-4	4.43±0.2	7.5± 0.3	1539 ±40
WPU-5	1.45± 0.8	0.8 ±0.01	115 ±12

The increment in PEG content initially enhances the tensile properties, yet, more than 6% PEG cause regression in the mechanical performance likely due to agglomeration which was also seen in Table 11 and Figure 48c. The elongation at break of WPU-2 was higher than that of WPU-4 and WPU-5 which can be attributed to the greater flexibility of PEG chains over PTMO and PDMS polyols. Meanwhile, WPU-4 had the highest Young's modulus (4.4MPa) and stress at break (7.5 MPa) among all WPU films in accordance with its maximum PTMO content. In WPU-5, PDMS content significantly weakened the mechanical properties due to its low molecular weight, low oxygen content and low flexibility.

Within the scope of this study, efforts have been made to improve surface slipperiness by adding polyvinylpyrrolidone (PVP) to the synthesized WPU dispersions using the ex-situ method[140]. PVP is a polymer with a rich methylene content, lipophilic properties, and a flexible chain structure, Figure 49. The lactam groups contained in the pyrrolidone ring impart high polarity to the chain, thus exhibiting hydrophilic properties. PVP is also a highly stable material; it can remain stable without oxidation for up to 100 hours at 60°C in a 3% H_2O_2 solution. Consequently, a stable hydration layer forms between PVP and H_2O molecules, reducing electrostatic forces between biological molecules and the coating, thus preventing adhesion. Utilizing these properties, the aim was to enhance the antifouling characteristic of the synthesized dispersions by adding PVP to the already present hydrophilic PEG chains. The associated problems of bacterial biofilm formation. the surface properties of a hydrophilic poly(vinyl pyrrolidone) coating applied to polyurethane and determined its suitability for use as a urinary tract biomaterial by comparing its lubricity and ability to resist bacterial adherence, lubricity and ability to resist bacterial adherence[140–142].

In this study, PVP with a molecular weight of 10,000 g/mol and the synthesized WPU-1 dispersion were mixed in different ratios to obtain homogeneous films with slippery surfaces. As seen in Figure 49, examinations were conducted with PVP amounts added at 1%, 5%, and 10% of the total weight of the dispersion. Homogeneous and compatible films were successfully obtained with 1% and 5% PVP additions, and the slippery structure becoming prominent on the upper surfaces of the films was noteworthy. It was determined that 10% PVP addition was the maximum limit; at this ratio, the added PVP agglomerated, disrupting the compatibility with the dispersion and negatively affecting film formation by creating phase separation. The successful integration of PVP into the dispersions ex-situ offers both process ease and economic advantages on the path to the target application.

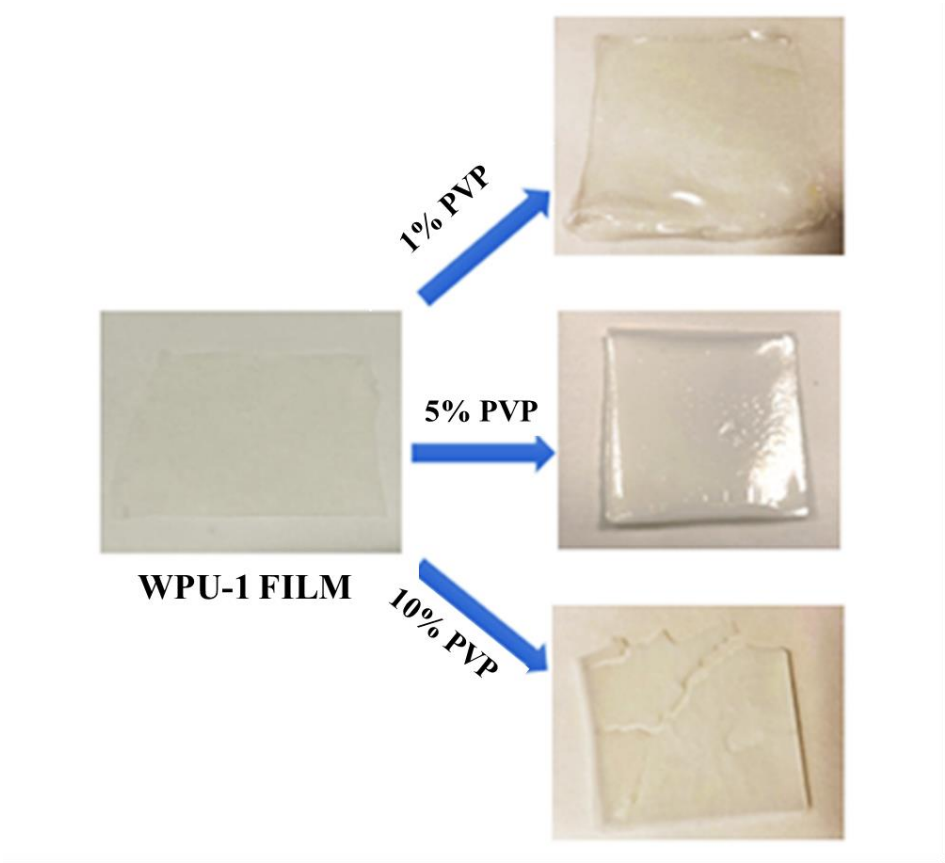

Figure 49: PVP addition into WPU-1 matrice

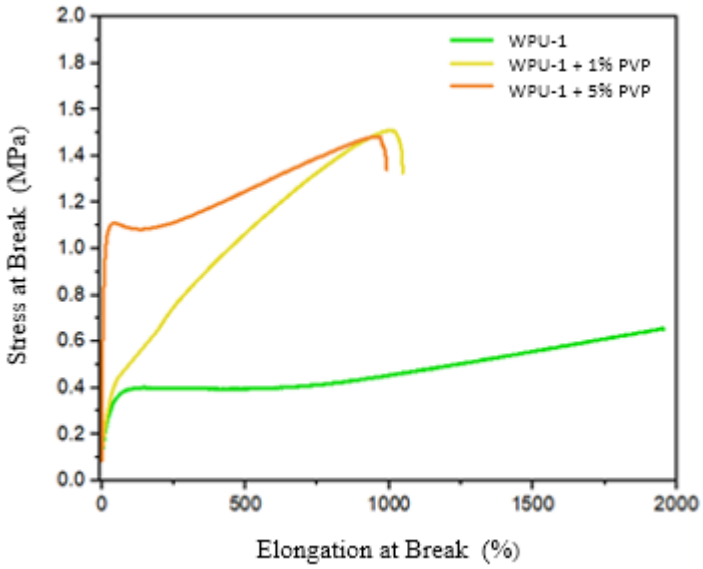

Figure 50: Tensile profiles of PVP added films

The new films obtained by adding PVP were examined using mechanical testing seen in Figure 50. The effect of PVP addition on the mechanical properties was consistent with the literature; depending on the additive added to the polymer matrix, the Young's modulus and tensile strength increased, while the elongation at break values decreased. According to the mechanical test results, there was a significant increase in the Young's modulus of the material in direct proportion to the added PVP additive. As it is reported in Table 12, with the addition of 1% PVP, the Young's modulus value rose to 1.33 MPa, and with the addition of 5% PVP, it showed a 1300% increase, reaching 13.7 MPa .The tensile strength increased by 120% compared to the original film sample, reaching a level of 1.5 MPa. In direct proportion to the amount of added PVP additive, a decrease in the elongation at break values of the material was observed. In the case of 1% PVP additive, the flexibility of the film samples decreased by 48%; with 5% PVP additive, a decrease of 51% occurred.

Table 12: Mechanical properties of PVP loaded films

	E_t (MPa)	σ_β (MPa)	ε_b (%)
WPU-1	1.28	0.67	1938.50
WPU-1 + 1% PVP	1.33	1.50	1006.30
WPU-1 + 5% PVP	13.7	1.49	960.20

The PVP nanofiller added ex-situ to the WPU-1 sample has produced the expected effect on the mechanical properties. Accordingly, the modulus value has increased. Similarly, the stress at break point has also significantly increased. As is commonly observed in matrices with added nanofillers, the elongation amount has decreased, and the elasticity, which was notable in the original films, has diminished. When we look at the tensile graphs, it is also noticeable that the films have moved away from exhibiting elastomeric properties. It was previously explained in earlier sections that the 10% filler does not exhibit the characteristic of forming a homogeneous film.

4.4.2. Biofilm Studies

The antifouling effect of WPU films was also demonstrated with their ability to kill bacteria[143]. WPU films were tested on Pseudomonas aeruginosa, as a Gram-negative model microorganism and *S. aureus*, as a Gram-positive model bacteria[120]. Their anti-fouling and anti-biofilm performance was confirmed by a culture-based method in broth media, with the biofilm formation factor against Gram-positive (S. aureus) and Gram-negative bacterial strains (E. coli).

The antibacterial activity of the WPU films against the S. aureus and P. manas bacteria was evaluated by determining the viability of the bacteria that had been in contact with the film surface[137]. As illustrated in Figure 51, WPU coatings demonstrated strong killing activity. Especially, WPU-3 had an outstanding antibacterial activity against both bacteria species with a 4-log reduction in the number of viable bacteria.

A reduction of 4log against *S. aureus* and 5log against *P.* m*anas* was identified, which means that at least 99% of the bacteria was successfully vanished from the surface. Such antimicrobial effect of PEG units with antimicrobial activity was reported earlier[137].

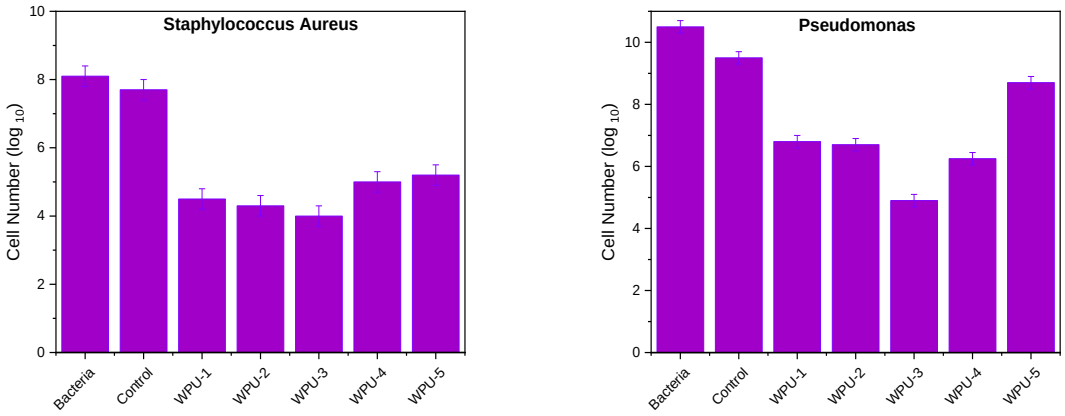

Figure 51: Biofilm test results against a) S. aureus b) P.monas

4.4.3. Antifouling Paint Examinations

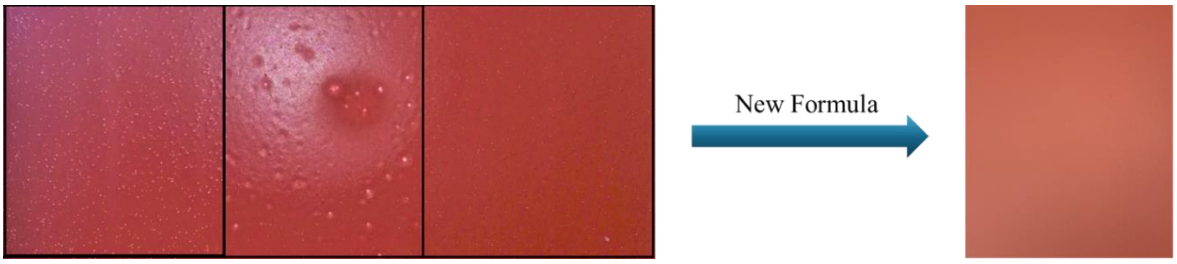

Figure 52: Surface Improvement with new formula

When applied, large silicone voids were observed on the surface. Therefore, the surface agent was removed from the formula, suspecting an excess presence. Although the silicone voids disappeared in the modified formula, a spreading issue was noticed on the surface, leading to a reduction in the co-solvent ratio. In light of this information, a new formula devoid of co-solvent, wetting agent, and surface agent was introduced. To prevent foam formation in this formula, a foam suppressant was added. The application of this formula has been determined to yield the best surface achieved so far as seen in Figure 52.

Table 13: Paint formulation of the Anti-fouling Paint

PAINT INGREDIENTS	
Resin	68%
Calcite	20%
Iron Oxide	6%
Anti-Foaming Agent	0.3%
Dispersant	0.7%
Thickener	0.5%
pH Regulator	0.05%

Metal plates were painted with the WPU-based biofouling paints to investigate their adhesion and impact tests. The results showed that the dry paints showed high impact resistance and adhesion, at best, GT0 level. Drying time was also observed to be impressively fast. On the other hand, regarding the long-term exposition to marine environment, contact angle measurements were also performed and seen that the paint could remain its hydrophobicity for a long period of time. Initially, the coating showed a superhydrophobic nature, upon exposure the sea water, the contact angle values were relatively reduced. Yet, the hydrophobicity was kept constant over time at 98 ± 1 º. The adhesion of the paint, which form a soft and flexible film, was determined to be at GT 0 level, and their impact resistance was found to be 70 kg.cm, as shown in the Figure 53.

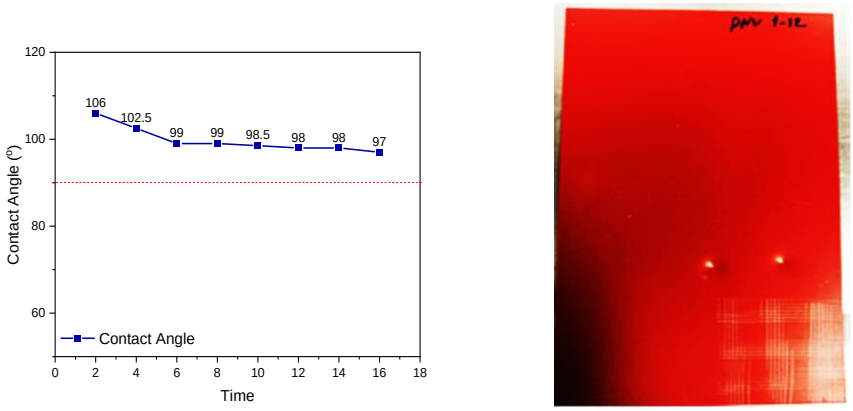

Figure 53: WPU based hull paint characterizations a) Contect angle b) Impact test

To conduct a comparative test in the sea, a similar application was carried out using a water-based acrylic binder (222-T) in the same formula for the paint to be used as a blank. The prepared panels were placed in the cage system located at Poliport harbor and submerged in the sea to be checked every five months. In order to see the real-life applicability of our material, painted plates were submersed into Marmara Sea and their surfaces were observed for 5 months. At the end of the examination period, plates were taken out. It was obviously seen in the Figure 54, the plates painted with the anti-fouling WPU based biofouling paint had a smoother and cleaner surface compared to the control panel. The control panel had much more fouling issue than theWPU-2 painted plate. These results were such promising that the application experiments took a step forward and a real boat was decided to paint with our WPU-2 based paint.

In order to see the real-life applicability of our material, painted plates were submersed into Marmara Sea and their surfaces were observed for 5 months. At the end of the examination period, plates were taken out. It was obviously seen in Figure 54, the plates painted with our WPU based biofouling paint had a smoother and cleaner surface compared to the control panel. The control panel had much more fouling issue than our WPU painted plate. These results were such promising that, the application experiments took a step forward and a real boat was decided to paint with our WPU based paint.

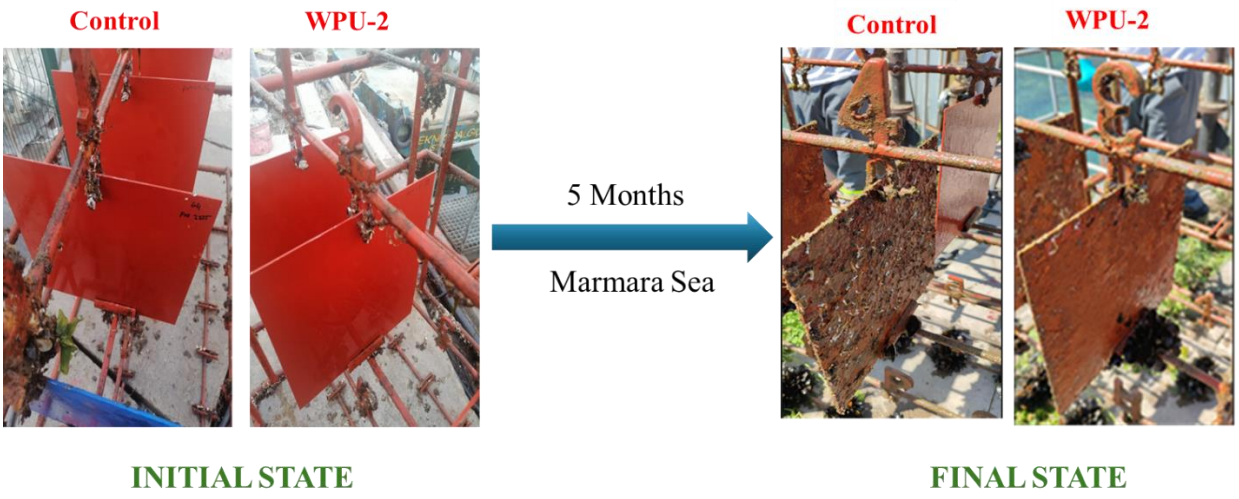

Figure 54: Plates submerged into Marmara Sea

The paint made with the WPU-2 binder, which was hung in position number 3 in the test cage and sent most recently, showed minimal contamination after 5 months. Having seen the successful preliminary studies, the WPU dispersion is scaled-up and the produced paint is applied on a fishing boat. The boat has been investigated for 3 months and at the end of season, it was seen that the biofilm formation was in a minimum level (Figure 55). Moreover, the surface could be easily cleaned with standard tools such as sponge. There was no barnacle or oyster like marine creature which could be attached if the coating was not successful. There was only a superficial layer of moss which was easily detached from the surface.

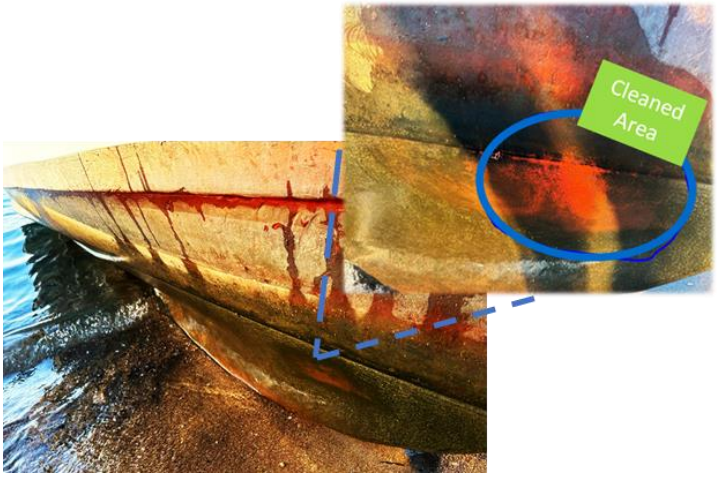

Figure 55: Fishing boat coated with WPU-based anti-fouling paint

4.5. Other Applications

4.5.1. Waterborne Polydopamine-Polyurethane/Polyethylene Glycol- Based Phase Change Films for Solar-to-Thermal Energy Conversion and Storage

Form-stable phase change films composed of a polydopamine-polyurethane polymer matrix with photothermal conversion properties and polyethylene glycol (PEG) are described. To create these films, environmentally friendly waterborne polyurethane (WPU) particles in aqueous dispersions were coated with polydopamine, resulting in a stable waterborne dispersion of the polydopamine-polyurethane (PDA-WPU) matrix with notable photothermal conversion properties. PEG was then directly mixed into the PDA-WPU matrix in its dispersion form. Successful film formation was achieved at a PDA-WPU to PEG ratio of 1:1 and higher, leading to form-stable, homogeneous PDA-WPU/PEG phase change films. The incorporation of PEG into the amorphous PDA-WPU matrix imparted a semicrystalline structure, enhancing the films' thermal stability and thermal conductivity. As the PEG content increased, the Young's modulus of the PDA-WPU/PEG films rose, while tensile strength and elongation at break decreased, although the films remained flexible. For the films with the highest PEG content (PDA-WPU1:1), the melting and solidifying enthalpies were 81.1 and 77.9 J/g, respectively, and these enthalpies remained stable over 60 heating-cooling cycles. Under 20 minutes of solar irradiation at 150 mW/cm², the PDA-WPU 1:1 film reached 74.8°C, with a solar-to-thermal energy conversion efficiency of 72.9%. In colder environments, the PDA-WPU/PEG films and their surroundings heated up more and retained warmth longer than control samples under solar light. After 30 minutes of sunlight exposure, the temperature around the PDA-WPU/PEG film was 10°C higher than that of the control environment, and it took 10 minutes longer to cool down to ambient temperature once sunlight was stopped. These form-stable, flexible, and durable films efficiently capture and store solar energy, showing strong potential as solar-driven thermoregulating materials[144].

4.6. Conclusions

The first examples of four component co-soft segmented waterborne polyurethanes are successfully synthesized via acetone method. PPG, PTMO, PDMS and PEG polyols are found to be compatible with each other up to a certain ratio. The molecular weight of PEG is found to be highly critical to obtain a well-defined WPU dispersion. Low molecular weight PEG polyol may not balance the hydrophobicity of the rest of the chain; high molecular weight PEG polyol may cause viscosity problems due to enhanced intermolecular H-bonds and entanglement (agglomeration).
This specific WPU formulation is a promising candidate for paint applications thanks to its low modulus and high hydrolytic stability. Furthermore, PEG units potentially provide biocompatible and biofouling properties.

Novel antifouling marine coating binders were successfully synthesized and provided to the industry in order to produce a complete paint formulation. Meanwhile, new experiments with PVP addition were done to increase lubricancy on the surface. The present paint formulation was found to be compatible and stable, so we passed to the next step and started to test them in real-world conditions. Upon immersion test into Marmara sea for 5 months, it was seen that the panel coated with our product was really free-of fouling, showing a remarkable performance even better than the commercial competitor. Therefore, a fishing boat was painted and observed. At the end of the season, there couldn’t be found any barnacle or sea creature attached to the surface.

CHAPTER 5: UV-CURABLE WATERBORNE POLYURETHANE DISPERSIONS AND FILMS

5.1. Abstract

The increasing demand for environmentally friendly materials and cleaner productions has made the substitution of conventional solvent-based systems and high energy-requiring processes with promising alternatives essential. In this sense, waterborne polyurethanes [145],[146] are prominent candidates since they form resistant, durable, flexible, non-toxic products[147] with a negligible amount of volatile organic compounds (VOC), which are widely used in coatings[148], adhesives[149],[150], textiles[151], inks[152], and corrosion resistance applications[153]. Although they already exhibit many outstanding properties, several approaches have been developed to enhance their mechanical, physical, and chemical properties. Studies have mostly focused on cross-linking[154], nanoparticle addition[155], [156],[157] and end-group modifications[158] strategies.

5.2. Introduction

UV active polymers may respond to different types of irradiations, at different wavelengths (or frequencies/energies) such as UV-Vis-NIR or sunlight. The wavelength ranges are : UV-C (100–280 nm), UV-B (280–315 nm), UV-A (315–400 nm), visible (400–780 nm), near-infrared (NIR) (780–2500 nm), and the solar irradiation covering the UV-Vis–NIR region.

UV irradiation has a lower wavelength and higher energy. Therefore, it is highly capable to penetrate deep tissues and probably damage the living tissue besides the possibility of destructing the microstructure of the polymer network as well. Consequently, UV-irradiated polymers are commonly used for in-vitro and industrial applications such as photo-curing coating systems or stimulating the shape memory behavior of polymers. The UV-activation may be endowed with functional groups such as vinyl, acrylate or methacrylate derivatives.

Photo-curing systems have received great attention over the last years where the uncured system can be cured via photochemical reactions by photon irradiation and form a crosslinked (tridimensional) network. This process can be classified as "green" approach since it provides an environmentally friendly method with energy saving, low cost, and easy applicability at mild temperatures, even via portable devices[159].

Therefore, this technology has become crucial for the polymer and coating industry to protect porous substrates like wood and paper, besides the adhesives, inks, and paints for a wide range of substrates, textile fabrics, anti-wrinkle applications, plastics, and leather where the drying stage can be dramatically shortened thanks to UV-curing[160][161][162][163].

In polyurethanes, the curing process is generally carried out with UV irradiation rather than moisture curing, radiation curing or thermal curing methods. Herein, the crucial parameters that affect the final properties of the cured structure can be classified into two main groups: 1) Curing parameters 2) Chemical Structure and composition. The curing parameters such as, the light source, wavelength, the distance between the specimen and the curing time can differ and easily optimized depending on each specific case. On the other hand, the structure of the polyurethane and the type, concentration, and compatibility of photoinitiator, and/or the filler's nature compose the chemical parameters. The UV-curable PU systems consist of a UV-active PU chain, photoiniator and a reactive diluent that reduces the system's viscosity.

The UV-active PU chains should bear vinyl groups, generally they contain photo-active acrylate or acrylate derivatives such as methacrylates.

The acrylate groups are able to easily polymerize upon UV irradiation and form crosslinked networks. These kinds of systems are also called polyurethane-acrylate (PUA) and have been subject to many studies since the structure of PUA eventually affects the polymerization

kinetics and the final properties of the cured films. As acrylate double bonds undergo polymerization, the hardness of the PUA coating increases with the formation of a glassy, chemically resistant material.

In this manner, the drying time, gelation points, rheological behaviors, mechanical and thermal properties are the primary behaviors getting affected[164].

In the system, another light sensitive moiety, the photoinitiator (PI) has an essential role as it absorbs UV light at a certain wavelength from the source and initiate the chemical reaction instantly, moreover, to control both the initiation rate and the penetration depth of the incident light. The photoinitior thus induces the polymerization of acrylate and the curing process can be accomplished. The chemistry of the photoinitior and its compatibility with the surrounding PU medium is also a highly crucial parameter that directly affects the final properties of the cured material. In UV-curable polyurethane combination, the most preferred photonitiators are such: Darocur 1173, Darocur 2959, Irgacure 184, Irgacure 819, Irgacure 2959, Irgacure 651, Irgacure 1173 ,and Darocur 4265.

The crosslinking density is a crucial parameter in the cured network. The control of the double bond content of the acrylate incorporated into the PU structure greatly influences the polymer's final properties and higher double bond concentration will provide films with a higher crosslink density after curing. While the cross-linking density brings high mechanical performance of material and hardness, it also yields brittleness, the elongation at break faces the risk of dropping dramatically. So, the crosslinking density should be controlled and kept at a certain level. The photoinitiator concentration is a key parameter as well as it dominates the C=C intensity and distribution over the system.

This photochemical reaction can be followed by an FTIR instrument, focusing on the disappearance of C=C double bonds. Furthermore, the C—C conversion rate and the kinetics of the curing process can be monitored via real-time FTIR (RT-IR)[165].

Several groundbreaking studies have been conducted to extend the application range of UV-Curable PUs. For instance, Wu et al. have used UV-Curable Polyurethane acrylates as polymer electrolytes in lithium metal batteries where the crosslinked PUA network was filled with TiO_2 particles[166]. Che et al. prepared a tree dimensional network with UV-curable PUA

resin to form a composite material with copper nanowires (Cu NWs) to bridge the modified hBN. The uncured hBN@PEI–Cu NWs/PUA composite precursor was loaded into a syringe and accurately injected into the interface voids. After a short time to fully penetrate and fill the void, it is irradiated by UV light until it cures, and the formed composites that perfectly fit with the shape of the mold and can be taken out individually in addition to great insulating properties and thermal conductivity[167].

Bakhshandeh et al. have prepared a siloxane modified UV-curable waterborne acrylate polyurethane with a three-step method in acetone. The soft segment was composed of PDMS and PTMG, IPDI was used as the isocyanate, chains were extended with DMPA, acrylate groups were incorporated with HEMA and hydroquinone (HQ) was used as inhibitor. They used a specific photo-rheometer to observe the in situ chemical and mechanical characteristics during photopolymerization reaction. After evaluating the effect of Mw of PDMS, enhanced drying time and gelation points were observed upon increasing Mw and content of PDMS with a reduction of the final storage modulus proving incomplete curing of the Si-WPUA sample affected by flexible PDMS chains[164].

Gobert et al., have found a new slant on the large-scale production of UV-PUDs based on the optimization of the neutralization and dispersion processes and both steps were combined in a single full continuous setup. Consequently, they claimed that continuous processing using static mixers and high-shear mixing is a viable option for the neutralization and dispersion of UV-PUDs. Indeed, this study revealed that neutralization step is mixing-sensitive, and the temperature of the neutralized prepolymer influences the particle size, yet the amount of shear force applied during the dispersion step has a limited effect on the particle size[168].

Recently, Xu et al. developed a new biomass silicone/vaniline based UV-curable polyurethane pressure sensitive adhesive for functional glass application. They decorated the vaniline with double bonds via the reaction with methacrylic anhydride and then, prepared silicone/vaniline monomers which polymerized with PU prepolymers under UV irradiation. The introduction of silicone/vaniline monomer into polyurethane matrix, improves the residual carbon rate and the ball number, 180◦ peel strength and shear strength[169] .

Waterborne UV-curable coatings are crosslinked through a two-step process: water evaporation, and UV-curing. Before applying the UV-WPU dispersions on a substrate, the

photo-polymerizer is added to the solution, which is then exposed to a temperature for the evaporation of water. There are several methods for preparing UV-WPU coatings, such as physical blending, emulsion polymerization, and the interpenetrating polymer network (IPN)-based technique. The most preferred method is to end-chain polyurethane with a single-hydroxyl acrylate or to introduce a double bond from hydroxyl-terminated polybutadiene, or even to incorporate vinyl groups into the polymer[160].

In UV-curable systems, the waterborne PU systems have a special place. In the case of waterbased systems, the photoinitiator must be uniformly distributed in the film after the drying stage. For most PIs, this can be achieved only by incorporating the photoinitiator into the PUA resin before dispersion in water. The PI molecules will remain in the micelles and, after coalescence upon water removal, they will be randomly distributed in the dry coating[170].

The ultraviolet light absorbed by the photoinitiator produces free radicals that promote the reaction between the prepolymer and the reactive monomers or diluents, generating the cured films. The dispersion stability and particle size, in addition to the product's final properties, will be influenced by the ionic group's content, rigid/flexible segments molar ratio, structure of the monomers, neutralization degree, acrylate double bond percentage, curing conditions, photoinitiator amount, and others. Moreover, the reaction parameters, such as temperature, stirring, component's feeding rate, and order of addition, significantly affect the aqueous dispersion properties.

Highly branched structures, combining short chains via branching points, play a crucial role in polymer science since they possess multiple functional end groups allowing further modifications for versatile materials[171],[172]. The first hyperbranched polyurethane architectures were reported by Spindler and Fréchet by using AB_2 monomers with protected or blocked isocyanates[173], Kumar and Ramaknishnan were conducted *in-situ* synthesis to achieve aromatic hyperbranched polyurethanes[174]. Furthermore, researches revealed that the oligomeric A_2+B_3 approach provides a greater number of possible functionalization to combine complementary properties depending on the target application, even in large scale production[175],[176]. By means of this approach, Bruchmann and Schrepp were synthesized hyperbranched poly(urethane urea)s from commercially available isocyanates[177]. Recently,

the oligomeric A_2+B_3 approach, wherein A_2 is an isocyanate end-capped difunctional oligomer and B_3 is a triamine monomer, was reported for the synthesis of highly branched poly(urethane urea) elastomers[178] and highly branched waterborne polyurethane acrylates[179].

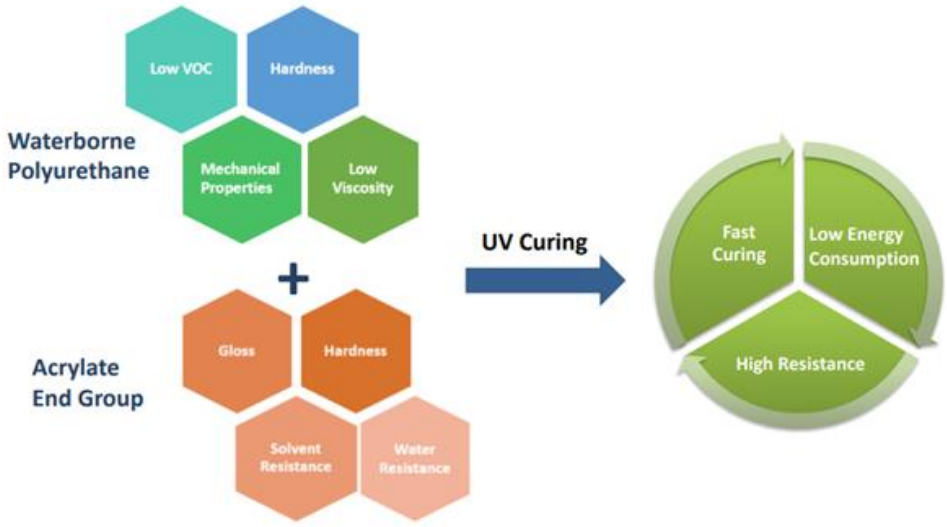

Figure 56: Properties of UV-curable WPUs

There has been little report in the literature on the synthesis and characterizations of UV-curable waterborne highly branched polyurethane dispersions focusing on the crosslinking efficiency, thermal and mechanical properties. In this study, novel methacrylate end functionalized highly branched waterborne poly(urethane-urea) dispersions (HBWPUD)s were synthesized via A_2+B_3 approach, without using any catalyst. As seen in Figure 56, the UV-cured films were prepared to investigate the complementary effect of A_2: B_3 ratio, photoinitiator concentration and curing energy on the final film properties.

5.3. Materials and Methods

5.3.1. Chemicals

Hexamethylene diisocyanate (HDI) and polyol of adipic acid/ diethylene glycol/ butanediol/ ethylene glycol (M_n=1060 g/mol) were provided by Bayer Material Science. Sodium 2-[(2-aminoethyl)amino]ethanesulphonate (AEAS) was kindly donated by Evonik Industries. Diethylene triamine and acetone (99.5 %) were purchased from Sigma-Aldrich. 2-isocynatoethyl methacrylate was provided from abcr (GmbH) and Irgacure 500 (50wt. % 1-Hydroxy-cyclohexyl-phenyl-ketone, 50 wt. % Benzophenone) was provided from BASF. Polyol was degassed by vacuum at 100 ^oC for 15 minutes before usage.

5.3.2. Synthesis of Highly Branched Waterborne Polyurethane Dispersions (HBWPUD)s

As shown in Figure 53, the highly branched waterborne polyurethane dispersions (HBWPUD)s were synthesized via the oligomeric A_2+B_3 method in four steps. The same reaction protocol was applied for the synthesis of HBWPUD-1 and HBWPUD-2 with the different A_2:B_3 ratios, which were 0.80 and 0.65, respectively. The dispersion formulations expressed as equivalents of the components were summarized in Table 12. The polyester polyol and HDI were fed at pre-calculated amounts into four-necked, round bottomed flask equipped with a thermocouple, reflux condenser, and an overhead mechanical stirrer. The pre-polymerization reaction was kept at 80 ^oC until the actual -NCO content reaches the theoretical -NCO content, which was regularly controlled by the standard dibutylamine back-titration method (ASTM D2572-97). The prepolymer was cooled down to 60 ^oC, acetone was added dropwise to dissolve -NCO terminated prepolymer. Afterwards, the chain extension

(emulsification) was realized with the addition of AEAS/water via addition-funnel; thus, A_2 oligomer was obtained.

The B_3 oligomeric structure, composed of diethylenetriamine/acetone/water mixture, was prepared in a separated round bottomed reaction flask. The prefabricated A_2 prepolymer was slowly poured into the B_3 system at 50 ºC to obtain the branching by avoiding gelation. 2-isocyanatoethyl methacrylate was added to endcape the branched polymer and finally, water was incorporated with a high-speed mechanical stirring. Vacuum drying was applied to remove the acetone from the system; hence the targeted methacrylate end-functionalized, highly branched waterborne poly(urethane-urea) dispersion (HBWPUD) was obtained with a 35% solid content.

5.3.3. Preparation of free-standing UV- Cured HBWPU Films

HBWPUDs were diluted with distilled water to 10 wt.%, the photoinitiator (IRGACURE 500) was applied in concentrations of 2wt% and 4wt% and casted onto Teflon molds at room temperature. Films were dried under ambient conditions overnight. Prepared films were kept in an oven at 120 ºC for 1 hour and stored in desiccator. After the complement of the flash-off process, UV curing process was performed in a UV- chamber using UV lamp (main wavelength: 315-400 nm., *low* pressure mercury lamps, 6.6 J/s) equipped with a photometer where the distance between UV-lamp and sample was 30 cm.

The liquid photoinitiator (IRGACURE 500) was stored at dark conditions, avoiding exposure to sunlight, under 18 ºC. HBWPUDs were diluted with distilled water to 10 wt.%, the photoinitiator (IRGACURE 500) was applied in concentrations of 2wt% and 4wt% and casted onto Teflon molds at room temperature.

The dispersion and photoinitiator mixture were well mixed and uniformly distributed. Over 4 wt% of photoinitiator, non-uniform curing behavior was observed due to the partial overconcentration issue. The films were dried under ambient conditions overnight. Pre-dried films were kept in an oven at 120 ºC for 1 hour and stored in desiccator in a dark environment. After the complement of the flash-off process, UV curing process was performed in a UV-

chamber using UV lamp (main wavelength: 315-400 nm., *low* pressure mercury lamps, 6.6 J/s) equipped with a photometer where the distance between UV-lamp and sample was 30 cm. The mold was placed to the middle of the rotating platform which spins at 1 RPM speed, in order to sustain a uniform curing Figure 57).

Figure 57: a) UV-Curing Chamber b) UV-Cured HBWPU Film

5.3.4. Characterization Methods

Particle size and distribution of HBWPUDs were measured by dynamic light scattering (Malvern- Zetasizer NaNo-Zs equipped with laser diffraction and polarized light of three wave detectors) after homogenizing the samples with deionized water at room temperature and the refractive index of HBWPUDs are 1,5.

The ATR-FT-IR spectra were recorded by a ThermoScientific Nicolet iS10 with a minimum of 64 scans.

Thermal stability of the films was determined by thermogravimetric analysis (TGA) by a DTG-60H, Shimadzu instrument using a heat rate of 10 $^{o}C.min^{-1}$ from room temperature to 600 ^{o}C under nitrogen atmosphere.

Differential scanning calorimetry (DSC) was performed in the temperature range between -120 ºC and 150 ºC with a heating rate of 10 ºC/min by TA Instruments – MDSCQ2000 with three cycles.

The measurements of molecular weight and polydispersity index of the HBWPUDs were carried out by triple detection Viscotek GPCmax-VE 2001 instrument, with HPLC grade DMF, 0,5 ml/min flow rate at 45 ºC. The ^{1}H NMR and ^{13}C NMR analysis were performed by a Varian Inova 500 MHz nuclear magnetic resonance instrument.

The mechanical test specimens of UV-cured films were prepared according to ASTM D1708-10 standards and tested by a universal testing machine Zwick Roell Z100 UTM, with a load cell of 200 N, 22 mm grip to grip separation and a crosshead speed of 25 mm/min.

In order to determine crosslink densities, the free standing UV-cured films were cut into the size 2cm x 2cm and gel contents were determined by Soxhlet apparatus by extracting for 24 hours with toluene. Gel contents were calculated according to the following formula after drying process:

$$\text{Gel Content (\%)} = \frac{m_1 - m_0}{m_0} \times 100$$

Equation 2: Calculation of Gel Content

where m_0 is the initial mass of the sample and m_1 is the final mass after extraction.

The water absorption (swelling ratio) of UV- cured films were measured by cutting samples into including the size of 2 cm x 1 cm. Pre-weighted samples were immersed into distilled water at room temperature for 24 hours; then, residual water on the film surface was wiped and weighted immediately. Swelling ratios were calculated according to their initial dry weight (W_d) and final wet weight (W_w) increment through the formula given below:

$$\text{\% Water Absorption} = \frac{W_w - W_d}{} \times 100$$

$$\frac{}{W_d}$$

Equation 3:Calculation of Water Absorption

5.4. Results And Discussion

In this study, novel hyperbranched waterborne polyurethane dispersion is synthesized via Acetone process. Once the dispersion is obtained, the photoinitiator is added and the mixture is poured in a Teflon mold and dried. Afterwards dry films were cured under UV irradiation as described in the Figure 58. Subsequently, several research parameters were investigated under three main stages since the final performance of UV-Cured films could be affected from different chemical and physical factors.

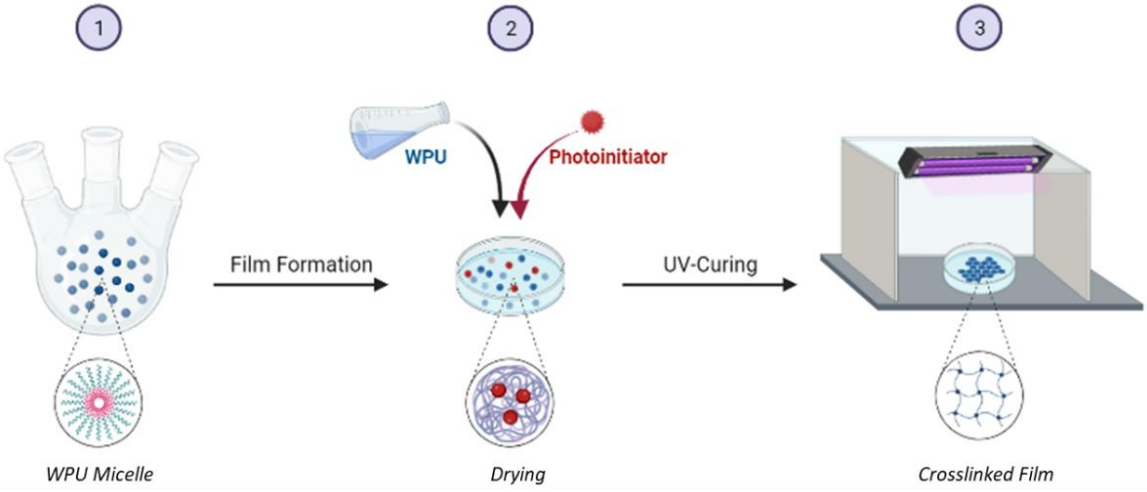

Figure 58: Preparation of UV-curable WPUs

In the first step, a formulation parameter influencing the branching degree was investigated. Hyperbranched waterborne polyurethanes at different A_2:B_3 ratio were synthesized, the critical gel point was determined and the effect of the increasing A_2:B_3 ratio on the resulting WPU latex and films were clarified. In the second stage, the effect of amount (%) of suitable

photoinitiator added to the dispersion system was investigated. Finally, the UV-Curing conditions (UV-light source, distance, curing energy) were studied to obtain the highest crosslinking degree.

The hyperbranched waterborne polyurethane dispersions (HBWPUD)s were synthesized via the oligomeric A_2+B_3 method in four steps, following the Acetone process. The same reaction protocol was applied for the synthesis of HBWPUD-1 and HBWPUD-2 with the different A_2:B_3 ratios, which were 0.80 and 0.65, respectively. The dispersion formulations expressed as equivalents of the components were summarized in Table 14. The polyester polyol and HDI were fed at pre-calculated amounts into four-necked, round bottomed flask equipped with a thermocouple, reflux condenser, and an overhead mechanical stirrer. The pre-polymerization reaction was kept at 80 ^{o}C until the actual -NCO content reaches the theoretical -NCO content, which was regularly controlled by the standard dibutylamine back-titration method (ASTM D2572-97). The prepolymer was cooled down to 60 ^{o}C, acetone was added dropwise to dissolve -NCO terminated prepolymer. Afterwards, the chain extension was realized with the addition of AEAS/water via addition-funnel; thus, A_2 oligomer was obtained.

The B_3 oligomeric structure, composed of diethylenetriamine/acetone/water mixture, was prepared in a separated round bottomed reaction flask. The prefabricated A_2 prepolymer was slowly poured into the B_3 system via addition funnel, at 50 ^{o}C to obtain the branching by avoiding gelation. 2- isocyanatoethyl methacrylate was added to endcape the branched polymer and finally, water was incorporated with a high-speed mechanical stirring. Vacuum distillation was applied to remove the acetone from the system; hence the targeted methacrylate end-functionalized, highly branched waterborne poly(urethane-urea) dispersion (HBWPUD) was obtained with a 35% solid content. The synthesis procedure is represented in Figure 59.

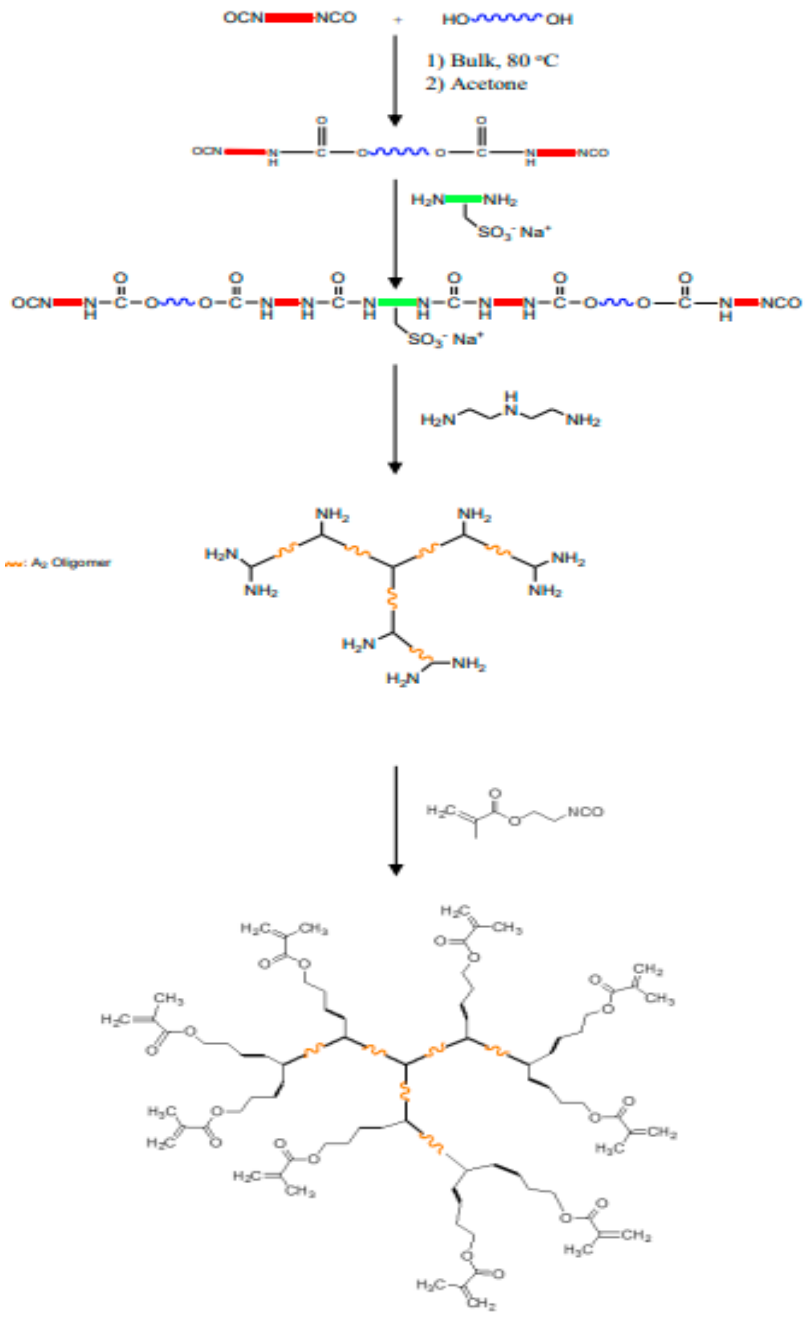

Figure 59: Synthesis of IV-Curable WPUs via A2+B3 method

Novel highly branched waterborne polyurethane dispersions (HBWPUD-1 and HBWPUD-2) were successfully prepared from HDI and polyester polyol with oligomeric A_2+B_3 approach at two different A_2:B_3 ratios (0.8 and 0.65). Fundamental characterizations of prepared HBWPUD-1 and HBWPUD-2 were carried out by DLS, GPC and NMR analysis. The particle size of the HBWPUD-1 and HBWPUD-2 were listed in Table 12 and their size distributions were presented in Figure 56. As seen in Figure 56 and Table 12, both dispersions possess unimodal distribution and the particle size distribution of HBWPUD-1 and HBWPUD-2 were found as 310 nm and 250 nm diameter, respectively.

Table 14 : Properties of Highly-branched Waterborne Polyurethanes

Sample item	**HBWPUD-1**	**HBWPUD-2**
A_2:B_3	0.80	0.65
HDI (mol)	0.1	0.1
Polyester polyol (mol)	0.05	0.05
AEAS (mol)	0.03	0.03
DETA (mol)	0.04	0.05
2-isocyanatoethyl methacrylate (mol)	0.018	0.027
M_w (Da)	53.999	30.939
PDI	2.9	2.42
Particle Size (nm)	310	250
pH	5	7
Solid Content (%)	35	35
Color & Appearance:	Milky White	Milky White

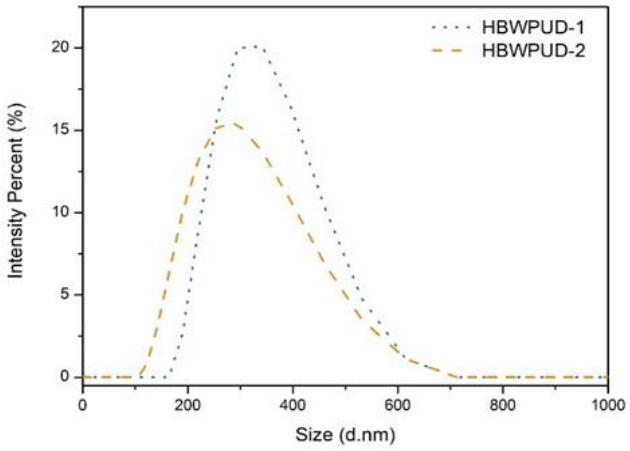

Figure 60 :Particle size distributions of HBWPUD-1 and HBWPUD-2

As presented in Figure 60, DLS measurements indicate that branching degree of the dispersions influence the mean size of resulting particles**.** At constant ionic content, significant decrease has been observed in the mean particle size with the decreasing A_2:B_3 ratio due to the less branching degree of the architecture and lower molecular weight.

The GPC data of the HBWPUD-1 and HBWPUD-2 are listed in Table 14. The weight average molecular weights (Mw) are about 200,000 and 24,000 Da respectively. The sharp decrease in the molecular weight reveals that tuning on the A_2:B_3 ratio from 0.8 to 0.65 has a dramatic impact on the molecular weight as well as the particle size.

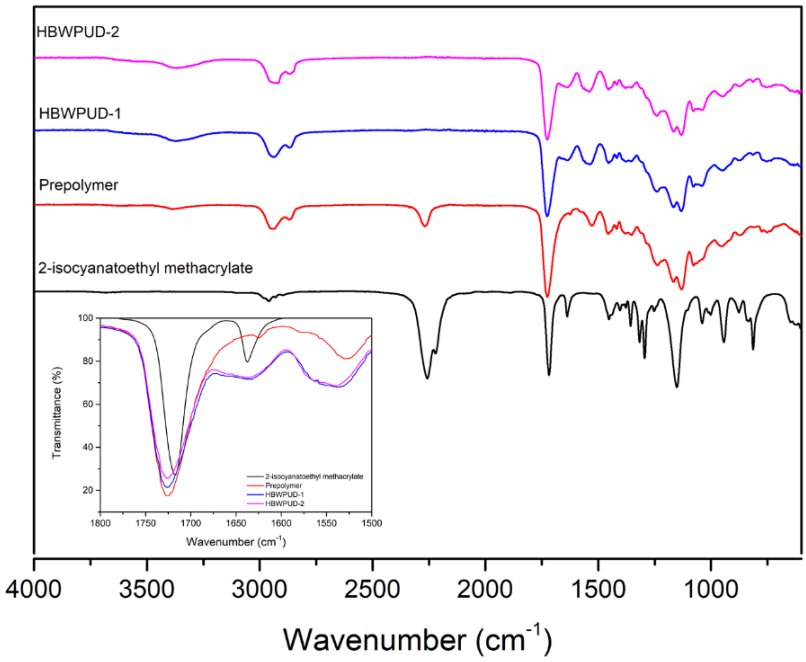

Figure 61: FT-IR spectra of monomer, prepolymer and HBWPUDs.

The evolution of the polymerization reaction was monitored with FT-IR analysis, and comparison of HBWPUDs with 2-isocyanatoethyl methacrylate monomer, prepolymer, and were shown in Figure 61. For the prepolymer, the absorption band at 2270 cm $^{-1}$ was attributed to the presence of unreacted -NCO groups which disappeared with the complete consumption of -NCO groups and completion of prepolymerization reaction. On the other hand, the methacrylate end-functionalization of the HBWPUDs was followed by the appearance of C=C stretching band at 1635 cm $^{-1}$. In the dispersion, the peaks around 3365-3385 cm $^{-1}$ were observed due to hydrogen bonds between -NH and C=O groups of urea and urethane, the peaks at 2870-2940 cm^{-1} region corresponded to the -CH stretching, and the strong absorption bands around 1725 cm $^{-1}$ were attributed to the carbonyl stretching region.

Upon the novel synthesis and structural characterization of HBWPUD-1 (A_2:B_3 = 0,8) and HBWPUD-2 (A_2:B_3= 0,65), 2%wt and 4%wt of photoinitiator were added into the dispersions and cured with different amount of energies under UV exposure. The UV-cured films were labeled according to their dispersion type, amount of energy (denoted with A,B,C,D according to increasing trend) and photoinitiator percent (2% and 4%) , respectively. The labeling and compositions of the UV-cured free-standing films were listed

in Table 15. Furthermore, the gel content, water absorption, thermal properties and mechanical behaviors of the UV-cured films were systematically analyzed. Neat HBWPUDs were not able to form films therefore they couldn't be evaluated in terms of thermal and mechanical properties for the comparison studies.

Table 15: Compositions and properties of UV-cured films.

Sample	Curing Energy (Joules)	Photoinitiator (wt%)	Gel Content (%)	Water Absorption (%)
HBWPUD-1-A2	120	**2%**	47	75
HBWPUD-1-B2	180	**2%**	67	36
HBWPUD-1-C2	240	**2%**	71	34
HBWPUD-1-D2	300	**2%**	65	30
HBWPUD-1-A4	120	4%	64	29
HBWPUD-1-B4	180	4%	60	35
HBWPUD-1-C4	240	4%	52	38
HBWPUD-1-D4	300	4%	50	59
HBWPUD-2-A2	120	2%	78	25
HBWPUD-2-B2	180	2%	80	20
HBWPUD-2-C2	240	2%	86	17
HBWPUD-2-D2	300	2%	79	22
HBWPUD-2-A4	120	4%	70	55
HBWPUD-2-B4	180	4%	67	35
HBWPUD-2-C4	240	4%	62	45
HBWPUD-2-D4	300	4%	43	78

As one of the major drawbacks compared with the solvent-based products, the water resistance of waterborne films has attracted extensive attention. Many factors influence the water resistance of the films, such as ionic groups and polyol structures. As it is stated in Table 13, there is a direct correlation between the gel content and the water absorption ratio. As the crosslinking density increases, the water absorption decreases.

Structural confirmation of HBWPUD-1 and HBWPUD-2 were also performed by NMR spectroscopy and results were given in Figure 62. Before the analysis, water dispersions of obtained HBWPUDs were dried at 100°C in an oven for removing of water medium.

Acquired white powders of HBWPUD-1 and HBWPUD-2 after the drying process were dissolved in *d*-$CDCl_3$ and NMR measurements were done.

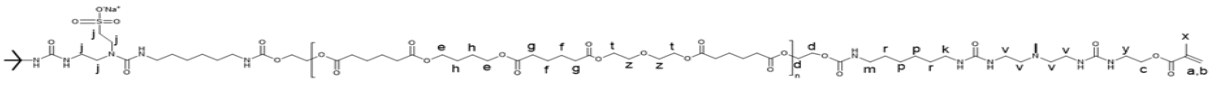

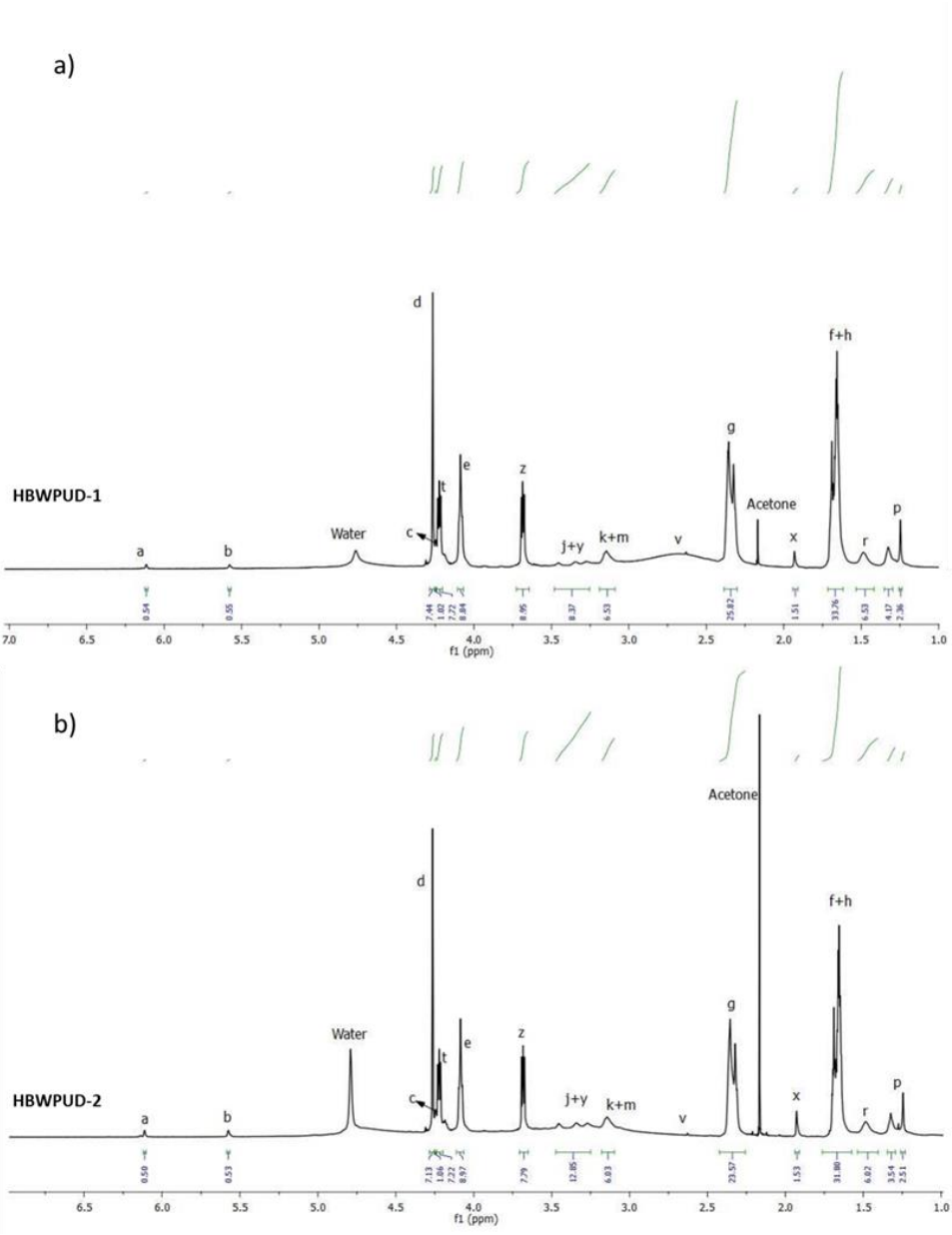

Figure 62: 1H NMR results of HBWPUD-1 (a) and HBWPUD-2

As seen in ^{1}H NMR spectrum of HBWPUD-1 and HBWPUD-2 (Figure 58), the peaks at 4.26, 4.21, 4.05, 3.69, 2.35 and 1.66 ppm corresponded to polyol segment of branched polymers. Peaks coming from methacrylate end-functional groups revealed at 6.11, 5.52ppm ($=CH_2$); 1.92 ppm ($-CH_3$) and 4.24 ppm ($-OCH_2$) that showed successful end functionalization. In addition, $-CH_2$ groups on HDI appeared in the range between 1-1.5ppm, and $-CH_2$ groups on chain extender part of polymer chain were detected in the region of 3.25-3.5 ppm on the spectrum. Moreover, any peak was not observed at 2 ppm and 2.5 ppm, suggesting that HBWPUDs were free of primary amine which could arise from B_3 monomer. It was also shown that HBWPUD-1 containing higher hyperbranched amount had a broader peak between 2.5 ppm – 3 ppm while HBWPUD-2 had less. This could be an important indicator of having higher branched points of HNWPUD-1 than HBWPUD-2 was, as expected. All peak assignments were confirmed by comparing the integral ratios of the signals on the spectrum.

5.5.1. Gel Contents of the UV-cured HBWPU Films

Following the synthesis and characterization of HBWPUD-1 and HBWPUD-2, the photoinitiator was incorporated at two different concentrations (2%wt and 4%wt) into the diluted dispersions. Films were cast onto Teflon molds, well dried, and cured with four different energy amounts. The compositions of the UV-cured films were listed in Table 13.

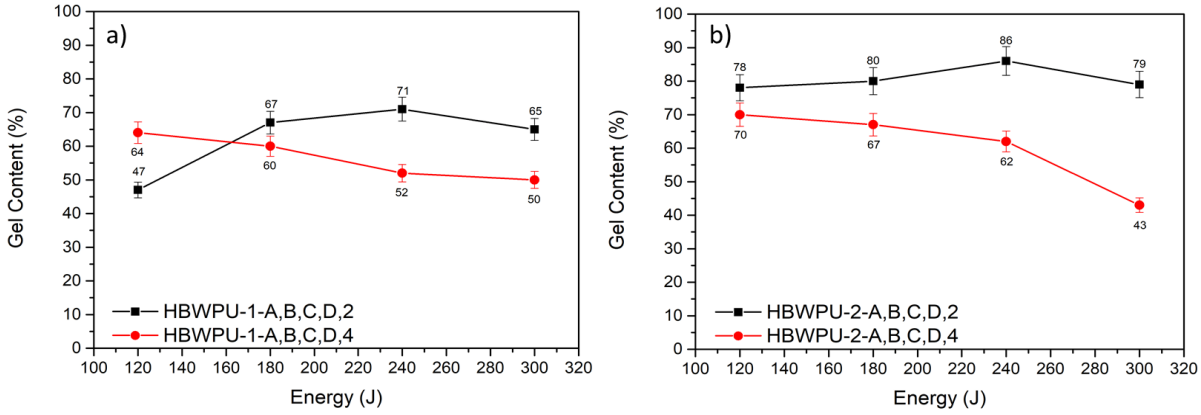

Figure 63 :Gel contents of UV-Cured films.

In order to determine the crosslink density of the UV-cured HBWPU films, their gel contents were measured as shown in Figure 59. It was observed that the crosslinking degrees of UV-cured films vary in a wide range from 43% to 86%. For the HBWPU-1 samples, 2 % photoinitiator had a positive effect on the gel content with increasing curing energy, while 4% photoinitiator had the opposite effect on the same curing conditions. For the HBWPU-2 series, 4% photoinitiator caused a significant decrease on the gel contents once again with the increasing curing energy, but the maximum average of the gel contents were obtained with the additive of 2% photoinitiator. This remarkable difference pointed out that the increasing amount of curing energy enhanced the crosslink density with the 2% photoinitiator added films; 4% photoinitiator had destructive effect with increasing curing energy for all the samples. Additionally, the films with higher A_2:B_3 ratio (HBWPU-1) showed lower gel contents when compared with their analogues (HBWPU-2) in the same curing conditions. These results claimed that the higher A_2:B_3 ratio pulled down the crosslinking efficiency.

The water absorption properties of the UV-cured HBWPU films were also measured to see their water resistance properties. The water absorption results, indicated in Table 13, showed an inverse proportion with the crosslinking density, as expected. Higher water resistance values were obtained with lower A_2: B_3 ratio and the most resistant sample was the one that has the maximum gel content. Both the gel content and the water absorption properties of the UV-cured films showed significantly different behaviors depending on the branching degree, photoinitiator amount and curing energy. The movement of molecule chains will be restricted at high crosslinking density, the remaining active groups cannot polymerize sequentially and the crosslinking density will tend to a constant.

5.5.2. Thermal and Mechanical Properties of the UV-Cured HBWPU Films

Thermal behaviors of the materials are crucial for the real-life applications. In order to investigate thermal properties of UV-cured films, TGA and DSC measurements were applied to the film samples. The UV-cured films are investigated with TGA and DSC analysis. Figure 64 shows the TGA curves and Table 3 includes the T_g values obtained from DSC analysis of the UV-cured films.

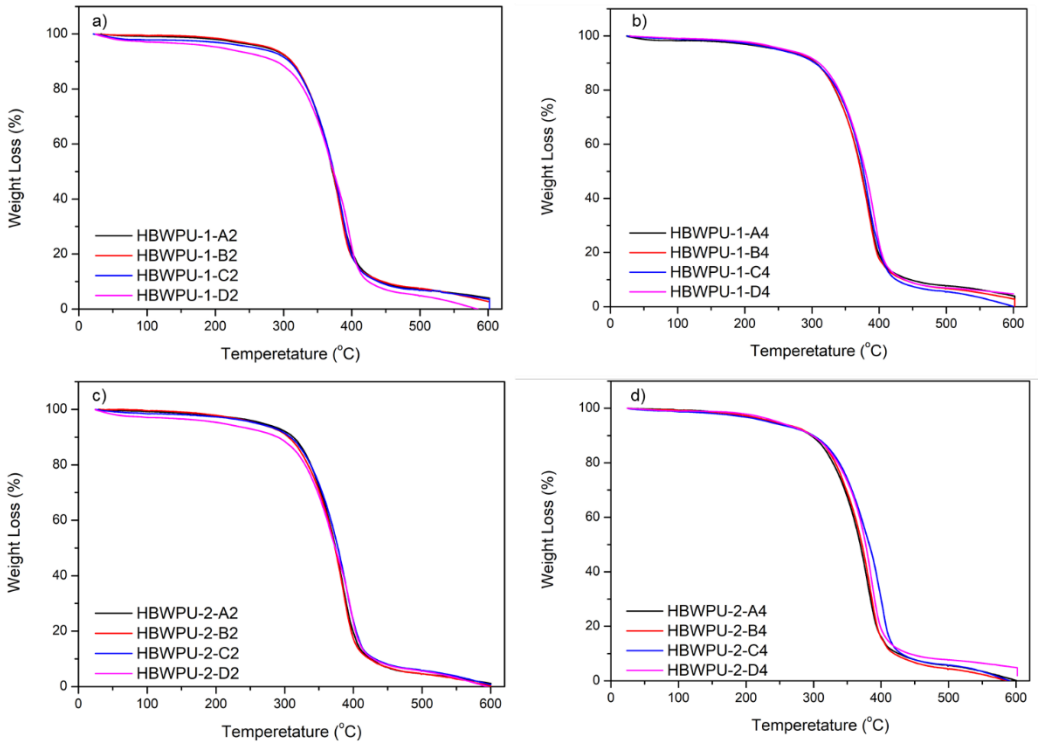

Figure 64: TGA curves of UV-Cured films.

Table 16: Glass Transition Temperatures of HBWPU films

T_g (°C)	HBPU-1		HBPU-2	
	2% PI	**4% PI**	**2% PI**	**4% PI**
Neat	-44.21		-43.08	
120	-42.58	-41.39	-42.4	-42.72
180	-40.56	-41.27	-43.43	-41.81
240	-42.55	-40.78	-42.31	-41.37
300	-41.78	-41.26	-41.57	-41.09

It was seen that the thermal decomposition of the UV-cured films occurred in one stage. For all the measured samples, the beginning of thermal decomposition was observed at around 275 °C and ended at 400 °C. The temperature of half decomposition ($T_{d,1/2}$) was determined as 375 °C for the free-standing films. Changing the parameters such as; A_2:B_3 ratio, photoinitiator concentration and the curing energy didn't have a significant impact on the thermal properties of the UV-cured HBWPU films.

The glass transition temperature (Tg) of a system is a direct measurement of molecular mobility and in a crosslinked sample it depends on its crosslinking degree. Glass transition temperatures (T_g) of UV-Cured films for different curing energy and photoinitiator concentration were investigated by DSC thermal cycles and results were listed in Table 16. It was observed that T_g values were lied between -43.3°C and - 40.6°C. When we interpreted the gel content data in relation to Tg values, it was seen that glass transition temperature shifted to higher temperature due to the crosslinking density increment. Although there was not significant changing in T_g values between all UV-cured films, glass transition temperatures of HBWPUD-2-B2 and HBWPUD-2-C2 samples, which have higher gel content percentage than other samples, were found as (-)40.8° and (-)40.6°C, respectively. The reason for obtaining higher T_g for HBWPUD-2-B2 and HBWPUD-2-C2 is that because higher gel content has provided a higher crosslinking density; thus, T_g values increased due to the ability of chain movement decreasing.

In addition to the thermal properties of Uv-cured films, mechanical properties were also examined, and stress-strain curves were presented in Figure 65. Elastic modulus ($E^{'}$), stress at break (σ_b) and elongation at break (ε_b) results were listed in Table 17.

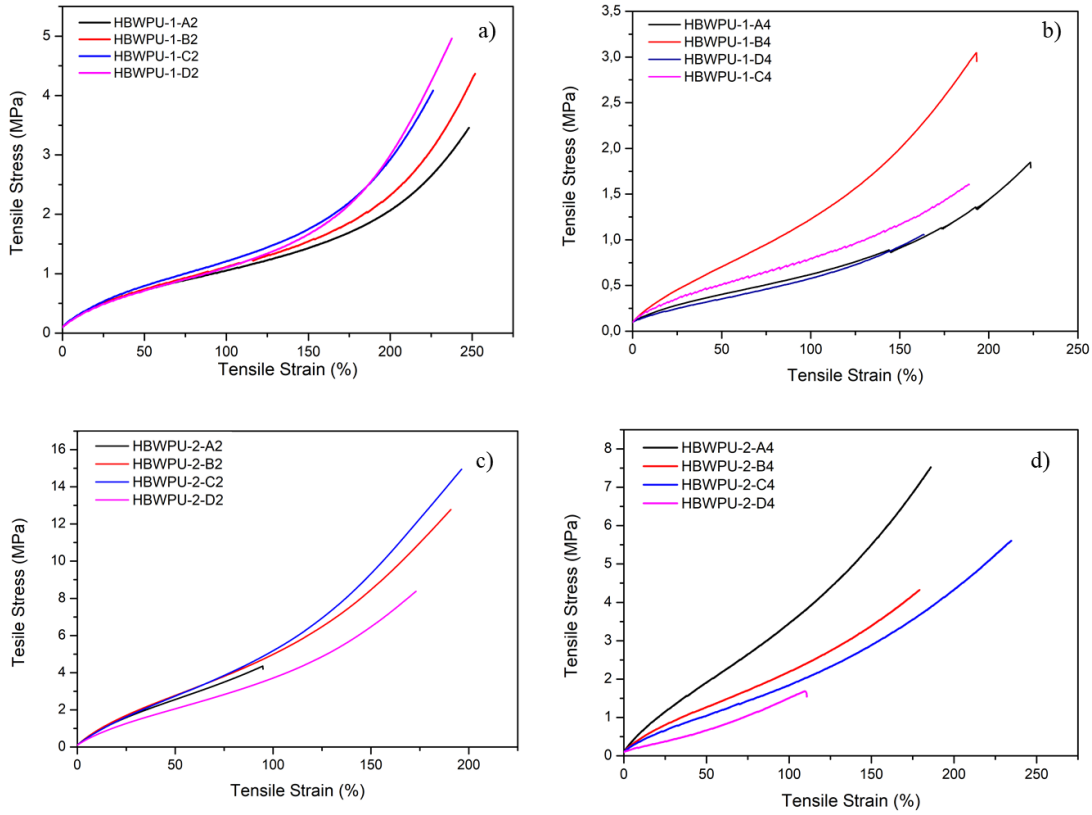

Figure 65: Tensile Properties of the cured films

According to results obtained from UTM tests, it is found that HBWPUD-2-B2 and HBWPUD-2-C2 films had higher elastic modulus values as 8.57 MPa and 7.90 MPa, respectively. These results demonstrated that elastic modulus values of UV-cured films having higher crosslinking density possessed almost 8 times higher than the films having less crosslinking density such as HBWPUD-2-D4. Mechanical properties enhancement of UV-cured films depending on crosslinking density of samples could also be seen in stress at break results. The sample coded as HBWPUD-2-C2 had resisted almost 12 times higher stress in comparison with HBWPUD-2-D4 before breaking.

Table 17: Mechanical properties of the cured films

Sample	T_g	E' (MPa)	σ_b (MPa)	ε_b (%)
HBWPUD-1-A2	-42.7	2.23 ± 0.30	2.48 ±0.94	219± 40.
HBWPUD-1-B2	-41.6	2.33 ± 0.14	3.70±0.93	247±6.
HBWPUD-1-C2	-41.4	2.90 ± 0.19	3.54±0.45	203±18
HBWPUD-1-D2	-41.3	2.37 ± 0.18	3.79±1.424	214±27
HBWPUD-1-A4	-41.8	0.82 ±0.24	1.09±0.65	193±39
HBWPUD-1-B4	-42.4	1.59 ± 0.50	2.38±0.94	170±32
HBWPUD-1-C4	-42.5	0.82 ± 0.28	1.92±0.78	200±45
HBWPUD-1-D4	-42.6	0.78 ± 0.22	0.91±0.17	177±12
HBWPUD-2-A2	-41.4	7.80 ± 0.47	5.84±2.10	119±34
HBWPUD-2-B2	-40.8	8.57± 0.18	8.21±3.99	128±24
HBWPUD-2-C2	-40.6	7.90 ± 0.38	12.69±2.03	183±12
HBWPUD-2-D2	-41.1	7.66 ± 0.64	6.12±0.18	128±5
HBWPUD-2-A4	-41.3	4.91 ±1.10	5.72±1.57	197.35±10.62
HBWPUD-2-B4	-41.8	4.06 ± 0.05	4.77±1.00	174.71±22.37
HBWPUD-2-C4	-42.3	3.20 ± 0.20	5.037±0.74	218.507±32.39
HBWPUD-2-D4	-43.3	1.19 ± 0.3	1.378±0.33	124.94±12.78

As seen in Table 17, mechanical properties of films improved according to their gel content percentage amounts.

5.5.3. The effect of photoinitiator concentration

The photoinitiator (PI) plays a key role in UV-radiation curing as it controls both the initiation rate and the penetration of the incident light (cure depth). In the case of waterborne systems, it is important that the photoinitiator be uniformly distributed in the film after the drying stage. Therefore, the optimum amount of photoinitiator is a highly critical parameter for the curing efficiency. Photoinitiator concentration at above or below the optimum amount can give rise to undesired effects. While deficient amount of photoinitiator causes an insufficient crosslinking; the excess amount of photoinitiator will absorb, reflect or scatter the incident UV light, furthermore, form a highly crosslinked layer on top of the surface which might block the penetration of UV light into the deep part of the film. This phenomenon is explained

by Beer- Lambert law and it was verified by the presented data and according to the Lambert–Beer's law, the light intensity was degressive in the form of exponential function when the content of the photoinitiator increased. When the content of the photoinitiator was excessive, the photoinitiator closed to the surface of the coating would absorb the most part of the Ultra Voilet, the light flux reached to the interior would decrease sharply, the number of the free radical produced by the photoinitiator and the velocity of the UV curable reduced. Besides, the cured film on the surface coating might hinder the molecular movement at the bottom coating, so that the gel content reduced and the curing degree decreased.

If the content of the Darocur 1173 was low, the energy may not effectively be used, and the number of the generated free radicals was lower than the reaction required, thus the curing speed would be slower. With the content of the Darocur 1173 increasing, the number of the generated free radicals increased, the curing speed would be quicker. But if the content of the Darocur 1173 was higher than the reaction required, there would be excess free radicals generated which could easily coupling each other, then terminated the chain growth and the curing speed would be slow at last. So, when the content of the Darocur 1173 was 4%, the surface drying time reached the minimum and the curing effect was the best. The results revealed that, for our system, 4%wt photoinitiator always caused a decrease on the gel contents and modulus values at the same polymeric and energetic conditions.

5.5.4.The effect of A_2:B_3 ratio

One of the main parameters dominating the crosslinking density and the final properties of the UV-cured films is the A_2:B_3 ratio of the dispersions. Since this ratio imposes the branching point distance, it is directly proportional to the diameter and the molecular weight of the latex particles. Our results showed that higher branching degree ends up with lower gel contents and mechanical properties for all curing conditions. Therefore, with lower A_2:B_3 ratio, favorable crosslinking densities and mechanical properties are obtained.

5.5.5. The effect of curing energy

The curing energy is related to the radiation dose and excitement of the free radicals. However, overdose energy given to the sample may cause a negative effect on the resulting properties. This effect can be easily seen with the films prepared with 4 wt% photoinitiator, which showed a decreasing trend in terms of gel content and mechanical properties with increasing curing energy. Thus, the optimum amount of curing energy is a critical parameter to obtain better characteristics. At the UV-curable prophase, the gel content gradually increased with the UV curing time increasing. This was due to the dual bond not being opened entirely when the curing time was too short. When the curing time reached 30 s, the gel content increased slightly but changed not obviously if the curing time continued to be increased. Because when the curing time was 30 s, dual bond was opened entirely and the curing reaction basically. completed. The curing degree basically remains unchanged even if prolongs the curing time.

5.5. Conclusions

Novel environmentally friendly dispersions, HBWPUD-1 and HBWPUD-2, have been successfully prepared at two different A_2:B_3 ratios and characterized. Afterwards, with the incorporation of2 wt% and 4 wt% photoinitiator, the films were UV-cured at four different amounts of energies. Our results revealed that with lower A_2:B_3 ratio, higher crosslink densities are obtained together with lower water absorption and remarkably better tensile properties. Moreover, thermal behaviors of crosslinked films didn't show crucial differences and they all have a great potential to serve in a wide range. The outstanding results, even superior properties than reported results with nanoparticle addition, yielded with HBWPUD-2-B2 sample. This film has A_2:B_3=0.65, 2 wt% photoinitiator and cured with 180 joules. In this case, gel content reached 86 %, water absorption dropped to 17%, elastic modulus increased to 8.57 MPa. On the contrary, HBWPUD-1-D4 sample exhibited the weakest properties due to higher A_2:B_3 ratio, overdose amount of photoinitiator and curing energy. In summary, this synthesis and crosslinking strategy provide a great potential for the green industry

6. OVERALL CONCLUSIONS AND FUTURE WORK

6.1. Overall Conclusions

The general conclusions of the thesis study according to the order of chapters flow can be listed as below:

- Acetone process is a highly suitable and adaptable synthesis method to prepare WPU dispersions for different applications.
- Self-healing waterborne polyurethanes can be successfully obtained only with non-covalent interactions, covalent interactions are not indispensable.
- For an efficient self-healing in WPU, besides the soft segment, ionic groups are also crucial. Therefore, ionic interactions also play a leading role in the rearrangement of the surface.
- The self-healing WPU dispersion is very well able to be incorporated into the industrial grade paint formulation.
- By fine tuning on the segmental composition and hydrophilic-hydrophobic balance in the WPU chain, anti-fouling properties can be gained even in the underwater conditions.
- Anti-fouling marine coatings can be prepared via environmentally friendly WPU binders.
- Highly branched WPU chains can be obtained via A_2+B_3 method. The effects of branching degree, curing energy and photoinitiator concentration can be directly detected on the dispersion and film properties.

- Additional photoinitiators can be successfully incorporated into the WPU dispersion.
- Overall, chemical, experimental and environmental factors are highly influential on the resulting WPU material and applications. New generation WPUs are highly promising to replace their toxic parents.

6.2. Future Work

The main conclusion from the studies conducted so far is that waterborne polyurethanes can be easily adapted to dozens of different application areas due to their segmental and functional chemical structure. Regarding that solid claim, numerous new studies and applications are included on the future work list. In this manner, the self-healing examination of the PDAPU described in Chapter 2 is one of the main research areas. Different parameters such as coating, and illumination differences have already been studied in a detailed way. Yet, there is still a lack of experience in the PDAPU films self-healing behavior toward different film and environmental parameters. Imagining that the PDAPU films are really used in outdoor applications, especially under dark and sun conditions, such a self-healing property would be fascinating. Photothermal materials together with self-healing performance will deserve credit for the next-generation materials.

On the other hand, UV-curable WPU study has an extendable application area, including alternating the photoinitiator, end groups, branching points and coating on different types of surfaces. In a holistic approach considering Chapters 1 &3, UV-curable 3D printing inks can be prepared in a suitable viscosity and curing efficiency. Stereolithography (SLA) is the specific type of 3D printing, curing liquid resin into solid parts, layer by layer. Therefore, environmentally friendly, high- precision and high-performance materials can be produced with a UV-curable WPU ink.

Last but not least, WPU has a huge potential on low VOC and environmentally friendly wood coating. High elasticity, transparency and hardness of WPU films are highly demanded on the industry. In addition to the existing features, implementation of hydrophobicity and oleophobicity will fulfill all the requirements that an end-user will need to. It is certain that WPU dispersions and films will have a extended application area in near future.

7. REFERENCES

1. De Souza, F. M., Kahol, P. K., & Gupta, R. K. (2021). Introduction to Polyurethane Chemistry. *Polyurethane Chemistry: Renewable Polyols and Isocyanates, Part 1 - Introduction to Polyurethane Chemistry*. https://doi.org/10.1021/bk-2021-1380.ch001

2. Król, P. (2007). Synthesis methods, chemical structures and phase structures of linear polyurethanes. Properties and applications of linear polyurethanes in polyurethane elastomers, copolymers and ionomers. In *Progress in Materials Science* (Vol. 52, Issue 6, pp. 915–1015). Pergamon. https://doi.org/10.1016/j.pmatsci.2006.11.001

3. Yilgor, E., Isik, M., & Yilgor, I. (2010). Novel synthetic approach for the preparation of poly(urethaneurea) elastomers. *Macromolecules*, *43*(20), 8588–8593. https://doi.org/10.1021/ma101770k

4. Akindoyo, J. O., Beg, M. D. H., Ghazali, S., Islam, M. R., Jeyaratnam, N., & Yuvaraj, A. R. (2016). Polyurethane types, synthesis and applications-a review. In *RSC Advances* (Vol. 6, Issue 115, pp. 114453–114482). Royal Society of Chemistry. https://doi.org/10.1039/c6ra14525f

5. Yilgör, I., Yilgör, E., & Wilkes, G. L. (2015). Critical parameters in designing segmented polyurethanes and their effect on morphology and properties: A comprehensive review. *Polymer*, *58*, A1–A36. https://doi.org/10.1016/J.POLYMER.2014.12.014

6. Kojio, K., Nozaki, S., Takahara, A., & Yamasaki, S. (2020). Influence of chemical structure of hard segments on physical properties of polyurethane elastomers: a review. *Journal of Polymer Research 2020 27:6*, *27*(6), 1–13. https://doi.org/10.1007/S10965-020-02090-9

7. Riehle, N., Athanasopulu, K., Kutuzova, L., Götz, T., Kandelbauer, A., Tovar, G. E. M., & Lorenz, G. (2021). Influence of Hard Segment Content and Diisocyanate Structure on the Transparency and Mechanical Properties of Poly(dimethylsiloxane)-Based Urea

Elastomers for Biomedical Applications. *Polymers*, *13*, 212. https://doi.org/10.3390/polym13020212

8. Li, R., Ton Loontjens, J. A., & Shan, Z. (2019). The varying mass ratios of soft and hard segments in waterborne polyurethane films: Performances of thermal conductivity and adhesive properties. *European Polymer Journal*, *112*, 423–432. https://doi.org/10.1016/J.EURPOLYMJ.2019.01.025

9. He, Y., Zhang, X., & Runt, J. (2014). The role of diisocyanate structure on microphase separation of solution polymerized polyureas. *Polymer*, *55*(3), 906–913. https://doi.org/10.1016/j.polymer.2014.01.001

10. Yang, C.-H., Yang, H.-J., Wen, T.-C., Wu, M.-S., & Chang, J.-S. (n.d.). *Mixture design approaches to IPDI-H 6 XDI-XDI ternary diisocyanate-based waterborne polyurethanes*.

11. Zia, K. M., Ahmad, A., Anjum, S., Zuber, M., & Anjum, M. N. (2014). Synthesis and characterization of siloxane-based polyurethane elastomers using hexamethylene diisocyanate: *Http://Dx.Doi.Org/10.1177/0095244314526746*, *47*(7), 625–635. https://doi.org/10.1177/0095244314526746

12. Fu, H., Liu, K., Yan, C., Chen, W., & Wang, Y. (2015). Phase morphology and mechanical properties of aliphatic waterborne polyurethane-Ureas: Effect of 1,6-Hexamethylene diisocyanate (HDI)/Isophorone diisocyanate (IPDI) Ratio. *Polymers and Polymer Composites*, *23*(3), 141–150. https://doi.org/10.1177/096739111502300304

13. Ma, J., Lee, G. H., Kim, J. H., Kim, S. W., Jo, S., & Kim, C. S. (2022). A Transparent Self-Healing Polyurethane-Isophorone-Diisocyanate Elastomer Based on Hydrogen-Bonding Interactions. *ACS Applied Polymer Materials*, *4*(4), 2497–2505. https://doi.org/10.1021/ACSAPM.1C01799/ASSET/IMAGES/LARGE/AP1C01799_0006.JPEG

14. Chattopadhyay, D. K., & Raju, K. V. S. N. (2007). Structural engineering of polyurethane coatings for high performance applications. *Progress in Polymer Science*, *32*(3), 352–418. https://doi.org/10.1016/j.progpolymsci.2006.05.003

15. Wang, T.-L., & Hsieh, T.-H. (1997). Effect of polyol structure and molecular weight on the thermal stability of segmented poly(urethaneureas). *Polymer Degradation and Stability*, *55*(1), 95–102. https://doi.org/10.1016/S0141-3910(96)00130-9

16. Yu, F., Saha, P., Suh, P. W., & Kim, J. K. (2015). Green polyurethane from dimer acid based polyether polyols: Synthesis and characterization. *Journal of Applied Polymer Science*, *132*(5), 41410. https://doi.org/10.1002/APP.41410

17. Zhang, J., Tu, W., & Dai, Z. (2012). Synthesis and characterization of transparent and high impact resistance polyurethane coatings based on polyester polyols and isocyanate trimers. *Progress in Organic Coatings*, *75*(4), 579–583. https://doi.org/10.1016/J.PORGCOAT.2012.05.005

18. Fuensanta, M., Jofre-Reche, J. A., Rodríguez-Llansola, F., Costa, V., Iglesias, J. I., & Martín-Martínez, J. M. (2017). Structural characterization of polyurethane ureas and waterborne polyurethane urea dispersions made with mixtures of polyester polyol and polycarbonate diol. *Progress in Organic Coatings*, *112*, 141–152. https://doi.org/10.1016/j.porgcoat.2017.07.009

19. Fuensanta, M., Jofre-Reche, J. A., Rodríguez-Llansola, F., Costa, V., Iglesias, J. I., & Martín-Martínez, J. M. (2017). Structural characterization of polyurethane ureas and waterborne polyurethane urea dispersions made with mixtures of polyester polyol and polycarbonate diol. *Progress in Organic Coatings*, *112*, 141–152. https://doi.org/10.1016/j.porgcoat.2017.07.009

20. Yilgor, I., Mather, B. D., Unal, S., Yilgor, E., & Long, T. E. (2004). Preparation of segmented, high molecular weight, aliphatic poly(ether-urea) copolymers in isopropanol. In-situ FTIR studies and polymer synthesis. *Polymer*, *45*(17), 5829–5836. https://doi.org/10.1016/J.POLYMER.2004.05.026

21. Liang, H., Feng, Y., Lu, J., Liu, L., Yang, Z., Luo, Y., Zhang, Y., & Zhang, C. (2018). Bio-based cationic waterborne polyurethanes dispersions prepared from different vegetable oils. *Industrial Crops and Products*, *122*, 448–455. https://doi.org/10.1016/J.INDCROP.2018.06.006

22. Fu, H., Wang, Y., Li, X., & Chen, W. (2016). Synthesis of vegetable oil-based waterborne polyurethane/silver-halloysite antibacterial nanocomposites. *Composites Science and Technology*, *126*, 86–93. https://doi.org/10.1016/j.compscitech.2016.02.018

23. Li, C., Xiao, H., Wang, X., & Zhao, T. (2018). Development of green waterborne UV-curable vegetable oil-based urethane acrylate pigment prints adhesive: Preparation and application. *Journal of Cleaner Production*, *180*, 272–279. https://doi.org/10.1016/J.JCLEPRO.2018.01.193

24. Lei, L., Zhong, L., Lin, X., Li, Y., & Xia, Z. (2014). Synthesis and characterization of waterborne polyurethane dispersions with different chain extenders for potential application in waterborne ink. *Chemical Engineering Journal*, *253*, 518–525. https://doi.org/10.1016/J.CEJ.2014.05.044

25. Ionita, D., Gaina, C., Cristea, M., & Banabic, D. (2015). *Tailoring the hard domain cohesiveness in polyurethanes by interplay between the functionality and the content of chain extender*. https://doi.org/10.1039/c5ra15190b

26. Panda, S. S., Panda, B. P., Mohanty, S., & Nayak, S. K. (2017). The castor oil based water borne polyurethane dispersion; effect of -NCO/OH content: synthesis, characterization and properties. *Green Processing and Synthesis*, *6*(3), 341–351. https://doi.org/10.1515/gps-2016-0144

27. Grzelak, A. W., Boinard, P., & Liggat, J. J. (2018). *The influence of diol chain extender on morphology and properties of thermally-triggered UV-stable self-healing polyurethane coatings*. https://doi.org/10.1016/j.porgcoat.2018.04.032

28. Fink, J. K. (2013). Poly(urethane)s. In *Reactive Polymers Fundamentals and Applications* (pp. 49–93). Elsevier. https://doi.org/10.1016/B978-1-4557-3149-7.00002-4

29. Honarkar, H. (2018). Waterborne polyurethanes: A review. *Journal of Dispersion Science and Technology*, *39*(4), 507–516. https://doi.org/10.1080/01932691.2017.1327818

30. Jaudouin, O., Robin, J. J., Lopez-Cuesta, J. M., Perrin, D., & Imbert, C. (2012). Ionomer-based polyurethanes: A comparative study of properties and applications. *Polymer International*, *61*(4), 495–510. https://doi.org/10.1002/pi.4156

31. Król, P., & Król, B. (2020). Structures, properties and applications of the polyurethane ionomers. In *Journal of Materials Science* (Vol. 55, Issue 1, pp. 73–87). Springer New York LLC. https://doi.org/10.1007/s10853-019-03958-y

32. Santamaria-Echart, A., Fernandes, I., Barreiro, F., Corcuera, M. A., & Eceiza, A. (2021). Advances in Waterborne Polyurethane and Polyurethane-Urea Dispersions and Their Eco-friendly Derivatives: A Review. *Polymers 2021, Vol. 13, Page 409*, *13*(3), 409. https://doi.org/10.3390/POLYM13030409

33. Chen, S. A., & Hsu, J. S. (1993). Polyurethane anionomers. I. Structure-property relationships. *Polymer*, *34*(13), 2769–2775. https://doi.org/10.1016/0032-3861(93)90119-U

34. Kim, B. K., Kim, K., & Jeonc, H. M. (n.d.). *Aqueous Dispersion of Polyurethane Anionomers from H,MDI/IPDI, PCL, BD, and DMPA*. https://doi.org/10.1002/app.1994.070530315

35. Sardon, H., Irusta, L., Fernández-Berridi, M. J., Luna, J., Lansalot, M., & Bourgeat-Lami, E. (2010). Waterborne Polyurethane Dispersions Obtained by the Acetone Process: A Study of Colloidal Features. *J Appl Polym Sci*, *120*, 2054–2062. https://doi.org/10.1002/app.33308

36. Nanda, A. K., & Wicks, D. A. (2006). The influence of the ionic concentration, concentration of the polymer, degree of neutralization and chain extension on aqueous polyurethane dispersions prepared by the acetone process. *Polymer*, *47*(6), 1805–1811. https://doi.org/10.1016/J.POLYMER.2006.01.074

37. Anıl, D., Berksun, E., Durmuş-Sayar, A., Sevinis¸-Özbulut, E. B., & Ünal, S. (2020). Recent advances in waterborne polyurethanes and their nanoparticle-containing dispersions. In *Handbook of Waterborne Coatings* (pp. 249–302). Elsevier. https://doi.org/10.1016/b978-0-12-814201-1.00011-1

38. Kolgesiz, S., Berksun, E., Tas, C. E., Unal, S., & Unal, H. (2023). Flexible waterborne polyurethane nanocomposite foams incorporated with halloysites as fresh-keeping packaging inserts for fresh fruits. *Food Packaging and Shelf Life*, *40*, 101204. https://doi.org/10.1016/J.FPSL.2023.101204

39. Tas, C. E., Berksun, E., Koken, D., Unal, S., & Unal, H. (2021). Photothermal Waterborne Polydopamine/Polyurethanes with Light-to-Heat Conversion Properties. *ACS Applied Polymer Materials*, *3*(8), 3929–3940. https://doi.org/10.1021/ACSAPM.1C00495/SUPPL_FILE/AP1C00495_SI_001.PDF

40. Wang, J., Yan, R., Hu, Y., Du, G., Liao, G., Yang, H., Luo, Y., Zheng, X., Chen, Y., Wang, S., & Li, X. (2022). Density-Dependent Emission Colors from a Conformation-Switching Chromophore in Polyurethanes. *Angewandte Chemie*, *134*(1), e202112290. https://doi.org/10.1002/ANGE.202112290

41. Ahmed, N., Kausar, A., & Muhammad, B. (2015). Advances in Shape Memory Polyurethanes and Composites: A Review. *Polymer-Plastics Technology and Engineering*, *54*(13), 1410–1423. https://doi.org/10.1080/03602559.2015.1021490

42. Yang, R., Liu, W., Song, N., Li, X., Li, Z., Luo, F., Li, J., & Tan, H. (2022). NIR Photothermal-Responsive Shape Memory Polyurethane with Protein-Inspired Aggregated Chymotrypsin-Sensitive Degradable Domains. *Macromolecular Rapid Communications*, 2200490. https://doi.org/10.1002/MARC.202200490

43. Zhang, P., Wu, B., Huang, S., Cai, F., Wang, G., & Yu, H. (2019). UV–vis–NIR light-induced bending of shape-memory polyurethane composites doped with azobenzene and upconversion nanoparticles. *Polymer*, *178*, 121644. https://doi.org/10.1016/J.POLYMER.2019.121644

44. Cremaldi, J. C., & Bhushan, B. (2018). Bioinspired self-healing materials: Lessons from nature. *Beilstein Journal of Nanotechnology*, *9*(1), 907–935. https://doi.org/10.3762/BJNANO.9.85

45. Liang, J., Liu, J., Zhu, L., Gao, S., Liu, Y., Teng, X., Wang, R., Wang, X., Wang, S., Wang, J., & Xia, Y. (2022). Self-Healing Chameleon Skin Functioning in the Air Environments. *ACS Applied Polymer Materials*. https://doi.org/10.1021/ACSAPM.2C01529

46. den Brabander, M., Fischer, H. R., & Garcia, S. J. (2019). Self-Healing Polymeric Systems: Concepts and Applications. *Smart Polymers and Their Applications*, 379–409. https://doi.org/10.1016/B978-0-08-102416-4.00011-9

47. Hager, M. D., Greil, P., Leyens, C., van der Zwaag, S., & Schubert, U. S. (2010). Self-Healing Materials. *Advanced Materials*, *22*(47), 5424–5430. https://doi.org/10.1002/adma.201003036

48. Yang, Y., & Urban, M. W. (2013). Self-healing polymeric materials. *Chemical Society Reviews*, *42*(17), 7446. https://doi.org/10.1039/c3cs60109a

49. Leeuwenburgh, S. C. G., De Belie, N., & van der Zwaag, S. (2018). Self-Healing Materials are Coming of Age. *Advanced Materials Interfaces*, *5*(17), 1800736. https://doi.org/10.1002/admi.201800736

50. Wool, R. P. (2008). Self-healing materials: A review. *Soft Matter*, *4*(3), 400–418. https://doi.org/10.1039/b711716g

51. Surendran, A., & Thomas, S. (2020). Self-healing polymeric systems—fundamentals, state of art, and challenges. In *Self-Healing Polymer-Based Systems* (pp. 1–16). Elsevier. https://doi.org/10.1016/b978-0-12-818450-9.00001-5

52. Hoque, M. E., & Shafoyat, M. U. (2024). Self-healing polymer nanocomposite films and coatings. *Polymer Nanocomposite Films and Coatings*, 181–217. https://doi.org/10.1016/B978-0-443-19139-8.00010-3

53. Wu, D. Y., Meure, S., & Solomon, D. (2008). Self-healing polymeric materials: A review of recent developments. In *Progress in Polymer Science (Oxford)* (Vol. 33, Issue 5, pp. 479–522). https://doi.org/10.1016/j.progpolymsci.2008.02.001

54. Utrera-Barrios, S., Verdejo, R., López-Manchado, M. A., & Hernández Santana, M. (2020). Evolution of self-healing elastomers, from extrinsic to combined intrinsic mechanisms: A review. In *Materials Horizons* (Vol. 7, Issue 11, pp. 2882–2902). Royal Society of Chemistry. https://doi.org/10.1039/d0mh00535e

55. Malekkhouyan, R., Neisiany, R. E., Khorasani, S. N., Das, O., Berto, F., & Ramakrishna, S. (2021). The influence of size and healing content on the performance of extrinsic self-healing coatings. *Journal of Applied Polymer Science*, *138*(10), 49964. https://doi.org/10.1002/app.49964

56. Rule, J. D., Sottos, N. R., & White, S. R. (2007). Effect of microcapsule size on the performance of self-healing polymers. *Polymer*, *48*(12), 3520–3529. https://doi.org/10.1016/J.POLYMER.2007.04.008

57. Mattia, J., & Painter, P. (2007). *A Comparison of Hydrogen Bonding and Order in a Polyurethane and Poly(urethane-urea) and Their Blends with Poly(ethylene glycol)*. https://doi.org/10.1021/ma0626362

58. Dahlke, J., Zechel, S., Hager, M. D., & Schubert, U. S. (2018). How to Design a Self-Healing Polymer: General Concepts of Dynamic Covalent Bonds and Their Application for Intrinsic Healable Materials. *Advanced Materials Interfaces*, *5*(17), 1800051. https://doi.org/10.1002/admi.201800051

59. Luo, Y., Chen, X., Chen, J., Wu, Z., Ma, H., Liu, X., Xiang, B., Ma, X., & Luo, Z. (2021). A combined experimental and molecular dynamics simulation study of an intrinsic self-healing polyurethane elastomer based on a dynamic non-covalent mechanism. *Soft Matter*, *17*(8), 2191–2204. https://doi.org/10.1039/d0sm02085k

60. Li, R., Fan, T., Chen, G., Xie, H., Su, B., & He, M. (2020). Highly transparent, self-healing conductive elastomers enabled by synergistic hydrogen bonding interactions. *Chemical Engineering Journal*, *393*. https://doi.org/10.1016/j.cej.2020.124685

61. Xie, Z., Hu, B. L., Li, R. W., & Zhang, Q. (2021). Hydrogen Bonding in Self-Healing Elastomers. *ACS Omega*, *6*(14), 9319–9333. https://doi.org/10.1021/ACSOMEGA.1C00462/ASSET/IMAGES/LARGE/AO1C00462_0018.JPEG

62. Cummings, S. C., Dodo, O. J., Hull, A. C., Zhang, B., Myers, C. P., Sparks, J. L., & Konkolewicz, D. (2021). *Quantity or Quality: Are Self-Healing Polymers and Elastomers Always Tougher with More Hydrogen Bonds? 15*, 19. https://doi.org/10.1021/acsapm.9b01095

63. Shang, X., Jin, Y., Du, W., Bai, L., Zhou, R., Zeng, W., & Lin, K. (2023). Flame-Retardant and Self-Healing Waterborne Polyurethane Based on Organic Selenium. *ACS Applied Materials & Interfaces*. https://doi.org/10.1021/ACSAMI.3C02251

64. Song, Y., Liu, Y., Qi, T., & Li, G. L. (2018). Towards Dynamic but Supertough Healable Polymers through Biomimetic Hierarchical Hydrogen-Bonding Interactions. *Angewandte Chemie - International Edition*, *57*(42), 13838–13842. https://doi.org/10.1002/anie.201807622

65. Chirila, T. V., Lee, H. H., Oddon, M., Nieuwenhuizen, M. M. L., Blakey, I., & Nicholson, T. M. (2014). Hydrogen-bonded supramolecular polymers as self-healing hydrogels: Effect of a bulky adamantyl substituent in the ureido-pyrimidinone monomer. *Journal of Applied Polymer Science*, *131*(4). https://doi.org/10.1002/app.39932

66. Peng, H., Du, X., Cheng, X., Wang, H., & Du, Z. (2021). Room-temperature self-healable and stretchable waterborne polyurethane film fabricated via multiple hydrogen bonds. *Progress in Organic Coatings*, *151*, 106081. https://doi.org/10.1016/j.porgcoat.2020.106081

67. Varley, R. J., & van der Zwaag, S. (2010). Autonomous damage initiated healing in a thermo-responsive ionomer. *Polymer International*, *59*(8), n/a-n/a. https://doi.org/10.1002/pi.2841

68. Hohlbein, N., Shaaban, A., Bras, A. R., Pyckhout-Hintzen, W., & Schmidt, A. M. (2015). Self-healing dynamic bond-based rubbers: Understanding the mechanisms in ionomeric elastomer model systems. *Physical Chemistry Chemical Physics*, *17*(32), 21005–21017. https://doi.org/10.1039/c5cp00620a

69. Jaudouin, O., Robin, J.-J., Lopez-Cuesta, J.-M., Perrin, D., & Imbert, C. (2012). Ionomer-based polyurethanes: a comparative study of properties and applications. *Polymer International*, *61*(4), 495–510. https://doi.org/10.1002/pi.4156

70. Das, A., Sallat, A., Bö, F., Suckow, M., Basu, D., Wießner, S., Stö, K. W., Voit, B., & Heinrich, G. (2015). Ionic Modification Turns Commercial Rubber into a Self-Healing Material. *ACS Appl. Mater. Interfaces*, *7*, 2021. https://doi.org/10.1021/acsami.5b05041

71. Scheiner, M., Dickens, T. J., & Okoli, O. (2016). Progress towards self-healing polymers for composite structural applications. In *Polymer* (Vol. 83, pp. 260–282). Elsevier Ltd. https://doi.org/10.1016/j.polymer.2015.11.008

72. Lee, W. J., Oh, H. G., & Cha, S. H. (2021). A Brief Review of Self-Healing Polyurethane Based on Dynamic Chemistry. *Macromolecular Research*, *29*(10), 649–664. https://doi.org/10.1007/S13233-021-9088-2

73. Blaiszik, B. J., Kramer, S. L. B., Olugebefola, S. C., Moore, J. S., Sottos, N. R., & White, S. R. (2010). Self-Healing Polymers and Composites. *Annual Review of Materials Research*, *40*(1), 179–211. https://doi.org/10.1146/annurev-matsci-070909-104532

74. Kim, Y. J., Huh, P. H., & Kim, B. K. (2015). Synthesis of self-healing polyurethane urea-based supramolecular materials. *Journal of Polymer Science Part B: Polymer Physics*, *53*(7), 468–474. https://doi.org/10.1002/POLB.23653

75. Joel, D., Pohl, G., & Hiller, W.-G. (1993). Polyurethane ureas with various urea structures. Solution behaviour and morphology. *Die Angewandte Makromolekulare Chemie*, *208*(1), 107–116. https://doi.org/10.1002/APMC.1993.052080110

76. Ahmed, S., Bae, M. J., Jeong, S., Lee, J. H., Kim, J. C., Park, Y. Il, & Cheong, I. W. (2022). Design of Eco-Friendly Self-Healing Polymers Containing Hindered Urea-Based Dynamic Reversible Bonds. *ACS Applied Polymer Materials*. https://doi.org/10.1021/ACSAPM.2C01087

77. Willocq, B., Khelifa, F., Odent, J., Lemaur, V., Yang, Y., Leclère, P., Cornil, J., Dubois, P., Urban, M. W., & Raquez, J. M. (2019). Mechanistic Insights on Spontaneous Moisture-Driven Healing of Urea-Based Polyurethanes. *ACS Applied Materials and Interfaces*, *11*(49), 46176–46182. https://doi.org/10.1021/acsami.9b16858

78. Kianfar, M., Mohajer, S., & Dorraji, M. S. S. (2022). Waterborne Polyurethanes for Self-Healing Applications. *Eco-Friendly Waterborne Polyurethanes*, 177–192. https://doi.org/10.1201/9781003173526-11

79. Ren, J., Dong, X., Duan, Y., Lin, L., Xu, X., Shi, J., Jia, R., Wu, D., & He, X. (2022). Synthesis and self-healing investigation of waterborne polyurethane based on reversible covalent bond. *Journal of Applied Polymer Science*, *139*(20), 52144. https://doi.org/10.1002/APP.52144

80. Chao Liu, Qing Yin, Qiming Yuan, Lifen Hao, Lei Shi, Yan Bao, Bin Lyu, & Jianzhong Ma. (2022). A wear-resistant, self-healing and recyclable multifunctional waterborne polyurethane coating with mechanical tunability based on hydrogen bonding and an aromatic disulfide structure. *Polymer Chemistry*. https://doi.org/10.1039/D2PY00958G

81. Xiao, Y., Huang, H., & Peng, X. (2017). Synthesis of self-healing waterborne polyurethanes containing sulphonate groups. *RSC Advances*, *7*(33), 20093–20100. https://doi.org/10.1039/C6RA28416G

82. Wan, T., & Chen, D. (2018). Preparation of β-cyclodextrin reinforced waterborne polyurethane nanocomposites with excellent mechanical and self-healing property. *Composites Science and Technology*, *168*, 55–62. https://doi.org/10.1016/J.COMPSCITECH.2018.08.049

83. Wan, T., & Chen, D. (2018). Mechanical enhancement of self-healing waterborne polyurethane by graphene oxide. *Progress in Organic Coatings*, *121*, 73–79. https://doi.org/10.1016/j.porgcoat.2018.04.016

84. Díez-García, I., Eceiza, A., & Tercjak, A. (2019). Self-Healable Nanocomposites with Enhanced Thermal Stability by Incorporation of TiO2 Nanoparticles to Waterborne Poly(urethane-urea) Matrices Based on Amphiphilic Triblock Copolymers. *Journal of Physical Chemistry C*, *123*(34), 21290–21298. https://doi.org/10.1021/acs.jpcc.9b06184

85. Chen, L., Dai, Z., Lou, W., Jiang, P., Zhang, P., Bao, Y., Gao, X., & Xia, | Jialiang. (2022). Synthesis of self-healing soybean oil-based waterborne polyurethane based on Diels–Alder reaction. *Journal of Applied Polymer Science*, e52694. https://doi.org/10.1002/APP.52694

86. Liu, H., & Sun, D. (2022). Synthesis of self-healing supramolecular waterborne polyurethane with quadruple hydrogen bonds via ureidotriazine. *Journal of Applied Polymer Science*, *139*(15), 51932. https://doi.org/10.1002/APP.51932

87. Bandekar, J., & Klima, S. (1991). FT-IR spectroscopic studies of polyurethanes Part I. Bonding between urethane C□O□C groups and the NH Groups. *Journal of Molecular Structure*, *263*(C), 45–57. https://doi.org/10.1016/0022-2860(91)80054-8

88. Diao, S., Zhang, Y., Zhao, C., Wang, M., & Yu, J. (n.d.). Preparation of waterborne polyurethane based on different polyols: the effect of structure and crystallinity. *Journal of Polymer Research*, *1*, 3. https://doi.org/10.1007/s10965-022-02960-4

89. Asplund, J. O. B., Bowden, T., Mathisen, T., & Hilborn, J. (2006). Variable hard segment length in poly(urethane urea) through excess of diisocyanate and vapor phase addition of water. *Macromolecules*, *39*(13), 4380–4385. https://doi.org/10.1021/ma060361k

90. Lu, Y., & Larock, R. C. (2008). Soybean-oil-based waterborne polyurethane dispersions: Effects of polyol functionality and hard segment content on properties. *Biomacromolecules*, *9*(11), 3332–3340. https://doi.org/10.1021/BM801030G/ASSET/IMAGES/LARGE/BM-2008-01030G_0010.JPEG

91. Ma, J., Lee, G.-H., Kim, J.-H., Kim, S.-W., Jo, S., & Kim, C. S. (2022). A Transparent Self-Healing Polyurethane–Isophorone-Diisocyanate Elastomer Based on Hydrogen-Bonding Interactions. *ACS Applied Polymer Materials*, acsapm.1c01799. https://doi.org/10.1021/ACSAPM.1C01799

92. Ylgör, E., & Ylgör, I. (2001). Hydrogen bonding: A critical parameter in designing silicone copolymers. *Polymer*, *42*(19), 7953–7959. https://doi.org/10.1016/S0032-3861(01)00293-2

93. Zhang, A., Li, J., Fan, H., Xiang, J., Wang, L., & Yan, J. (2022). Effect of mechanical properties on the self-healing behavior of waterborne polyurethane coatings. *Journal of Applied Polymer Science*, 52364. https://doi.org/10.1002/APP.52364

94. Jhon, Y.-K., Cheong, I.-W., & Kim, J.-H. (2001). Chain extension study of aqueous polyurethane dispersions. *Colloids and Surfaces A: Physicochemical and Engineering Aspects*, *179*, 71–78. www.elsevier.nl/locate/colsurfa

95. Lee, D. Il, Kim, S. H., & Lee, D. S. (2019). Synthesis of self-healing waterborne polyurethane systems chain extended with chitosan. *Polymers*, *11*(3). https://doi.org/10.3390/POLYM11030503/POLYMERS_11_00503_S001_PDF.PDF

96. Kim, C. K., & Kim, B. K. (1991). IPDI-based polyurethane ionomer dispersions: Effects of ionic, nonionic hydrophilic segments, and extender on particle size and physical properties of emulsion cast film. *Journal of Applied Polymer Science*, *43*(12), 2295–2301. https://doi.org/10.1002/app.1991.070431219

97. Cakić, S. M., Špírková, M., Ristić, I. S., B-Simendić, J. K., M-Cincović, M., & Poręba, R. (2013). The waterborne polyurethane dispersions based on polycarbonate diol: Effect of ionic content. *Materials Chemistry and Physics*, *138*(1), 277–285. https://doi.org/10.1016/J.MATCHEMPHYS.2012.11.057

98. Angeles Pe´rezpe´rez-Liminãna, M., Ara´n, F., Aı´s, A.-A., Torro´-, A. M., Palau, T.-, Ce´sar, A. C., Orgile´s-Barceloá, O., Jose´miguel, J., & Martı´n-Martı´nezmartı´nez, M. (2005). Characterization of waterborne polyurethane adhesives containing different amounts of ionic groups $. *International Journal of Adhesion & Adhesives*, *25*, 507–517. https://doi.org/10.1016/j.ijadhadh.2005.02.002

99. Kalista, S. J., Pflug, J. R., & Varley, R. J. (2013). Effect of ionic content on ballistic self-healing in EMAA copolymers and ionomers. *Polymer Chemistry*, *4*(18), 4910–4926. https://doi.org/10.1039/c3py00095h

100. Wang, X., Liang, D., & Cheng, B. (2020). Preparation and research of intrinsic self-healing elastomers based on hydrogen and ionic bond. *Composites Science and Technology*, *193*, 108127. https://doi.org/10.1016/j.compscitech.2020.108127

101. Cheng, B.-X., Gao, W.-C., Ren, X.-M., Ouyang, X.-Y., Zhao, Y., Zhao, H., Wu, W., Huang, C.-X., Liu, Y., Liu, X.-Y., Li, H.-N., & Li, R. K. Y. (2022). A review of microphase separation of polyurethane: Characterization and applications. *Polymer Testing*, 107489. https://doi.org/10.1016/J.POLYMERTESTING.2022.107489

102. Niemczyk, A., Piegat, A., Sonseca Olalla, Á., & El Fray, M. (2017). New approach to evaluate microphase separation in segmented polyurethanes containing carbonate

macrodiol. *European Polymer Journal*, *93*, 182–191. https://doi.org/10.1016/j.eurpolymj.2017.05.046

103. Noreen, A., Zia, K. M., Zuber, M., Tabasum, S., & Saif, M. J. (2016). Recent trends in environmentally friendly water-borne polyurethane coatings: A review. In *Korean Journal of Chemical Engineering* (Vol. 33, Issue 2, pp. 388–400). Springer New York LLC. https://doi.org/10.1007/s11814-015-0241-5

104. Montemor, M. F. (2014). Functional and smart coatings for corrosion protection: A review of recent advances. *Surface and Coatings Technology*, *258*, 17–37. https://doi.org/10.1016/J.SURFCOAT.2014.06.031

105. Alrashed, M. M., Jana, S., & Soucek, M. D. (2019). Corrosion performance of polyurethane hybrid coatings with encapsulated inhibitor. *Progress in Organic Coatings*, *130*, 235–243. https://doi.org/10.1016/J.PORGCOAT.2019.02.005

106. Koh, E., Kim, N.-K., Shin, J., & Kim, Y.-W. (2014). Polyurethane microcapsules for self-healing paint coatings. *RSC Adv.*, *4*(31), 16214–16223. https://doi.org/10.1039/C4RA00213J

107. Zhang, F., Ju, P., Pan, M., Zhang, D., Huang, Y., Li, G., & Li, X. (2018). Self-healing mechanisms in smart protective coatings: A review. *Corrosion Science*, *144*, 74–88. https://doi.org/10.1016/J.CORSCI.2018.08.005

108. Koh, E., Lee, S., Shin, J., & Kim, Y.-W. (2013). Renewable Polyurethane Microcapsules with Isosorbide Derivatives for Self-Healing Anticorrosion Coatings. *Ind. Eng. Chem. Res*, *52*, 33. https://doi.org/10.1021/ie402505s

109. Wu, Y., Guo, P., Zhao, Y., Liu, X., & Du, Z. (2019). Hydrophobic, transparent waterborne polyurethane-polydimethylsiloxane composites prepared from aqueous sol-gel process and applied in corrosion protection. *Progress in Organic Coatings*, *127*, 231–238. https://doi.org/10.1016/J.PORGCOAT.2018.06.002

110. Odarczenko, M., Thakare, D., Li, W., Venkateswaran, S. P., Sottos, N. R., & White, S. R. (2020). Sunlight-Activated Self-Healing Polymer Coatings. *Advanced Engineering Materials*, *22*(3), 1901223. https://doi.org/10.1002/adem.201901223

111. Xu, W. M., Rong, M. Z., & Zhang, M. Q. (2016). Sunlight driven self-healing, reshaping and recycling of a robust, transparent and yellowing-resistant polymer. *Journal of Materials Chemistry A*, *4*(27), 10683–10690. https://doi.org/10.1039/c6ta02662a

112. Wu, S., Li, J., Zhang, G., Yao, Y., Li, G., Sun, R., & Wong, C. (2017). Ultrafast self-healing nanocomposites via infrared laser and their application in flexible electronics. *ACS Applied Materials and Interfaces*, *9*(3), 3040–3049. https://doi.org/10.1021/acsami.6b15476

113. García, S. J., Fischer, H. R., White, P. A., Mardel, J., González-García, Y., Mol, J. M. C., & Hughes, A. E. (2011). Self-healing anticorrosive organic coating based on an encapsulated water reactive silyl ester: Synthesis and proof of concept. *Progress in Organic Coatings*, *70*(2–3), 142–149. https://doi.org/10.1016/J.PORGCOAT.2010.11.021

114. Jadhav, R. S., Hundiwale, D. G., & Mahulikar, P. P. (2011). Synthesis and characterization of phenol-formaldehyde microcapsules containing linseed oil and its use in epoxy for self-healing and anticorrosive coating. *Journal of Applied Polymer Science*, *119*(5), 2911–2916. https://doi.org/10.1002/app.33010

115. Fang, C., Zhou, X., Yu, Q., Liu, S., Guo, D., Yu, R., & Hu, J. (2014). Synthesis and characterization of low crystalline waterborne polyurethane for potential application in water-based ink binder. *Progress in Organic Coatings*, *77*(1), 61–71. https://doi.org/10.1016/J.PORGCOAT.2013.08.004

116. Vadillo del Ser, J. (2020). *Design, synthesis and characterization of inks based in waterborne polyurethane urea dispersions suitable for direct ink writing 3D-printing.* https://addi.ehu.es/handle/10810/50578

117. Vadillo, J., Larraza, I., Calvo-Correas, T., Gabilondo, N., Derail, C., & Eceiza, A. (2021). Design of a Waterborne Polyurethane–Urea Ink for Direct Ink Writing 3D Printing. *Materials 2021, Vol. 14, Page 3287*, *14*(12), 3287. https://doi.org/10.3390/MA14123287

118. MADINEH RASTGOO. (2023). *Direct ink writing of waterborne polyurethane as a biomedical matrix: Assessing mechanical properties and the performance of controlled release*. Sabancı University.

119. Alkan-Taş, B., Berksun, E., Taş, C. E., Ünal, S., & Ünal, H. (2022). NIR-responsive waterborne polyurethane-polydopamine coatings for light-driven disinfection of surfaces. *Progress in Organic Coatings*, *164*, 106669. https://doi.org/10.1016/J.PORGCOAT.2021.106669

120. Taş, B. A., Berksun, E., Taş, C. E., Ünal, S., & Ünal, H. (2022). Lysostaphin-Functionalized Waterborne Polyurethane/Polydopamine Coatings Effective against S. Aureus Biofilms. *ACS Applied Polymer Materials*. https://doi.org/10.1021/ACSAPM.2C00254

121. Sundaran, S. P., Reshmi, C. R., & Sujith, A. (2018). Tailored design of polyurethane based fouling-tolerant nanofibrous membrane for water treatment. *New Journal of Chemistry*, *42*(3), 1958–1972. https://doi.org/10.1039/C7NJ03997B

122. Zhang, Y., Ge, T., Li, Y., Lu, J., Du, H., Yan, L., Tan, H., Li, J., & Yin, Y. (2023). Anti-Fouling and Anti-Biofilm Performance of Self-Polishing Waterborne Polyurethane with Gemini Quaternary Ammonium Salts. *Polymers 2023, Vol. 15, Page 317*, *15*(2), 317. https://doi.org/10.3390/POLYM15020317

123. Fusetani, N. (2004). Biofouling and antifouling. *Natural Product Reports*, *21*(1), 94–104. https://doi.org/10.1039/B302231P

124. Adkins, J. D., Mera, A. E., Roe-Short, M. A., Pawlikowski, G. T., & Brady, R. F. (1996). Novel non-toxic coatings designed to resist marine fouling. *Progress in Organic Coatings*, *29*(1–4), 1–5. https://doi.org/10.1016/S0300-9440(96)00646-7

125. Sinha, S., Kumar, R., Anand, J., Gupta, R., Gupta, A., Pant, K., Dohare, S., Tiwari, P., Kumar Kesari, K., Krishnan, S., & Kumar Gupta, P. (2023). Nanotechnology-Based Solutions for Antibiofouling Applications: An Overview. *ACS Applied Nano Materials*, *0*(0). https://doi.org/10.1021/acsanm.3c01539

126. Chambers, L. D., Stokes, K. R., Walsh, F. C., & Wood, R. J. K. (2006). Modern approaches to marine antifouling coatings. *Surface and Coatings Technology*, *201*(6), 3642–3652. https://doi.org/10.1016/J.SURFCOAT.2006.08.129

127. Magin, C. M., Cooper, S. P., & Brennan, A. B. (2010). Non-toxic antifouling strategies. *Materials Today*, *13*(4), 36–44. https://doi.org/10.1016/S1369-7021(10)70058-4

128. Cao, X., Pan, J., Cai, G., Hu, Y., Zhang, X., & Dong, Z. (2022). Degradation mechanisms of corrosion and biofouling resistance of superhydrophobic coatings in harsh marine conditions. *Progress in Organic Coatings*, *173*, 107222. https://doi.org/10.1016/J.PORGCOAT.2022.107222

129. Tong, Z., Guo, H., Di, Z., Sheng, Y., Song, L., Hu, J., Gao, X., Hou, Y., Zhan, X., & Zhang, Q. (2022). Squid inspired elastomer marine coating with efficient antifouling strategies: Hydrophilized defensive surface and lower modulus. *Colloids and Surfaces B: Biointerfaces*, *213*, 112392. https://doi.org/10.1016/J.COLSURFB.2022.112392

130. Rahman, M. M., Lee, I., Chun, H.-H., Kim, H. Do, & Park, H. (2014). Properties of waterborne polyurethane-fluorinated marine coatings: The effect of different types of diisocyanates and tetrafluorobutanediol chain extender content. *Journal of Applied Polymer Science*, *131*(4), n/a-n/a. https://doi.org/10.1002/app.39905

131. Caki C, S. M., Risti C B, I. S., Krakovský, I., Stojiljkovi C A, D. T., Elský, P. B., & Kollová, L. (n.d.). *Crystallization and thermal properties in waterborne polyurethane elastomers: Influence of mixed soft segment block*. https://doi.org/10.1016/j.matchemphys.2013.12.008

132. Yang, Z., & Wu, G. (n.d.). Effects of soft segment characteristics on the properties of biodegradable amphiphilic waterborne polyurethane prepared by a green process. *Journal of Materials Science*, *55*. https://doi.org/10.1007/s10853-019-04237-6

133. Li, S., Liu, Z., Hou, L., Chen, Y., & Xu, T. (2020). Effect of polyether/polyester polyol ratio on properties of waterborne two-component polyurethane coatings. *Progress in Organic Coatings*, *141*, undefined-undefined. https://doi.org/10.1016/J.PORGCOAT.2020.105545

134. Yen, M. S., & Tsai, P. Y. (2003). Study on polyethylene glycol/polydimethylsiloxane mixing soft-segment waterborne polyurethane from different mixing processes. *Journal of Applied Polymer Science*, *90*(1), 233–243. https://doi.org/10.1002/APP.12640

135. Yang, C.-H., Li, Y.-J., & Wen, T.-C. (1997). *Mixture Design Approach to PEG-PPG-PTMG Ternary Polyol-Based Waterborne Polyurethanes*. https://pubs.acs.org/sharingguidelines

136. Gündüz, G., & Kısakürek, R. R. (2004). Structure–Property Study of Waterborne Polyurethane Coatings with Different Hydrophilic Contents and Polyols. *Journal of Dispersion Science and Technology*, *25*(2), 217–228. https://doi.org/10.1081/DIS-120030668

137. Chen, X., Zhang, G., Zhang, Q., Zhan, X., & Chen, F. (2015). *Preparation and Performance of Amphiphilic Polyurethane Copolymers with Capsaicin-Mimic and PEG Moieties for Protein Resistance and Antibacteria*. https://doi.org/10.1021/ie505062a

138. Chen, S., Li, L., Zhao, C., & Zheng, J. (2010). Surface hydration: Principles and applications toward low-fouling/nonfouling biomaterials. *Polymer*, *51*(23), 5283–5293. https://doi.org/10.1016/J.POLYMER.2010.08.022

139. Meng, Q. B., Lee, S.-I., Nah, C., & Lee, Y.-S. (2009). Preparation of waterborne polyurethanes using an amphiphilic diol for breathable waterproof textile coatings. *Progress in Organic Coatings*, *66*, 382–386. https://doi.org/10.1016/j.porgcoat.2009.08.016

140. Yuan, H., Qian, B., Zhang, W., & Lan, M. (2016). Protein adsorption resistance of PVP-modified polyurethane film prepared by surface-initiated atom transfer radical polymerization. *Applied Surface Science*, *363*, 483–489. https://doi.org/10.1016/J.APSUSC.2015.12.072

141. Khandwekar, A. P., & Doble, M. (2011). Physicochemical characterisation and biological evaluation of polyvinylpyrrolidone-iodine engineered polyurethane (Tecoflex®). *Journal of Materials Science: Materials in Medicine*, *22*(5), 1231–1246. https://doi.org/10.1007/S10856-011-4285-8/FIGURES/12

142. Paradowska, A. E., Kaÿmierska, K. A., & Ciach, T. (2010). Influence of the coating process parameters on the quality of PUR/PVP hydrogel coatings for PVC medical devices. *Polish Journal of Chemical Technology*, *12*(2), 10. https://doi.org/10.2478/v10026-010-0016-z

143. Li, Q., Wang, L., Yu, L., Li, C., Xie, X., Yan, H., Zhou, W., Wang, C., Liu, Z., Hou, G., & Zhao, Y.-Q. (n.d.). *Polysaccharide-Based Coating with Excellent Antibiofilm and Repeatable Antifouling-Bactericidal Properties for Treating Infected Hernia*. https://doi.org/10.1021/acs.biomac.3c01175

144. Tas, C. E., Berksun, E., Koken, D., Kolgesiz, S., Unal, S., & Unal, H. (2021). Waterborne Polydopamine-Polyurethane/Polyethylene Glycol-Based Phase Change Films for Solar-to-Thermal Energy Conversion and Storage. *Industrial and Engineering Chemistry Research*, *60*(41), 14788–14800. https://doi.org/10.1021/ACS.IECR.1C02751/ASSET/IMAGES/LARGE/IE1C02751_0009.JPEG

145. Akindoyo, J. O., Beg, M. D. H., Ghazali, S., Islam, M. R., Jeyaratnam, N., & Yuvaraj, A. R. (2016). Polyurethane types, synthesis and applications – a review. *RSC Advances*, *6*(115), 114453–114482. https://doi.org/10.1039/C6RA14525F

146. Xiao, Y., Fu, X., Zhang, Y., Liu, Z., Jiang, L., & Lei, J. (2016). Preparation of waterborne polyurethanes based on the organic solvent-free process. *Green Chemistry*, *18*(2), 412–416. https://doi.org/10.1039/C5GC01197C

147. Hsu, S. H., Hung, K. C., Lin, Y. Y., Su, C. H., Yeh, H. Y., Jeng, U. S., Lu, C. Y., Dai, S. A., Fu, W. E., & Lin, J. C. (2014). Water-based synthesis and processing of novel biodegradable elastomers for medical applications. *Journal of Materials Chemistry B*, *2*(31), 5083–5092. https://doi.org/10.1039/c4tb00572d

148. Florian, P., Jena, K. K., Allauddin, S., Narayan, R., & Raju, K. V. S. N. (n.d.). *Preparation and Characterization of Waterborne Hyperbranched Polyurethane-Urea and Their Hybrid Coatings*. https://doi.org/10.1021/ie900840g

149. Patel, M. R., Shukla, J. M., Patel, N. K., & Patel, K. H. (2009). Biomaterial based novel polyurethane adhesives for wood to wood and metal to metal bonding. *Materials Research*, *12*(4), 385–393. https://doi.org/10.1590/S1516-14392009000400003

150. Ángeles Pérez-Limiñana, M., Arán-Aís, F., Torró-Palau, A. M., Orgilés-Barceló, C., Martín-Martínez, J. M., & Miguel Martín-Martínez, J. (2006). Structure and properties of waterborne polyurethane adhesives obtained by different methods. *J. Adhesion Sci. Technol*, *20*(6), 519–536. https://doi.org/10.1163/156856106777213320

151. Mao, H., Qiang, S., Xu, Y., & Wang, C. (2017). Synthesis of polymeric dyes based on UV curable multifunctional waterborne polyurethane for textile coating. *New Journal of Chemistry*, *41*(2), 619–627. https://doi.org/10.1039/C6NJ03159E

152. Zhang, J., Xu, H., Hu, L., Yang, Y., Li, H., Huang, C., & Liu, X. (2017). Novel Waterborne UV-Curable Hyperbranched Polyurethane Acrylate/Silica with Good Printability and Rheological Properties Applicable to Flexographic Ink. *ACS Omega*, *2*(11), 7546–7558. https://doi.org/10.1021/acsomega.7b00939

153. Org, W. E., Cui, J., Zhang, Y., Hu, X., Chu, P. K., Wang, F., Wang, X., & Xu, Y. (2016). ELECTROCHEMICAL SCIENCE Synthesis of UV-Cured Hyperbranched Polyurethane Acrylate Coatings and Its Corrosion Resistance Revealed by Electrochemistry. *Int. J. Electrochem. Sci*, *11*, 3727–3737. https://doi.org/10.20964/110268

154. Yu, F., Cao, L., Meng, Z., Lin, N., & Liu, X. Y. (2016). Crosslinked waterborne polyurethane with high waterproof performance. *Polymer Chemistry*, *7*(23), 3913–3922. https://doi.org/10.1039/C6PY00350H

155. Lv, C., Hu, L., Yang, Y., Li, H., Huang, C., & Liu, X. (2015). Waterborne UV-curable polyurethane acrylate/silica nanocomposites for thermochromic coatings. *RSC Advances*, *5*(33), 25730–25737. https://doi.org/10.1039/C5RA01687H

156. Chen, S., Zhang, S., Li, Y., & Zhao, G. (2015). Synthesis and properties of novel UV – curable hyperbranched waterborne polyurethane/Fe $_3$ O $_4$ nanocomposite films with excellent magnetic properties. *RSC Advances*, *5*(6), 4355–4363. https://doi.org/10.1039/C4RA13683G

157. Yao, S., Shi, J., Du, X., Lu, M., Liu, Y., Liang, L., & Lu, M. (2020). Preparation, Characterization and Application of Cyclodextrin-Containing UV-Curable Waterborne Polyurethane Based on Guest Regulation. *ChemistrySelect*, *5*(7), 2255–2262. https://doi.org/10.1002/slct.201904348

158. Chen, S., Guo, L., Du, D., Rui, J., Qiu, T., Ye, J., & Li, X. (2016). Waterborne POSS-silane-urethane hybrid polymer and the fluorinated films. *Polymer*, *103*, 27–35. https://doi.org/10.1016/J.POLYMER.2016.09.034

159. Fu, J., Wang, L., Yu, H., Haroon, M., Haq, F., Shi, W., Wu, B., & Wang, L. (2019). Research progress of UV-curable polyurethane acrylate-based hardening coatings. *Progress in Organic Coatings*, *131*, 82–99. https://doi.org/10.1016/J.PORGCOAT.2019.01.061

160. Dall Agnol, L., Dias, F. T. G., Ornaghi, H. L., Sangermano, M., & Bianchi, O. (2021). UV-curable waterborne polyurethane coatings: A state-of-the-art and recent advances review. *Progress in Organic Coatings*, *154*, 106156. https://doi.org/10.1016/J.PORGCOAT.2021.106156

161. Wang, L., Zheng, Q., Xu, P., Li, Y., Tan, Y., Wang, R., & Hao, L. (2022). Amphiphilic alginate stabilized UV-curable polyurethane acrylate as a surface coating to improve the anti-wrinkle performance of cotton fabrics. *Progress in Organic Coatings*, *162*, 106595. https://doi.org/10.1016/J.PORGCOAT.2021.106595

162. Zhang, X., Zhu, M., Wang, W., & Yu, D. (2018). Silver/waterborne polyurethane-acrylate's antibacterial coating on cotton fabric based on click reaction via ultraviolet radiation. *Progress in Organic Coatings*, *120*(March), 10–18. https://doi.org/10.1016/j.porgcoat.2018.03.004

163. Cui, G., Zhang, C., Wang, A., Zhou, X., Xing, X., Liu, J., Li, Z., Chen, Q., & Lu, Q. (2021). Research progress on self-healing polymer/graphene anticorrosion coatings. *Progress in Organic Coatings*, *155*, 106231. https://doi.org/10.1016/J.PORGCOAT.2021.106231

164. Bakhshandeh, E., Sobhani, S., Croutxé-Barghorn, C., Allonas, X., & Bastani, S. (2021). Siloxane-modified waterborne UV-curable polyurethane acrylate coatings:

Chemorheology and viscoelastic analyses. *Progress in Organic Coatings*, *158*, 106323. https://doi.org/10.1016/J.PORGCOAT.2021.106323

165. Xu, J., Jiang, Y., Zhang, T., Dai, Y., Yang, D., Qiu, F., Yu, Z., & Yang, P. (2018). Synthesis of UV-curing waterborne polyurethane-acrylate coating and its photopolymerization kinetics using FT-IR and photo-DSC methods. *Progress in Organic Coatings*, *122*, 10–18. https://doi.org/10.1016/J.PORGCOAT.2018.05.008

166. Wu, Q., Yang, Y., Ma, C., Chen, Z., Su, Q., Zhu, C., Gao, Y., Ma, R., & Li, C. (2021). *Flexible Nanocomposite Polymer Electrolyte Based on UV-Cured Polyurethane Acrylate for Lithium Metal Batteries*. https://doi.org/10.1021/acssuschemeng.1c00467

167. Che, Y., Liu, C., Li, N., Guo, W., Xi, M., Zhang, S., & Wang, Z. (2022). UV curing polyurethane–acrylate composites as full filling thermal interface materials. *New Journal of Chemistry*, *46*(17), 7979–7986. https://doi.org/10.1039/D2NJ00397J

168. Gobert, S. R. L., Vancleef, A., Clercx, S., Braeken, L., & Thomassen, L. C. J. (2021). Continuous Production of Water-Based UV-Curable Polyurethane Dispersions Using Static Mixers and a Rotor-Stator Mixer. *ACS Omega*, *6*(40), 25884–25891. https://doi.org/10.1021/ACSOMEGA.1C01525/ASSET/IMAGES/MEDIUM/AO1C01525_0011.GIF

169. Xu, C. an, Liang, W., Wu, X., Jiao, E., Lu, M., Wu, K., Hao, X., & Shi, J. (2022). Effect of novel silicone/vanillin monomer on the thermal stability and adhesion properties of UV-curable polyurethane pressure sensitive adhesive and its application in functional glass. *Progress in Organic Coatings*, *171*, 107019. https://doi.org/10.1016/J.PORGCOAT.2022.107019

170. Masson, F., Decker, C., Jaworek, T., & Schwalm, R. (2000). UV-radiation curing of waterbased urethane-acrylate coatings. *Progress in Organic Coatings*, *39*(2–4), 115–126. https://doi.org/10.1016/S0300-9440(00)00128-4

171. Gurunathan, T., Mohanty, S., & Nayak, S. K. (2016). Hyperbranched Polymers for Coating Applications: A Review. *Polymer-Plastics Technology and Engineering*, *55*(1), 92–117. https://doi.org/10.1080/03602559.2015.1021482

172. Han, W., Lin, B., Yang, H., & Zhang, X. (2013). Synthesis of UV-curable hyperbranched polyurethane (meth)acrylate oligomers via thiol-ene “click” chemistry. *Journal of Applied Polymer Science*, *128*(6), 4261–4270. https://doi.org/10.1002/app.38584

173. Spindler, R., & Fréchet, J. M. J. (1993). Synthesis and Characterization of Hyperbranched Polyurethanes Prepared from Blocked Isocyanate Monomers by Step-Growth Polymerization. In *Macromolecules* (Vol. 26).

174. Kumar, A., & Ramakrishnan, S. (1993). A novel one-pot synthesis of hyperbranched polyurethanes. *Journal of the Chemical Society, Chemical Communications*, *18*, 1453–1454. https://doi.org/10.1039/C39930001453

175. Lin, Q., Unal, S., Fornof, A. R., Yilgor, I., & Long, T. E. (2006). Highly Branched Poly(arylene ether)s via Oligomeric A2 + B3 Strategies. *Macromolecular Chemistry and Physics*, *207*(6), 576–586. https://doi.org/10.1002/macp.200500503

176. Sheth, J. P., Unal, S., Yilgor, E., Yilgor, I., Beyer, F. L., Long, T. E., & Wilkes, G. L. (2005). A comparative study of the structure-property behavior of highly branched segmented poly(urethane urea) copolymers and their linear analogs. *Polymer*, *46*(23), 10180–10190. https://doi.org/10.1016/j.polymer.2005.07.068

177. Bruchmann, B., & Schrepp, W. (2003). *The AA* + B*B 2 approach A simple and convenient synthetic strategy towards hyperbranched polyurea-urethanes* (Issue 014).

178. Unal, S., Yilgor, I., Yilgor, E., Sheth, J. P., Wilkes, G. L., & Long, T. E. (2004). *A New Generation of Highly Branched Polymers: Hyperbranched, Segmented Poly(urethane urea) Elastomers*. https://doi.org/10.1021/ma049472e

179. Zhang, Y., Asif, A., & Shi, W. (2011). Highly branched polyurethane acrylates and their waterborne UV curing coating. *Progress in Organic Coatings*, *71*(3), 295–301. https://doi.org/10.1016/J.PORGCOAT.2011.03.022